

CHALMERS



Influence of Tyre Inflation Pressure on Fuel Consumption, Vehicle Handling and Ride Quality

Modelling and Simulation

ALEXANDER VARGHESE

Department of Applied Mechanics
Division of Vehicle Engineering and Autonomous Systems
Vehicle Dynamics Group
CHALMERS UNIVERSITY OF TECHNOLOGY
Göteborg, Sweden 2013
Master's thesis 2013:75

MASTER'S THESIS IN AUTOMOTIVE ENGINEERING

**Influence of Tyre Inflation Pressure on Fuel
Consumption, Vehicle Handling and Ride Quality
Simulation and Modelling**

ALEXANDER VARGHESE

Department of Applied Mechanics
Division of Vehicle Engineering and Autonomous Systems
Vehicle Dynamics Group
CHALMERS UNIVERSITY OF TECHNOLOGY
Göteborg, Sweden 2013

Influence of Tyre Inflation Pressure on Fuel Consumption, Vehicle Handling and Ride Quality

Simulation and Modelling

ALEXANDER VARGHESE

© ALEXANDER VARGHESE, 2013

Master's Thesis 2013:75

ISSN 1652-8557

Department of Applied Mechanics

Division of Vehicle Engineering and Autonomous Systems

Vehicle Dynamics Group

Chalmers University of Technology

SE-412 96 Göteborg

Sweden

Telephone: + 46 (0)31-772 1000

Influence of Tyre Inflation Pressure on Fuel Consumption, Vehicle Handling and Ride Quality

Simulation and Modelling

ALEXANDER VARGHESE

Department of Applied Mechanics

Division of Vehicle Engineering and Autonomous Systems

Vehicle Dynamics Group

CHALMERS UNIVERSITY OF TECHNOLOGY

Göteborg, Sweden 2013

ABSTRACT

It is well understood that fuel economy directly influences the CO₂ emissions in vehicles. Thus, a straightforward approach to reduce the tailpipe CO₂ emissions is to reduce the overall fuel consumption of the vehicle. In this thesis work the role of tyre inflation pressure on the fuel economy is investigated. Apart from the benefits of reduced fuel consumption, tyre pressure also plays an important role in deciding vehicle handling and passenger comfort.

Three mathematical vehicle models have been developed in the Matlab/Simulink[®] interface, to capture and represent the influence of tyre pressure on fuel consumption, vehicle handling and ride characteristics. The first model is a full-vehicle model developed to enable quick and reliable estimation of fuel consumption with the change in tyre pressure. The second model is a two-track vehicle model developed to study the changes in vehicle lateral behaviour when the tyre inflation pressure is changed. The third model is a half-car model that is designed to evaluate the changes in vertical acceleration response of the vehicle with change in tyre pressure.

When the full-vehicle model was simulated for the New European Driving Cycle (NEDC city cycle), fuel consumption reduction up to 5 % was observed simply by increasing the tyre inflation pressures from 2 bar to 3 bar. The vehicle handling also improved considerably especially when tyre pressure was maintained higher on the outer wheels and lower on the inner wheels of the vehicle in a turn. For smooth roads found within city limits, it was observed that the tyre pressure affected the ride comfort only marginally. However as road roughness increased, the impact of tyre pressure on ride comfort also increased. Through these findings, a foundation is established for the development of a dynamic Tyre Pressure Regulating System (TPRS) that is capable of regulating the tyre pressure in all four wheels, independently and continuously.

Keywords: Tyre inflation pressure, Rolling Resistance, Tyre model, Fuel estimation, QSS TB[®], TNO Delft-Tyre[®], Two-Track vehicle model, Four-DOF vehicle model.

CONTENTS

1	INTRODUCTION	9
1.1	Background	9
1.2	Aim	10
1.3	Scope and limitations	10
2	LITERATURE REVIEW	12
2.1	Contribution of the tyre rolling resistance to fuel consumption	12
2.1.1	Influence of temperature	13
2.1.2	Influence of load	15
2.1.3	Influence of speed	16
2.1.4	Influence of size and construction of tyres	17
2.1.5	Influence of tyre wear	18
2.1.6	Influence of tyre pressure	19
2.2	Importance of having appropriate tyre pressure	20
2.3	Influence of tyre pressure on braking performance	22
2.4	Influence of tyre pressure on vehicle handling	24
2.4.1	Lateral force	24
2.4.2	Self-aligning moment	25
2.4.3	Longitudinal force	26
2.5	Influence of tyre pressure on vehicle ride characteristics	28
3	MODELLING AND SIMULATION	30
3.1	Fuel estimation	30
3.1.1	Mathematical modelling approach	31
3.1.2	Rolling resistance models	32
3.1.3	QSS vehicle model	36
3.2	Vehicle lateral handling characteristics	40
3.2.1	Modelling approach	40
3.2.2	Tyre models	41
3.2.3	Two-track vehicle model	48
3.3	Vehicle ride characteristics	55
3.3.1	Modelling approach	55
3.3.2	Four DOF half-car model	56

4	RESULTS AND DISCUSSION	64
4.1	QSS vehicle model: Fuel estimation	64
4.1.1	Contribution of rolling resistance to overall fuel consumption	64
4.1.2	Influence of tyre pressure on rolling resistance	66
4.2	Two track model	68
4.2.1	Vehicle response to a step input	68
4.2.2	Vehicle response to ramp input	75
4.2.3	Sine-With-Dwell input	81
4.3	Four DOF half-car model	87
4.3.1	Response to step input	87
4.3.2	Response to sinusoidal input	90
4.3.3	Frequency response	91
5	CONCLUSIONS AND FUTURE WORK	97
5.1	Conclusion	97
5.1.1	QSS vehicle model / Fuel consumption	97
5.1.2	Two-track model / Handling	97
5.1.3	Four DOF half-car model / Comfort	98
5.2	Future work	99
6	REFERENCES	101
7	APPENDIX I	104

Preface

In this research work, the influence of tyre inflation pressure on fuel consumption has been examined with emphasis on the corresponding change in vehicle ride characteristics and handling. This thesis work was carried out from April, 2013 to November, 2013 under the supervision of Associate Professor Jenny Jerrelind of KTH The Royal Institute of Technology, Prof. Professor Bengt Jacobson of Chalmers University of Technology and Fredrik Lotto at Yovinn AB, Sweden. The work is part of a research project initiated by Ivar Frischer, Chief Designer at Yovinn AB, in collaboration with Centre for ECO² Vehicle Design to develop a dynamic Tyre Pressure Regulating System (TPRS) for a passenger car. This system should be capable of regulating tyre pressure continuously and independently in each tyre, based on different driving conditions without adversely affecting safety, driving performance and passenger comfort. The project is carried out at the Department of Aeronautical and Vehicle Engineering, KTH, Sweden. The project is financed by Vinnova AB through the Centre for ECO² Vehicle Design and Yovinn AB.

I would like to thank the supervisors, staff and PhD students at the research group of vehicle dynamics at KTH for their time and guidance despite their hectic schedules and responsibilities. I would also like to thank Julien Brondex, who worked on the design of this adaptive tyre pressure regulating system, for his valuable inputs via questions that has helped me in my work. I would like to extend my deepest gratitude to TNO[®], Netherlands and Delft University, Netherlands for their indirect participation in this thesis work through the supply of an advanced, validated tyre model, MF-Tyre and the guidance from Docent Mathias Lidberg of Chalmers University of Technology.

An acknowledgment is also due to ETH Zürich for making available a Matlab QSS toolbox[®] for building full vehicle models for educational research. This toolbox was obtained via the course, "TME095 Hybrid vehicles and control", offered at Chalmers University of Technology in 2012.

Stockholm, November 2013

Alexander Varghese

Notations

Abbreviations

DOF	Degree Of Freedom
DSC	Dynamic Stability Control
EPA	Environmental Protection Agency
ESC	Electronic Stability Control
EU	European Union
FMVSS	Federal Motor Vehicle Safety Standards
KTH	Kungliga Tekniska Högskolan (Royal Institute of Technology)
MERF	Mean Equivalent Rolling Force
mph	Miles Per Hour
NEDC	New European Driving Cycle
NHTSA	National Highway Traffic Safety Administration
NVH	Noise, Vibration and Harshness
psi	Pounds per square Inch
QSS TB	Quasi-Static Simulation ToolBox
RMS	Root Mean Square
RR	Rolling Resistance
SAE	Society of Automotive Engineers
SWD	Sine-With-Dwell
TNO	Toegepast Natuurwetenschappelijk Onderzoek
TPRS	Tyre Pressure Regulating System

Roman upper case letters

B	Stiffness factor Magic Tyre Formula [-]
B_f	2*Front suspension spring damping [Ns/m]
B_r	2*Rear suspension spring damping [Ns/m]
B_{tf}	2*Front tyre vertical damping [Ns/m]
B_{tr}	2*Rear tyre vertical damping [Ns/m]
C	Shape factor Magic Tyre Formula [-]
C_{RR}	Coefficient of rolling resistance [-]
C_α	Cornering stiffness coefficient [N/rad]
D	Peak value in Magic Tyre Formula [-]
E	Curvature factor Magic Tyre Formula [-]
F_x	Longitudinal tyre force [N]
F_y	Lateral tyre force [N]
\bar{F}_y	Non-dimensional Lateral force [-]
F_{R0}	Tyre rolling resistance at load F_{Z0} and pressure p_0 [N]
F_{RR}	Tyre rolling resistance force [N]
$F_{RR(drum)}$	Rolling resistance force measured on test drum [N]
F_{xLi}	Rolling resistance force, left tyre [N]
F_{xRi}	Rolling resistance force, right tyre [N]
F_Z	Tyre load of interest [N]
F_{Z0}	Reference/Nominal tyre vertical load [N]
ΔF_{zlong}	Load transfer longitudinal [N]
ΔF_{zlat}	Load transfer lateral [N]

I_{xx}	Moment of inertia about x axis at COG [Nm]
I_{yy}	Moment of inertia about y axis at COG [Nm]
I_{zz}	Moment of inertia about z axis at COG [Nm]
K	Tyre vertical stiffness [N/m]
K_0	Tyre vertical stiffness at nominal pressure [N/m]
K_f	2*Front suspension spring stiffness [N/m]
K_L	Slope of load dependency of F_{RR} [-]
K_P	Slope of reciprocal pressure dependency of F_{RR} [-]
K_r	2*Rear suspension spring stiffness [N/m]
K_{tf}	2*Front tyre's vertical stiffness [N/m]
K_{tr}	2*Rear tyre's vertical stiffness [N/m]
L	Wheelbase [m]
M	Weight of the vehicle [kg]
M_B	Sprung mass of the vehicle [kg]
M_z	Self-aligning moment [Nm]
M_x	Overturning moment [Nm]
M_{RR}	Rolling resistance moment [Nm]
M_{uf}	Un-sprung mass at front axle [kg]
M_{ur}	Un-sprung mass at rear axle [kg]
M_{us}	Un-sprung mass of the vehicle [kg]
$M_{\phi i}$	Roll stiffness moment about roll centre [Nm/rad]
P_{Fz1}	Pressure effect on vertical stiffness [-]
R_{class}	Road roughness coefficient [m ³ /cycle]
$S_{rd}(n)$	PSD of elevation of road profile [m ³]

T_e	Equilibrium temperature of tyre [$^{\circ}\text{C}$]
V_{sy}	Lateral tyre slip velocity [m/s]
V_x	Longitudinal velocity at the wheel centre [m/s]
Y_{RR}	Yaw Rate Response [%]
Z_B	Displacement of sprung mass [m]
Z_{uf}	Displacement of un-sprung mass at the front axle [m]
Z_{ur}	Displacement of un-sprung mass at the rear axle [m]

Roman lower case letters

a_1	Distance from COG to front axle [m]
a_2	Distance from COG to rear axle [m]
a_x	Longitudinal acceleration [m/s^2]
a_y	Lateral acceleration [m/s^2]
dp_i	Non-dimensional pressure increment = $\frac{p_i - p_0}{p_0}$ [-]
f	Frequency [Hz]
h	Height of COG from the ground [m]
h_i	Roll centre height at axle number, i [m]
i	Axle number; 1=front and 2=Rear [-]
n	Spatial frequency of interest [cycles/m]
n_0	Spatial frequency at the discontinuity [cycles/m]
p_0	Reference/Nominal tyre pressure (2.2 bar assumed) [Pa]
p_1, p_2	Slope of the log-log curve [-]
p_i	Tyre pressure of interest [pa]
r	Yaw rate [rad/s]

r_{peak}	Peak yaw rate [rad/s]
r_t	Yaw rate at time, t [rad/s]
s_1	Half track width at the front axle [m]
s_2	Half track width at the rear axle [m]
t_0	Driving cycle start time [s]
t_f	Driving cycle end time [s]
v_x	Longitudinal velocity in vehicle's coordinate axis system [m/s]
v_y	Lateral velocity in vehicle's coordinate axis system [m/s]

Greek lower case

α_{slip}	Slip angle [rad]
$\bar{\alpha}_{slip}$	Non-dimensional slip angle [-]
α_{Li}	Left tyre side-slip angle [rad]
α_{Ri}	Right tyre side-slip angle [rad]
β	Body slip angle [rad]
δ	Steered wheel angle at the tyres [rad]
$\delta_{steering}$	Steering wheel angle [rad]
γ	Camber angle [rad]
θ	Pitch [rad]
κ	Slip ratio [-]
μ	Surface friction coefficient [-]
ψ	Turn slip velocity of the tyre [rad/s]
ω	Angular frequency [rad/s]

1 Introduction

According to a recent report filed by the United Nation Framework Convention on Climate Change (UNFCCC) in April 2013, Carbon Dioxide (CO₂) emissions from road transport have increased by 21 % between 1990 and 2011 and account for 23 % of the European Union's (EU) total CO₂ emissions. The EU, in its effort to meet the greenhouse gas emission targets set under the Kyoto Protocol, has pushed vehicle manufacturers to find solutions to limit the tailpipe emissions of CO₂. After reviewing data on the fleet average CO₂ emissions from cars introduced after the year 2012, the European Commission had set the fleet average CO₂ emission target at 130 g/km for cars in 2015 and a projected target of 95 g/km for 2021. For the first time, these targets will be mandatory for all vehicle manufacturers within the EU. Failing to comply, will result in the vehicle manufacturer having to pay an excess emission premium for each new car registered.

The easiest way to reduce CO₂ emissions in a vehicle is to reduce its fuel consumption since the CO₂ emission is directly proportional to the amount of fuel consumed. Tyre inflation pressure plays an important role in the vehicle's fuel consumption. The results of a survey released by the US Department of Transportation's NHTSA in 2001 showed that a decrease of 0.55 bar, from the recommended inflation pressure, resulted in the reduction of fuel efficiency by 3.3%, in miles per gallon [1]. This survey also found that one in four cars on the road had at least one tyre that was under-inflated. With over 12 million cars added (in 2012) to the roads each year, it is possible to imagine the impact having proper tyre pressure can have on the economy and ecology of a nation.

1.1 Background

This thesis work is a pre-study to a project initiated by Ivar Frischer, Chief Design Engineer at Yovinn AB, in collaboration with the Centre for ECO² Vehicle Design at KTH The Royal Institute of Technology. The idea is to develop an on-board adaptive Tyre Pressure Regulating System (TPRS) for a passenger cars, that is capable of continuously varying an optimized amount of air in the tyres based on different driving conditions such as road quality and driving styles. On highways for example, the vehicle operates at a constant velocity most of the time and the tyres require a low rolling-resistance profile to achieve better fuel efficiency. However, having low rolling resistance profile reduces the acceleration, braking and cornering performance of the vehicle. Thus within city limits, a high-grip, wider tyre profile is required for effective acceleration, braking and cornering.

The inflation pressure indirectly affects the side wall stiffness and foot-print of the tyre which play an important role in determining vehicle handling and ride characteristics. Numerous tests have also shown significant fuel consumption benefits obtained by simply maintaining appropriate tyre pressure in all wheels [1]. All this

justifies the development of a dynamic TPRS that can not only improve overall fuel efficiency of the vehicle but possibly its handling and ride characteristics, without substantial changes to the basic vehicle design at high cost. Such systems are already in use in agricultural vehicles and have also become standard in wheeled military vehicles. They have been proven to offer better ride comfort, lower component failure and improved traction, particularly on rough terrain [2].

1.2 Aim

The main goal of this thesis work is to simulate and analyse the effects of tyre inflation pressure on the vehicle's overall fuel consumption. The corresponding changes in handling and ride characteristics of the vehicle are also analysed, based on the inputs from the road and driver. The findings from this work should be able to justify the development of an on-board adaptive TPRS, which is capable of estimating and regulating an optimum amount of air required in the tyres under different driving conditions to give the best possible combination between fuel consumption, vehicle handling and ride comfort. To study the impact of tyre pressure on vehicle performance and fuel consumptions, vehicle models need to be developed. The tyre models used in these vehicle models should be able to capture and simulate the effects of tyre pressure on the vehicle's lateral, longitudinal and vertical response.

1.3 Scope and limitations

In a vehicle, there are several sources of energy losses which affect the overall fuel consumption. In this thesis work only the rolling resistance losses from tyres are studied and modelled when estimating the fuel consumption of the vehicle. Losses due to tyre slip are not considered. Due to lack of tyre and road data, the tyre data on rolling resistance is borrowed from reference [3], which is a tyre smaller than that used in the other two vehicle models. Thus, a load constant is applied to the rolling resistance data to account for the difference in size. The fuel estimations are made only for the standard NEDC city driving cycle that closely represents the driving style of a vehicle within city limits, with a number of starts and stops.

The influence of tyre pressure on vehicle handling is studied for two surfaces, dry and wet, at different velocities and tyre pressures settings in the four tyres. Due to lack of data and for the sake of simplicity, the wet surface is modelled by reducing the peak lateral and longitudinal friction coefficient at the tyre road interface. The impact of factors such as tyre tread design, tread depth, standing water height, road surface roughness etc on tyre force and moment characteristics, are not modelled explicitly.

The influence of inflation pressure on vehicle's ride characteristics is evaluated at different inflation pressures and compared to the vehicle whose tyres are at the nominal inflation pressure. The RMS values of vertical acceleration is determined in a certain frequency range of interest and compared to the International Standards

Organization (ISO) 2631 standards for whole body vibration in the vertical direction. The frequency response of the vehicle's vertical acceleration and tyre's road holding are also examined. The ride analysis will be carried out only for vibrations in the frequency range of 1 Hz to 20 Hz and will not include the dynamic tyre behaviours such as standing waves, which are observed at higher frequencies.

Finally, as mentioned earlier, the TPRS is assumed to be continuous and independent in its operation i.e., it can take any value of tyre pressure within its operating range and does not require driver intervention. In order to take advantage of the handling benefits obtained by changing the tyre pressure, the TPRS is assumed to be instantaneous in its response i.e., the inflation pressure can be changed to the required value almost instantaneously. However in reality, to achieve a near instantaneous system, large valves and high pressure difference between the air tank and tyres are required to allow sufficient air flow into the tyres, which poses a serious design challenge.

2 Literature Review

In this section, the contribution of tyres to the vehicle's overall fuel consumption is discussed. In this respect, different parameters that affect the rolling resistance (RR) of tyres are discussed, with a special focus on the role of tyre inflation pressure on the RR of the tyres. The influence of tyre pressure on parameters that affect vehicle handling behaviour and ride characteristics are also discussed.

There are several factors that contribute to the overall fuel consumption of a vehicle. In general, these factors may be broadly classified into the following categories:

- I. Energy loss from tyres,
- II. Aerodynamic drag losses,
- III. Vehicle inertia during acceleration or deceleration.

The main resistive forces acting on a vehicle and its tyres can be seen in [Figure 1](#). Energy losses also arise from the vehicle driveline components and auxiliary devices. However, this report will only shed light on the losses from the tyres and the affect it has on the overall fuel consumption of the vehicle. Some of the main parameters affecting RR are discussed in the sections below.

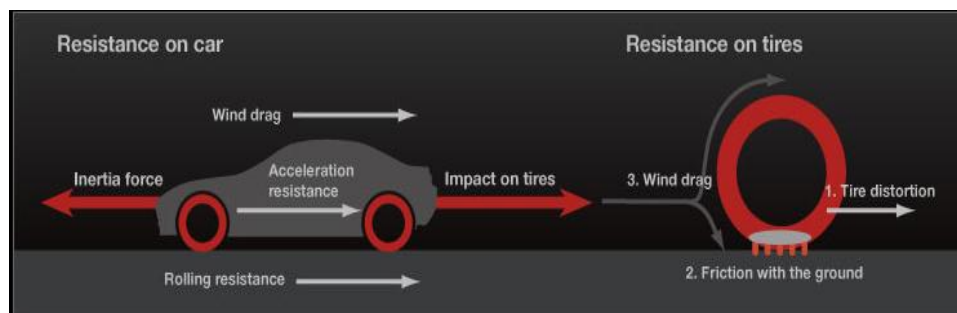


Figure 1: Resistive forces acting on the vehicle and tyre [32].

2.1 Contribution of the tyre rolling resistance to fuel consumption

Tyre rolling resistance is defined as the force required to maintain the forward movement of a loaded pneumatic tyre in a straight line, on a flat road, at a constant vehicle speed when no wind resistance is present [4]. The tyre losses may be attributed to three broadly classified mechanisms [5, 6]:

- I. Friction or scrubbing between tyre and roadway,
- II. Aerodynamic drag of the rolling wheels,
- III. Hysteretic losses of tyres due to cyclic stressing of the rubber compound.

Friction or scrubbing losses occur due to slippage at the tyre-road interface due to tangential forces and due to the difference in the Young's modulus and radii of curvature of rolling bodies in contact, resulting in shear tension and causing shear friction. However, scrubbing has low impact on the RR as it has been found to be hardly affected by lubrication of the surfaces in contact [6]. Though not much of the wheels are exposed in the direction of travel for a passenger car, the aerodynamic drag from the wheels can vary considerably based on the overall design of the tyre carcass and wheel hub. However, under normal operating conditions, majority of the tyre loss can be attributed to hysteresis of the tyre rubber element [5].

Rubber has both viscous and elastic response to deformation. The viscous response is proportional to the rate of deformation while the elastic response is proportional to the amount of deformation [7]. Hysteresis is an inherent property of all visco-elastic material where the material relaxation takes more time than material compression time.

Studies have shown that tyre RR has considerable impact on vehicle fuel efficiency. Fuel consumption improvements up to 4 % for urban driving and 7 % during highway driving have been estimated in theory. An estimation by Auto-industries and other sources show that for a 10 % reduction in RR, fuel efficiency could be improved up to 2 % [4]. The sub-sections below give an overview of the different parameters affecting the RR of tyres rolling on a smooth road surface.

2.1.1 Influence of temperature

The RR of tyres depend greatly on the temperature of tyre carcass. From data on tyres of different make it has been observed that a tyre reaches an equilibrium temperature in about 10 to 20 minutes of steady state operation [5]. Tiretrack.com [4], an organization specializing in the sale of wheels and tyres, performed a controlled experiment to see how the tyre temperature varied with time. Based on a 'Tyre Heating Cycle' experiment it was observed that the tyre pressure had increased consistently in the first 20 minutes by 1 psi (0.068 bar) every 5 minutes. After the first 20 minutes of the heating cycle the tyre temperature began to stabilize, resulting in only 1 psi increase in the next 20 minutes. Inflation pressure has a significant impact on the RR of tyres and is discussed in Section 2.1.5.

Thus analytical modelling of tyres for short trips should take into account this phenomenon for a more true representation while calculating fuel savings from RR reduction. The data from a survey in 1997 showed that 40 % to 50 % of the trips made by a vehicle in Sweden represents a short trip [8] (provided we define short trip as distance of 5 km to 6 km). Figure 2 shows the typical RR behaviour of a radial tyre whose temperature has been recorded over time, at constant speed. The tyre temperature reaches an equilibrium state when run in a steady state condition (highway-style driving) and consequently the RR reduces. However, in the case of

city-style driving the temperature fluctuates about a mean value. In other words, the RR of tyres with respect to fuel efficiency is dependent on the driving cycle used in simulations. Generally, the tyre is subjected to a heating cycle prior to actual RR measurements.

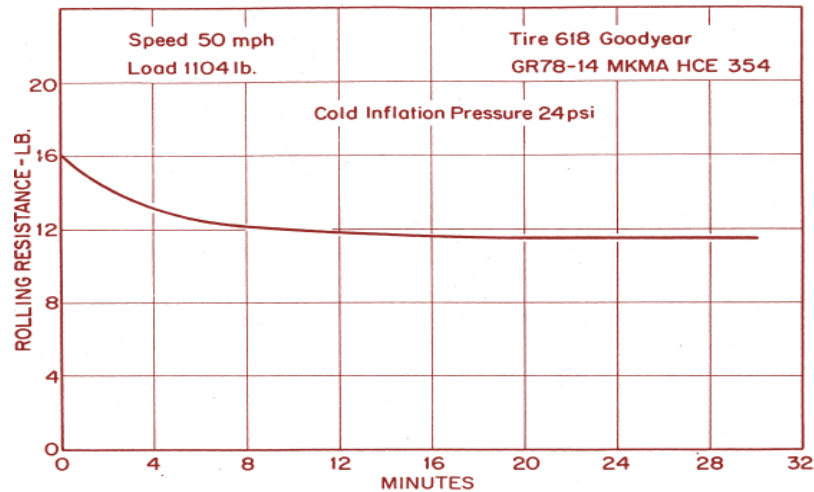


Figure 2: Influence of temperature on RR with passage of time [5].

This reduction of RR with temperature is caused by a combination of two actions; temperature sensitivity of hysteresis (i.e., hysteretic loss properties of most rubber compounds are temperature sensitive, being much higher at lower temperatures) and expansion of air inside the tyre due to increase in tyre temperature. As the tyre temperature increases, the pressure inside the tyre also increases thereby reducing the deflection and in turn lowering the loss due to hysteresis. Figure 3 shows the effect of temperature on hysteresis for a number of rubber compounds.

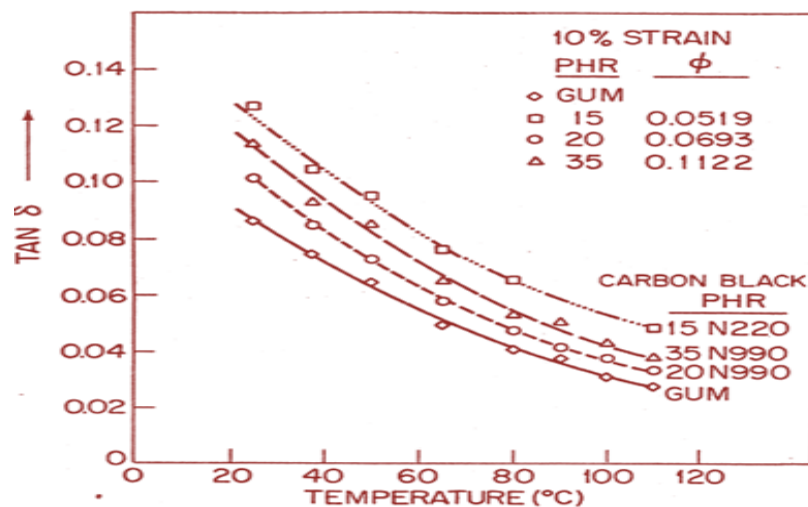


Figure 3: Effect of temperature on hysteresis [5].

Tan δ in Figure 3 is called the loss tangent (= loss elastic modulus/storage elastic modulus). It is a material property and is proportional to the hysteresis loss. From the figure it can be seen that the same decreasing trend holds true for all the compounds. A publication by Yokohama Rubber Co., Ltd has claimed that hysteresis of the tyre tread, among other tyre constituents, contributes to nearly 50 % of the total C_{RR} [9]. However, in this report the influence of temperature on RR will not be taken into account as it would require the study of rubber compounds used in each tyre, which vary from one manufacturer to the other. Instead it is assumed that the tyre is at its equilibrium temperature when estimating the fuel consumption.

2.1.2 Influence of load

Several interesting facts come to light when RR of a tyre is plotted against the vertical load at different temperatures. From Figure 4, it is seen that there is significant reduction in RR of the tyres five minutes after the start of rolling, with very little reduction to its equilibrium temperature after the five minutes mark. A linear relationship develops between load and RR as the operating temperature increases.

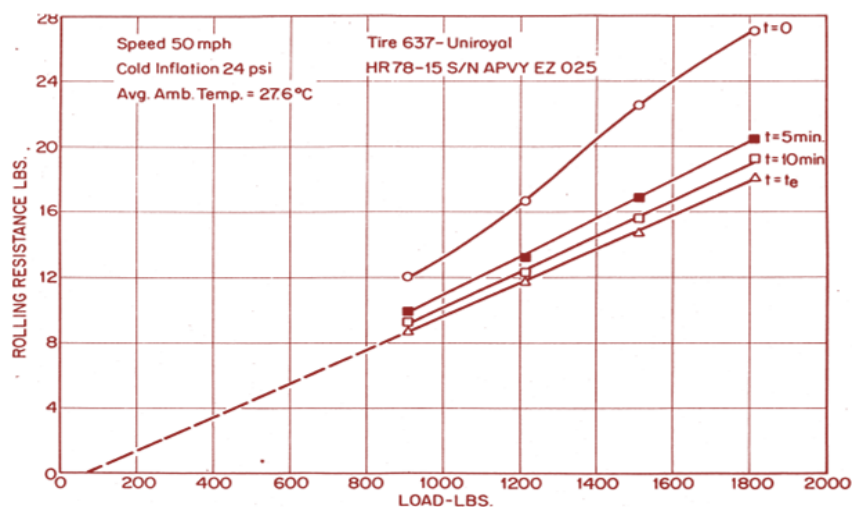


Figure 4: Rolling resistance versus vertical load [5].

In Figure 4, a backward extension of the curve (at equilibrium temperature, $t = t_e$) nearly intersects the origin, implying that the RR is nearly zero at zero load. This linear relationship of equilibrium RR versus load gives rise to the concept of coefficient of RR, C_{RR} . This trend is observed in all tyres and thus serves as a reliable parameter to compare the efficiency of tyres. It can be seen from Figure 5 that C_{RR} is nearly independent of load at equilibrium temperature.

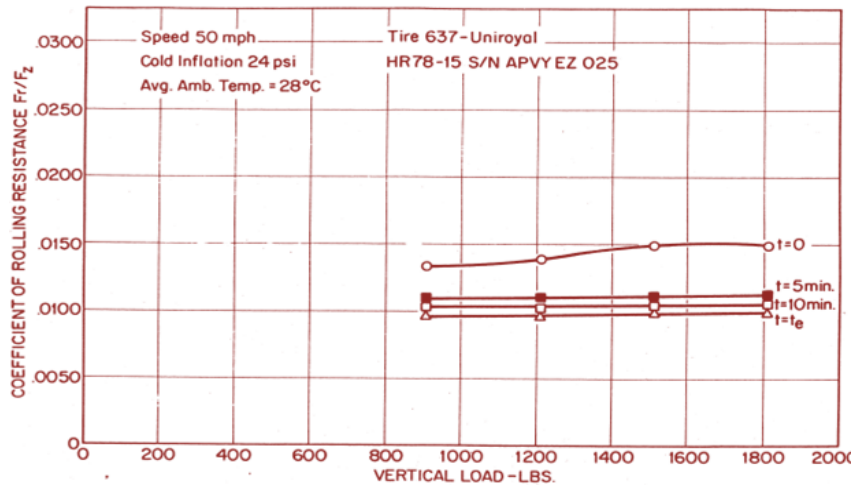


Figure 5: Coefficient of rolling resistance versus vertical load [5].

2.1.3 Influence of speed

Variation of RR with speed has been disputed several times in the past as there exists contradicting experimental data which are both for and against the claim that speed is a function of RR. A number of tests conducted have shown that there is not much influence of speed on RR at normal operating/legal speeds, though there is a tendency to increase at higher speeds [5]. Figure 6, shows the variation of RR with speed for a number of radial and bias-belted passenger car tyres.

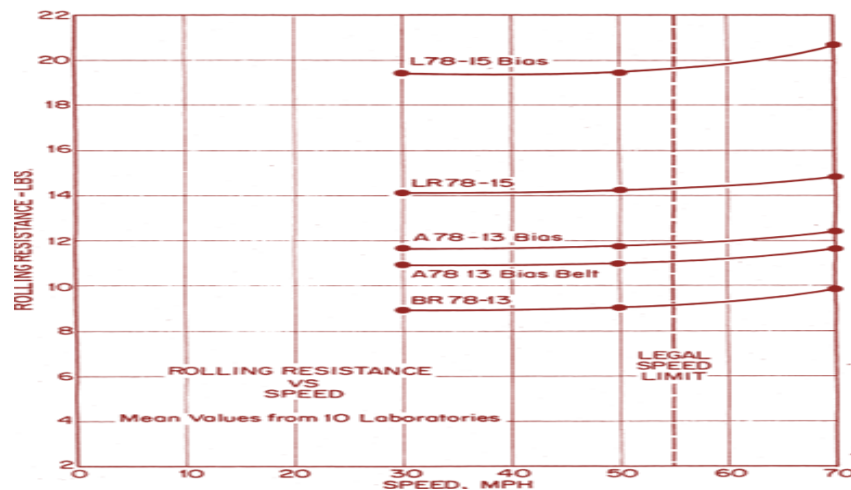


Figure 6: Rolling resistance versus speed [5].

It can be seen that the RR remains nearly constant up to speeds of 50 mph (80 km/h), beyond which there exists a non-linear trend. The tendency to increase with speed has been attributed to several reasons such as aerodynamic forces (which varies as the square of speed) and other dynamic tyre behaviour observed at higher speeds. Rubber, when vibrated, becomes stiffer with a dynamic modulus that is higher than static modulus [7]. In order to accurately estimate the fuel consumption, the influence of

speed on RR will be included in the fuel estimation simulation model developed for this thesis work.

2.1.4 Influence of size and construction of tyres

Larger tyres have been observed to have higher RR force but a lower RR coefficient C_{RR} , since the load carried by the larger tyre is also higher. This may also be due to the fact that the tyre tread can bend, stretch and recover more easily with increasing wheel diameter [4]. Regardless of the C_{RR} being smaller for larger tyres, the larger tyres require more effort to roll due to its physical characteristics. From experimental data on 65 different tyres of various sizes and constructions, the author of [5] observed that the RR force was lower for tyres with higher load rating, for a given vehicle. This tyre data was collected at the following parameters; tyre pressure, 1.65 bars; steady state speed, 80 km/h and vertical load, 80 % of the rated load. A summary of this study is presented in Figure 7.

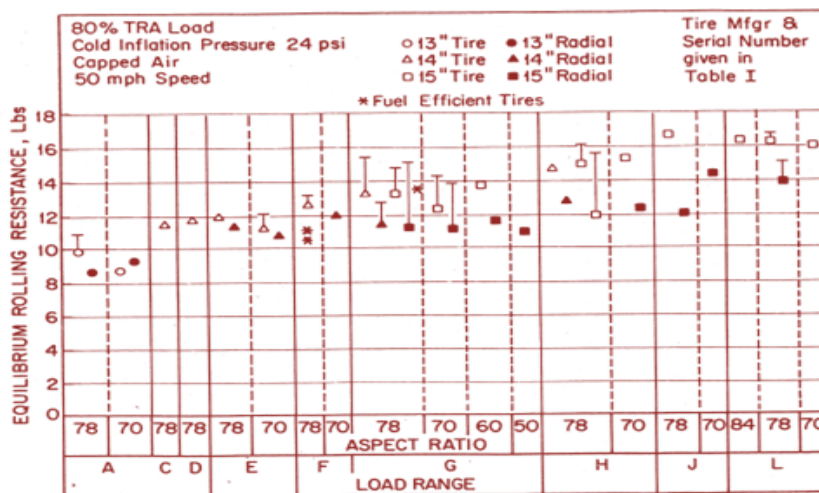


Figure 7: Equilibrium rolling resistance versus load rating for tyres of different size and construction [5].

Figure 7, shows the variation of equilibrium RR with load rating, increasing from left to the right, for a number of radial tyres and bias-ply tyres of different sizes. Based on the type of construction it has been observed that radial tyres roll more efficiently than bias-ply or bias-belted tyres of the same size and load rating [5]. Similarly the influence of aspect ratio on RR was also studied but no clear relations could be established. However, tyres with lower aspect ratio were observed to have lower RR from physical rolling considerations.

If RR is the only criterion in deciding a set of wheels for the vehicle then it's advisable to choose an oversize tyre and operate it in an under-load condition. This can be seen

from RR values in Figure 8, where the third column shows the operating load/Load Rating values for different tyres.

TIRE	MFR	LOAD / RATED LOAD	EQUILIBRIUM ROLLING RESISTANCE, lbs
C78-14	Goodyear 2P+2F/2P	840 / 1050	11.44
E78-14	Dunlop 2P+2F/2P	840 / 1190	10.03
F78-14	Dunlop 4P	840 / 1280	9.55
H78-14	Goodyear 2P+2F/2P	840 / 1510	9.63
GR78-15	Goodrich 2P+2S/2P	1104 / 1380	12.49
LR78-15	Goodrich 2P+2S/2P	1104 / 1680	11.97

Figure 8: Influence of tyre load on equilibrium rolling resistance based on tyre load rating [5].

2.1.5 Influence of tyre wear

When tyres wear, the volume of rubber in the tread reduces thereby reducing the hysteresis loss and in turn reducing the C_{RR} . Hence new tyres have slightly more RR than used tyres. A RR study carried out on two pairs of tyres, one pair fully worn while the other rarely used, it was seen that the worn-out tyre showed slightly lower equilibrium RR than the new tyre [5]. The findings are shown Figure 9.

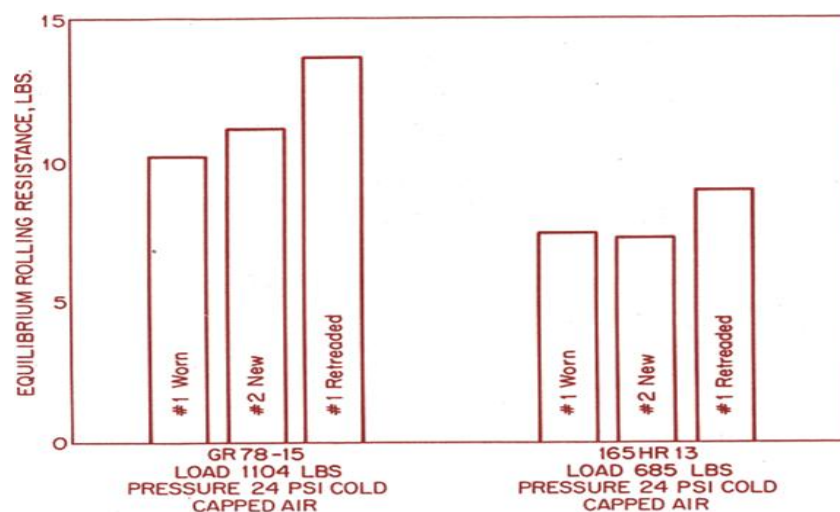


Figure 9: Equilibrium rolling resistance values for worn, new and re-treaded tyres [5].

Figure 9 also shows the difference in RR between new tyres and re-treated tyres. The worn out tyres when re-treaded showed considerably higher RR than the new tyres,

providing further proof of the contribution of tyre tread to hysteresis. However, this finding is not conclusive due to lack of data and the reduction of RR value between the worn tyres and re-treaded tyres bear no clear relation with regards to tread depth or pattern.

2.1.6 Influence of tyre pressure

It has been observed from data on several tyres that the RR varies nearly linearly with the reciprocal of tyre inflation pressure under steady-state conditions (i.e. constant load and speed) [5]. Figure 10, shows this near-linear behaviour especially as the tyre reaches T_e (equilibrium temperature).

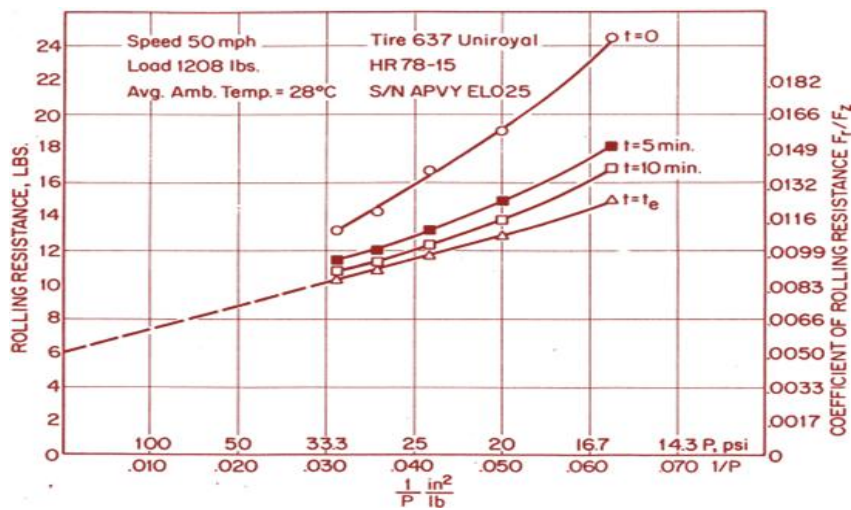


Figure 10: Rolling resistance and C_{RR} versus ($1/\text{pressure}$) [5].

Unlike the backward extrapolation of the RR versus load curve, the backward extrapolation of the above curve does not pass through zero RR. Thus, it can be concluded that there is still some RR even at very high tyre pressures. Figure 10 also shows that there exist no distinct relationship between load, pressure and initial RR under cold operating conditions.

2.2 Importance of having appropriate tyre pressure

The main motivation for properly inflated tyre is to distribute the vehicle load evenly across the tyre footprint thereby providing good contact with the road, passenger comfort, responsive handling and uniform tyre wear. It should be remembered that it is the air pressure inside the tyre that supports the weight of the vehicle. Two situations can arise with improperly inflated tyres namely, under-inflated and over-inflated.

In the case of under-inflated tyres, the tyre life could be reduced considerable if the tyre pressures is maintained low for long periods of time. Tyre manufacturers Michelin and Goodyear have claimed a reduction in tyre life of up to 30 % if tyres are operated 20 % below recommended pressure [10]. Tyre also bends and distorts more, resulting in over-heating and increased RR. In a test conducted by tiretrack.com [4], it was even found that the vehicle was a few seconds slower around a track on under-inflated tyres, with drivers reporting a detached feeling from the vehicle in the corners.

For the over-inflated case, the tyre could sustain damage when riding over road surface irregularities such as potholes and bumps. Passenger comfort is also marginally compromised. Increasing the tyre pressure results in a decrease in tyre-road contact area, resulting in slightly poorer traction and braking capabilities. Figure 11 shows typical tyre wear patterns observed for an under-inflated, recommended and over-inflated tyres. An under-inflated tyre tends to wear at the shoulders more than at the centre, since the pressure is not sufficient at the tyre centre to bear the load. For over-inflated tyres, the wear is severe along the centre due to bulging of the tyre structure at high pressures.



Figure 11: *Typical tyre wear patterns observed for different tyre inflation pressures [18].*

Proper tyre pressure becomes particularly important in wet weather conditions from a safety point of view. Tread depth, tyre footprint size and tread design play a vital role in determining the hydroplaning characteristics and wet traction performance of a tyre. From a series of test conducted by Michelin [4] it was concluded that the tyre pressure plays an important role in determining the tyre's contact patch surface area, especially at increasing vehicle speeds. Tests revealed that an under-inflated tyre would hydroplane at speeds lower than well inflated tyres for the same height of standing water.

Figure 12 a, shows a tyre properly inflated to 35 psi (2.41 bar) sitting in still water on a glass plate. Cameras placed beneath the glass plate capture the footprint size and shape. In the figure, the black area is where the tyre is pressed against the glass and the green area indicates the presence of water (dyed green). Figure 12 b, shows the same tyre being driven across the glass plate at 60 mph (96.5 km/h). If the glass plate were dry the footprint size would virtually be identical to that of the stationary tyre. However, since water is incompressible it must be evacuated from under the tyre sufficiently fast enough with a proper tread design and depth, to ensure proper road-tyre contact. From Figure 12 b it can be seen that the tyre footprint shows good contact with the surface although the contact area is slightly smaller compared to that in the stationary condition.

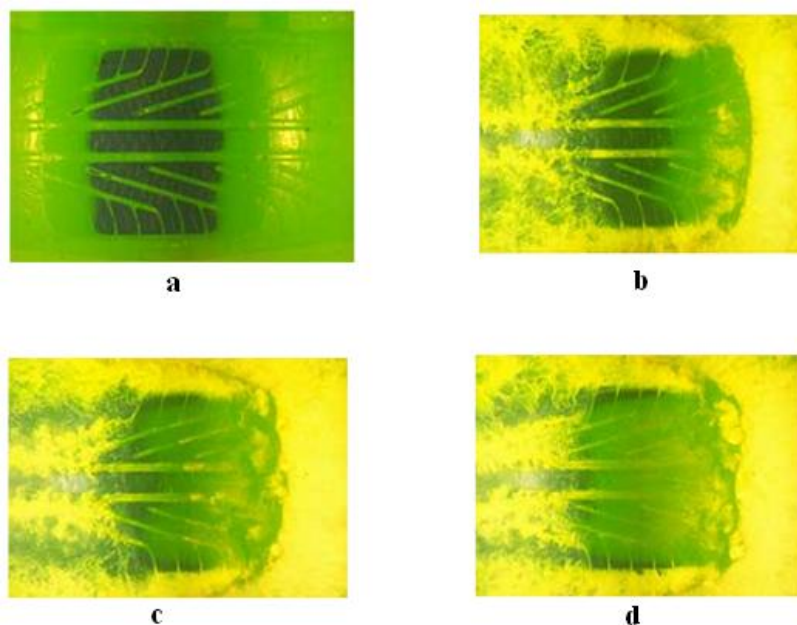


Figure 12: (a) Footprint of a stationary tyre in standing water at 35 PSI inflation pressure. Footprint of the same tyre rolling at 60 mph: (b) pressure - 35 PSI, (c) pressure- 30 PS, (d) pressure- 25 PSI [4]

Figure 12 c, shows the tyre at a pressure of 30 psi (2.07 bar). It is seen that the central portion of the contact patch has been lifted, forming a concave shape at the leading

edge of the tyre for the same test conditions. As a result the overall footprint of the tyre is now reduced considerably leaving only the shoulders in contact. The lack of sufficient inflation pressure has resulted in the collapse of the central part of tyre tread, trapping water rather than evacuating it through the tread. Figure 12 d, shows the same tyre, now at 25 psi (1.72 bar). The overall footprint has been reduced to contact at just the tyre shoulders, on the verge of whole tyre losing traction. Hence, even though the tread depth and design play a vital role in preventing hydroplaning, improper tyre pressure can render the role of tread design and tread depth completely useless.

2.3 Influence of tyre pressure on braking performance

Braking performance is a measure of how effective and stable a vehicle is under braking under both regular and emergency braking situations. A number of authors have concluded differently on the influence of tyre pressure as a function of braking distance or braking deceleration. Some authors have found in testing that 'dry peak traction' and available friction tended to decrease with a decrease in tyre pressure for radial tyres. In some cases, it was observed that the sliding friction was optimal around the nominal inflation pressure and slightly lower at pressures above and below this nominal value [12]. Gillespie [13], notes that peak and sliding friction coefficient are only mildly affected by tyre inflation pressure.

From a series of tests conducted by Marshek K. M. et al [12] on different vehicles, it was concluded that the ABS braking performance is optimum near the manufacturer recommended tyre pressure and slightly low both above and below this nominal pressure.

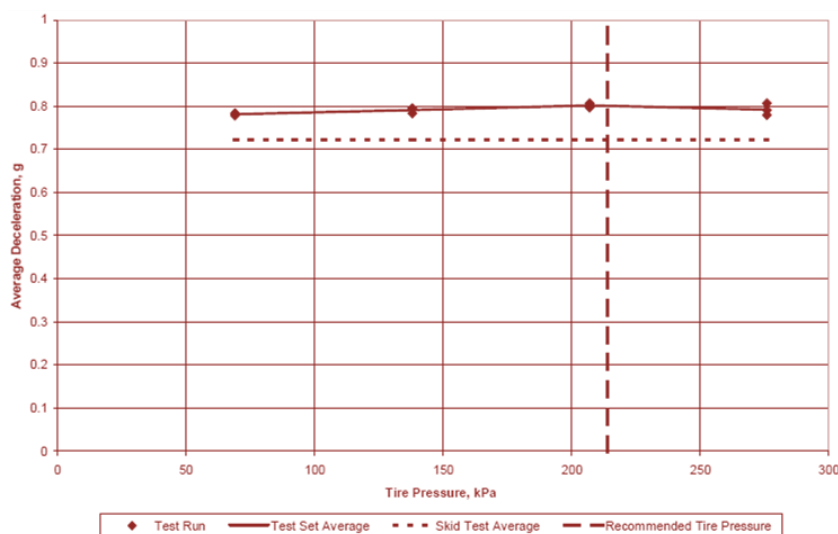


Figure 13: Vehicle braking deceleration versus tyre pressure [12].

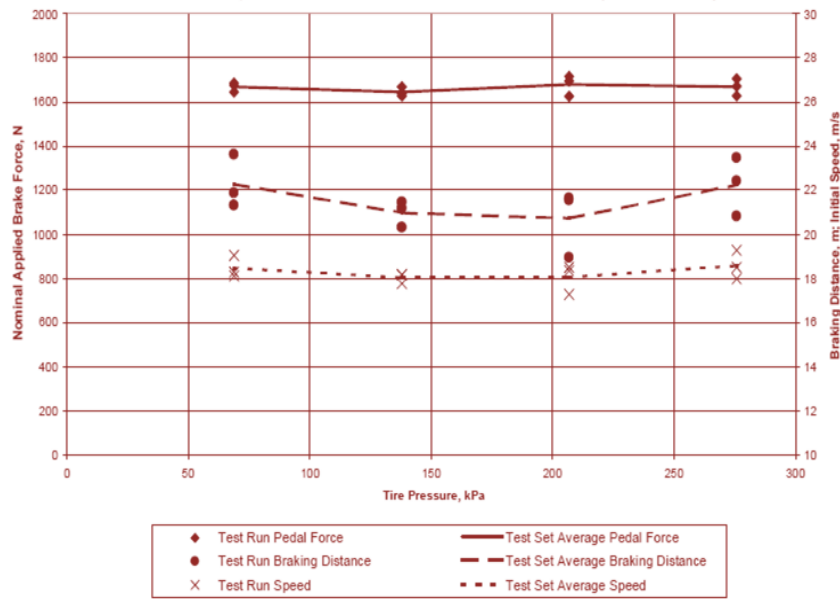


Figure 14: Brake pedal force, braking distance, initial speed versus tyre pressure [12].

Figure 13 and 14 show the results obtained from one of the vehicles, a 1989 Sterling 827SL limited edition, from the series of tests conducted by Kurt M. Marshek et al. In one of the tests, an emergency braking manoeuvre was performed to evaluate the braking distance and deceleration using an electro-pneumatic brake pedal application system, to eliminate the variation in the applied brake force in each test. Figure 13 shows the average deceleration recorded at different tyre pressures. It can be seen that the deceleration is slightly higher near the nominal pressure and lower for very low and high pressures. Ideally, it is best just below the nominal tyre pressure.

Figure 14 shows the applied brake force, initial velocity and corresponding stopping distance. Though it can be seen that the stopping distance is nearly 1 meter shorter near the nominal pressure, it may be attributed to other factors such as corresponding velocity being lower and force being higher (see Figure 14). A clear trend could not be established across all the vehicles tested [12]. Since the effects observed during emergency braking test were minimal and due time limitation on this thesis work, it did not warrant the need for a simulation model to further study this trend.

2.4 Influence of tyre pressure on vehicle handling

The overall stiffness of a tyre and its weight bearing capability is primarily decided by the air inside the tyre. Thus, the tyre inflation pressure can considerably affect the overall vehicle performance. This is clearly evident in racing applications where extreme care is taken to maintain appropriate air pressure in all the tyres since a trained driver is able to sense even the slightest variation in pressure, especially when driving at the limit. Thus, it is useful, and maybe even essential to capture the effects of tyre pressure in a tyre model for design and simulation purposes.

Traditionally, the lateral tyre characteristics were measured at fixed speeds and inflation pressures. This approach demanded a large number of tests and measurements to enable the study of tyre forces and moment characteristics across all operating parameters. Many of the tyre models developed over the years have either ignored the effects of tyre pressure in them or could not sufficiently validate the results obtained from it. The influence of tyre pressure on the three main handling parameters of tyres namely, longitudinal force F_x , lateral force F_y and aligning moment M_z , will be examined in the sections below.

2.4.1 Lateral force

Several authors [14, 15] have concluded that the lateral stability of a vehicle is largely governed by the tyre's cornering stiffness coefficient, C_α , which determines the lateral force characteristics of a tyre. In this section, the influence of tyre pressure on the tyre force and moment characteristics will be presented. Cornering stiffness is mathematically defined as follows, $C_\alpha = \frac{\partial F_y}{\partial \alpha}$ at $\alpha_{slip}=0$ [13, 15], i.e. the slope of the lateral force versus slip angle at zero slip angle.

Two clear trends emerge when studying the effect of air pressure on cornering stiffness. First, higher inflation pressure results in lower cornering stiffness at lower vertical loads on the tyre. This is clearly visible from Figure 15, which shows a typical relationship between inflation pressure and load, for a passenger car tyre. This behaviour can be explained by realizing that the tyre's overall stiffness increases with increase in air pressure thereby reducing the tyre deformation and in turn its contact patch length. A quick glimpse into the relationship between cornering stiffness and contact patch length in the Brush Tyre model also supports this explanation [6], see equation (1).

$$C_\alpha = \left(\frac{\partial F_y}{\partial \alpha}\right)_{\alpha=0} = 2 * c_{py} * a^2 \quad (1)$$

where, $2a$ is the contact patch length and c_{py} , the stiffness of the brush elements. It can be seen from the relation that a reduction in contact patch length results in lower cornering stiffness, C_α .

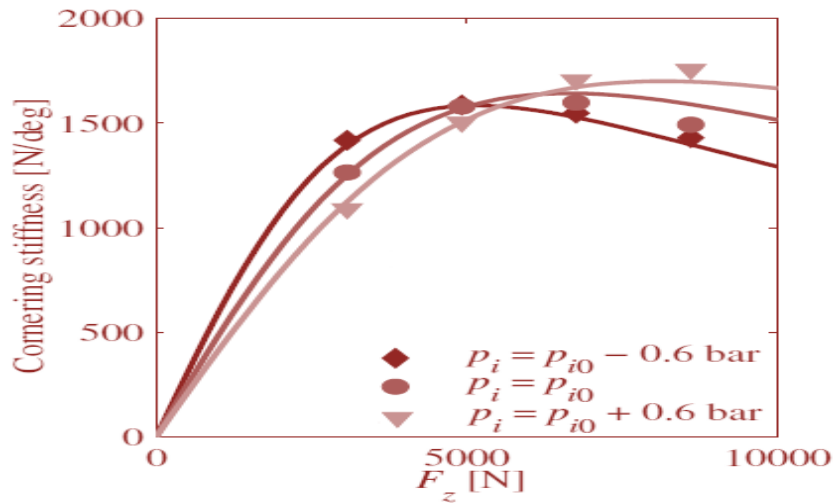


Figure 15: Effect of tyre pressure on cornering stiffness [31].

The second noticeable trend from Figure 15 is that the cornering stiffness is higher for high pressure tyres at higher vertical loads. The explanation provided earlier for the first trend breaks down at high vertical loads. At these loads, the tyre carcass stiffness and the inflation pressure dependency of the tyre belt stiffness play a prominent role in determining the overall cornering stiffness of the tyre [9].

2.4.2 Self-aligning moment

Experimental measurements have shown that an increase in tyre pressure results in a decrease in self-aligning moment. Figure 16 shows this trend for a typical passenger car radial tyre.

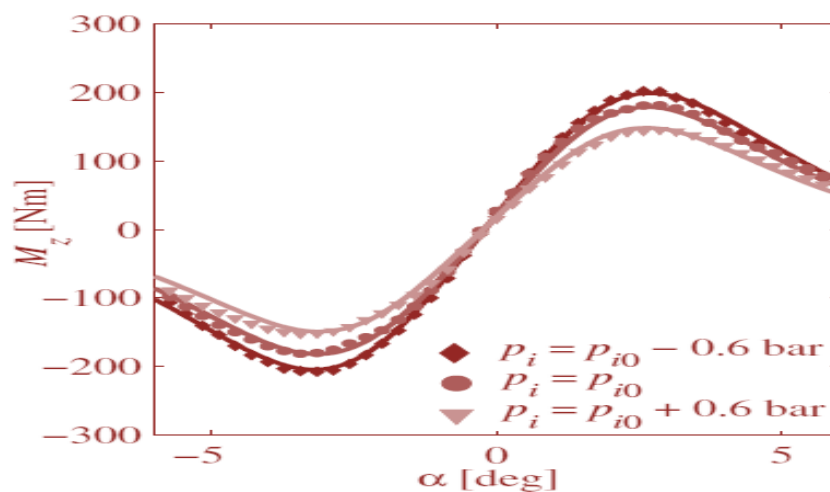


Figure 16: Effect of tyre pressure on self-aligning moment [31].

An increase in pressure results in an increase in the tyre stiffness (see also equation (2)), which in turn results in the decrease in the contact patch length. This decrease in contact length is accompanied by the decrease in the moment arm of the self-aligning moment, thereby exhibiting a lower peak value.

2.4.3 Longitudinal force

There is limited literature on the effects on inflation pressure on longitudinal force. However, a similarity in property has been observed between lateral slip curve and longitudinal slip curve. The longitudinal force is characterized by the longitudinal slip stiffness, κ . The longitudinal slip stiffness is mathematically defined as $C_\kappa = \left(\frac{\partial F_x}{\partial \kappa}\right)_{\kappa=0}$, similar to cornering stiffness. Direct measurements performed by the author of [9] on two tyres, gave conflicting results and no clear trend could be established.

Figure 17 and 18 show the results obtained for two tyres of the same brand but different sizes. It can be seen that the trends are completely inverted for the two tyres. A series of measurements carried out on different tyres using a tyre-test trailer at TNO's tyre-test facility showed that the larger tyres behaved more or less in a manner depicted by Figure 17. However, the smaller tyres showed an optimum value of slip stiffness for a particular pressure, above or below which the slip stiffness was lower. This finding can also be seen in the work by Marshek K. M. et al [12].

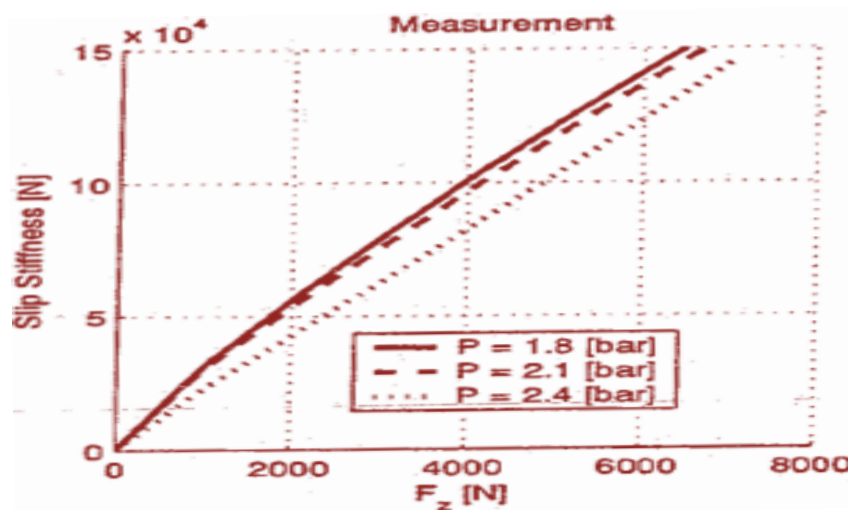


Figure 17: Effect of tyre pressure on longitudinal slip stiffness; Continental 225/55R16 [9].

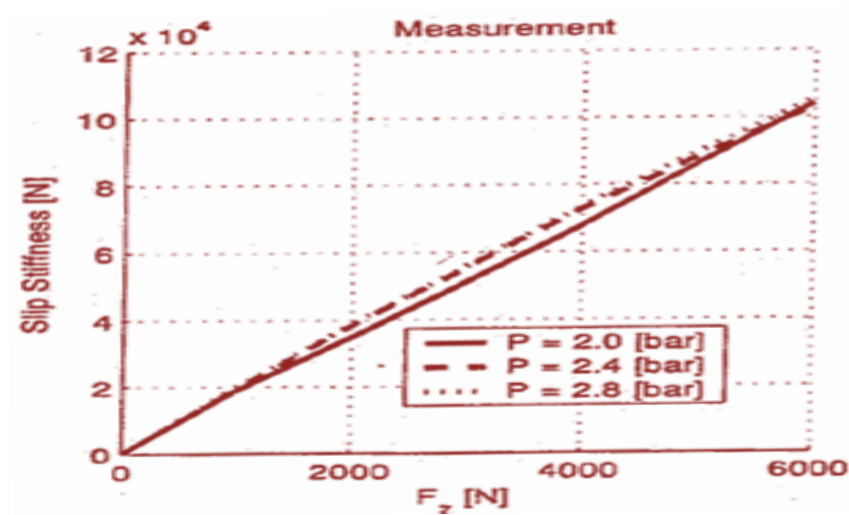


Figure 18: Effect of tyre pressure on longitudinal slip stiffness; Continental 155/70 R13 [9].

2.5 Influence of tyre pressure on vehicle ride characteristics

The primary objective of study of vehicle ride characteristics is to provide guiding principles for the effective control of vehicle body excitations and vibrations that cause passenger discomfort and/or vehicle components failure. The assessment of human response to vibration is a complex task and subjective in nature i.e., it depends on an individual's tolerance to such response. The human body in general responds to different vibration frequencies in different ways. At higher frequencies, the human body tissue act as suspension systems and effectively isolate the body and organs from vibrations. However, between 4 Hz and 8 Hz the organs of the body tend to resonate, thus causing most harmful effect [2, 16]. Below 1 Hz, passengers can experience motion sickness.

A vehicle is subjected to vibrations from a number of different sources. Some of the main sources are road surface irregularities, engine and driveline vibrations, aerodynamic forces and mass imbalances in the rotating components. In this report only the low frequency road surface excitations will be considered and the other sources of vibration and noise will be excluded. The vertical tyre stiffness of a tyre is influenced by several parameters such as inflation pressure, normal load, speed, camber angle etc. The tyre design parameters such as tread pattern, tread depth, number of plies, materials used in plies and crown angle also affect the overall tyre stiffness. However, keeping design and construction unchanged, the parameters of interest then become the inflation pressure, normal load and speed.

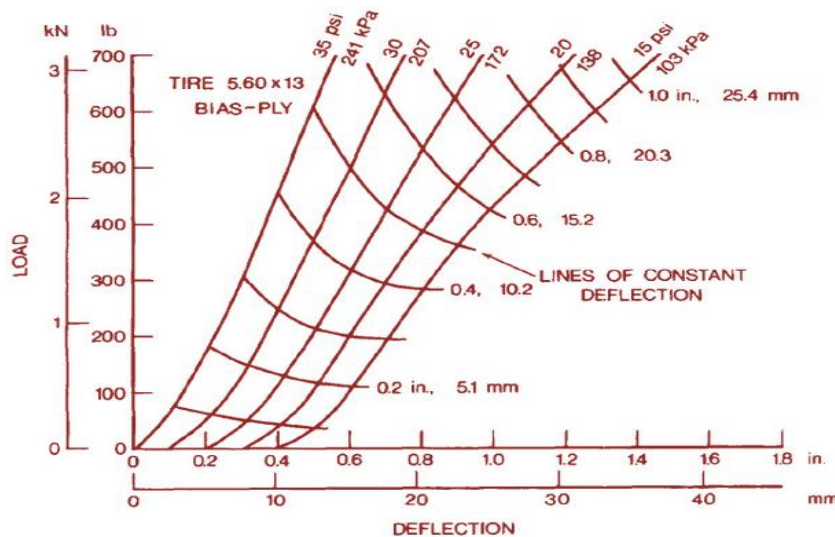


Figure 19: Static Load-Deflection relationship for a radial tyre [7].

Figure 19, for example, shows the relationship between tyre inflation pressure, static load and corresponding tyre deflection for a radial tyre [15]. This is a lattice plot in which the origin of load deflection curve is shifted along the x-axis in proportion to

inflation pressure. Not much validated literature is available on the influence of tyre pressure on the operating and design parameters of the tyre. In order to study the influence of tyre pressure on vehicle ride characteristics, a mathematical vehicle model is developed in the Matlab/Simulink[®] interface. The relation between inflation pressure and vertical tyre stiffness will be mathematically modelled using a semi-empirical relationship developed by TNO, Netherlands in collaboration with and TU-Delft University of Technology, Netherlands. The relationship is given by the equation (2).

$$K = (1 + P_{Fz1} dp_i) * K_0 \quad (2)$$

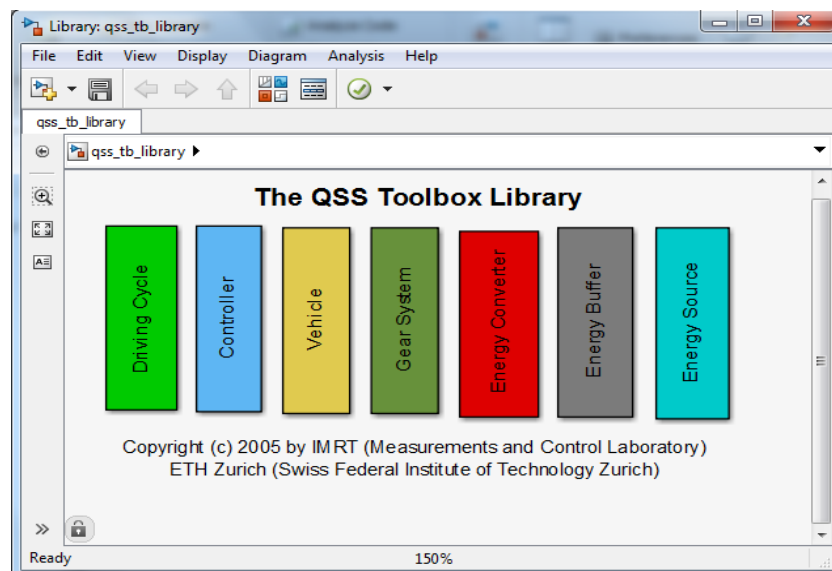
K_0 is the tyre stiffness at nominal inflation pressure, p_0 . P_{Fz1} is an empirical constant which accounts for the effect of inflation pressure on tyre vertical stiffness. dp_i is a non-dimensional pressure increment variable, mathematically defined as $\frac{p_i - p_0}{p_0}$. p_i is the tyre inflation pressure of interest. The effect of pressure on the vertical damping of the tyre is not included due to lack of data on this subject. Since the tyre damping is several orders lower than the damping of the suspension system, it may be neglected without much loss in accuracy. Equation (2), has been used in the extensively validated MF-Tyre/MF-Swift tyre model to define the vertical stiffness of the tyre and is thus a reliable relationship. Once a vehicle model is built, it will be subjected to a number of inputs to analyse the changes in vehicle response with corresponding change in inflation pressures.

3 Modelling and simulation

This section presents the methodology and tools used to build mathematical vehicle models capable of capturing and representing the influence of tyre inflation pressure on the fuel consumption, lateral handling and vertical ride characteristics of the vehicle. Three vehicle models, one each for fuel consumption, lateral handling and vertical ride comfort, are built in the Matlab/Simulink[®] interface. This section also reviews different tyre models which accounts for the effects of inflation pressure on these parameters.

3.1 Fuel estimation

A complete vehicle model based on the specifications of a medium sized passenger car is developed in Simulink[®] using the Quasi-Static Simulation Toolbox[™] library (QSS TB). The QSS TB, developed by ETH Zürich for educational research purposes, permits fast and simple estimation of fuel consumption for different power-train configurations. The toolbox library has build in models of different vehicle's components such as engines, transmissions, motors, batteries etc, with which it is possible to build a complete vehicle, both conventional Internal Combustion (IC) engine vehicles or hybrid vehicles. Figure 21 (a) shows a snapshot of this toolbox in the Simulink[®] interface.



(a)

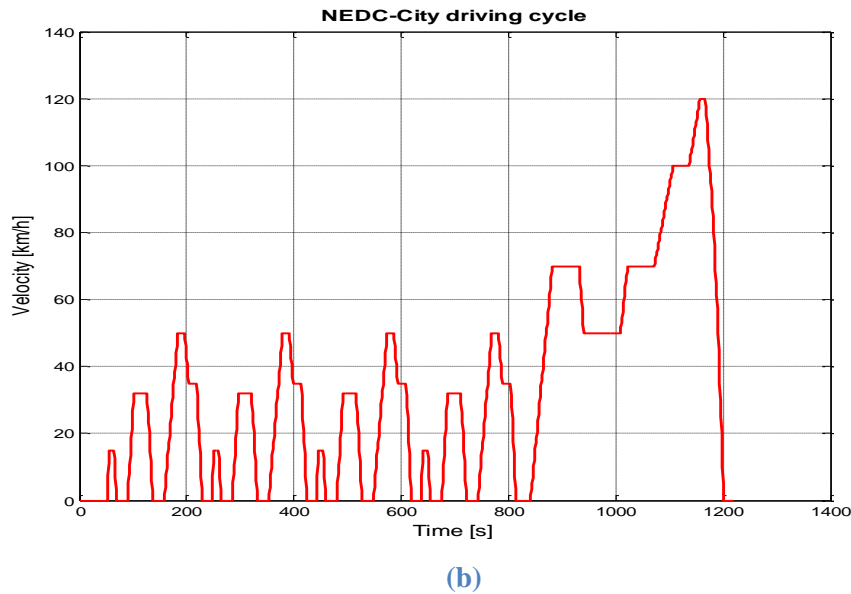


Figure 20: (a) QSS toolbox in the Matlab/Simulink® interface; (b) NEDC city driving cycle velocity profile.

For this thesis work, the model of a simple IC engine vehicle with the specifications shown in Table 10 (in Appendix I) was built. This model is capable of predicting the fuel consumption for a given driving cycle, based on a number of vehicle inputs, including tyre pressure. However, due to lack of tyre data the vehicle model only gives results for tyre pressure inputs between 2 and 3 bars. This model does not account for the losses in the tyres due to tyre slippage. Only the losses due to RR forces are modelled.

This model is simulated for a NEDC city cycle and the fuel consumption of the vehicle is estimated in L/100 km. The NEDC cycle is supposed to represent the driving scenario present in a typical urban environment with a number of vehicle starts and stops [21]. Figure 20 (b) shows the velocity profile for an NEDC city cycle.

3.1.1 Mathematical modelling approach

Dynamic systems can be modelled in different ways based on the parameters of interest. The QSS TB used in developing the complete vehicle model uses, as its name suggests, a quasi-static approach of modelling a dynamic system. Traditionally, dynamic systems are modelled such that the speed and acceleration of a system are calculated from forces acting on the system. However in the quasi-static approach, the forces acting on the system are calculated from the speed and acceleration of the system i.e., the cause and effect relationships are reversed. For the sake of clarity, consider one of the equations used in Section 3.2.3.

The system

$$M * a_y = F_{yL2} + F_{yR2} + (F_{yL1} + F_{yR1}) \cos(\delta) + (F_{xL1} + F_{xR1}) \sin(\delta)$$

In the traditional approach

Cause: Forces. F_{yL2} , F_{yR2} , F_{yL1} , F_{yR1} , F_{xL1} , and F_{xR1} .

Effect: Acceleration. a_y .

In the quasi-static approach

Cause: Acceleration, a_y .

Effect: Forces, F_{yL2} , F_{yR2} , F_{yL1} , F_{yR1} , F_{xL1} , and F_{xR1} .

In this toolbox, the RR force of tyre is analytically defined using the conventional linear relationship between load and RR force i.e., $F_{RR} = C_{RR} * \text{Load}$. This relationship is independent of factors such as tyre speed and pressure, which becomes particularly important when the fuel estimations are made for driving cycles with velocity profiles ranging up to speeds of 120 km/h. In the next sub section a few tyre RR models that captures the influence of tyre inflation pressure are presented.

3.1.2 Rolling resistance models

Several RR tyre models were investigated for the purpose of estimating the contribution of RR to fuel consumption in the vehicle. From the literature survey described in Section 2.1 and 2.2, we see that a number of parameters such as load, speed, tyre pressure, temperature, size, construction, tyre wear and road roughness together influence the overall RR of tyres. Among these parameters only the load, tyre pressure and speed show common trends across different tyre manufacturers. Hence, only these properties will be considered for modelling the RR of a tyres in the complete vehicle model. Although temperature shows a consistent trend and plays a crucial role in determining the tyre's RR it will not be considered as this parameter is difficult to control in real driving scenarios.

References [6, 17] show some mechanical models of RR which are used primarily when there is large variation in the road surface texture and its hardness. With regards to the QSS full vehicle model, the stiffness of the road is assumed to be much greater than that of the tyre i.e., the road surface is non-deformable. Since the focus of this report is on the influence of tyre pressure on fuel consumption, three semi-empirical RR models that account for tyre pressure are discussed below. These models are described by equations (3), (4) and (5). Here on out these models will be referred to as Model 1, Model 2 and Model 3, respectively.

Model 1, accounts for the influence of load and pressure on the RR force. Using this model, the tyre RR can be estimated at different loads and pressures based on RR data measured at some fixed number of points [5]. In the measurement procedure, one parameter (load or pressure) is held fixed while the other is varied. The empirical relation is given as follows:

$$F_{RR} = F_{R0} + K_L * (F_Z + F_{Z0}) + K_P * \left(\frac{1}{p_i} + \frac{1}{p_0}\right) \quad (3)$$

where, F_{RR} is the tyre RR force at a load F_Z and pressure p_i . F_{R0} is the tyre RR force at reference load F_{Z0} and reference pressure p_0 . K_L is slope of load dependency of F_{RR} at a fixed pressure, p_0 . K_P is the slope of reciprocal pressure ($1/p$) dependency of F_{RR} at fixed load, F_{Z0} . When the load dependency and pressure dependency of the RR is plotted together, we get a carpet plot as shown in Figure 21.

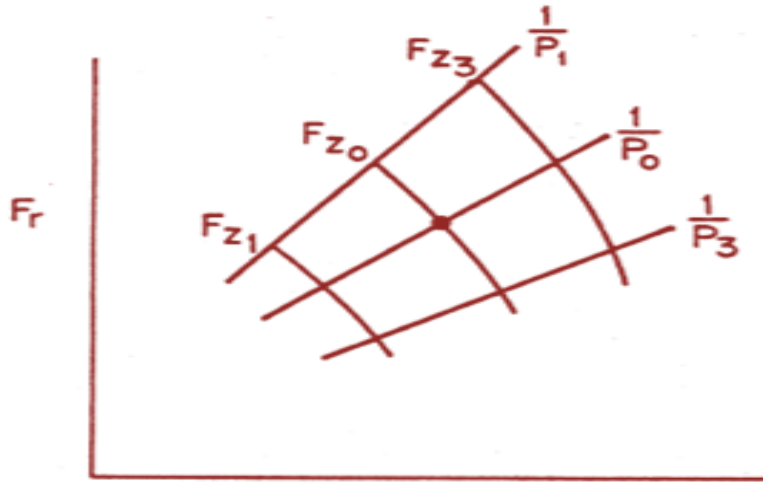


Figure 21: Load and pressure dependency of rolling resistance [5].

Model 2 is also based on the load and pressure dependency of RR. However, this model does not require as much pre-calculated data as Model 1 for the prediction of RR. It is given by the following empirical formula, equation (4) [5];

$$F_{RR} = F_{R0} * \left(\frac{F_Z}{F_{Z0}}\right) * \left(c_P * \frac{p_0}{p} + c_T\right) \quad (4)$$

where, $c_P + c_T = 1$ and c_T, c_P are constants obtained from the regression analysis of measured data. Model 2 is able to predict the RR at any given pressure and load provided there is data on F_{R0} and the value of c_P or c_T .

Model 3 [3, 18, 19] accounts for the influence of load, inflation pressure and speed on the RR of tyres. This Model is used in conjunction with the SAE J2452 coast-down procedure [19], where the RR of the tyre is measured at some predetermined speeds while the tyre speed is varied from a speed of 110 km/h to 15 km/h. Figure 22 shows this coast-down procedure as defined by SAE J2453 methodology.

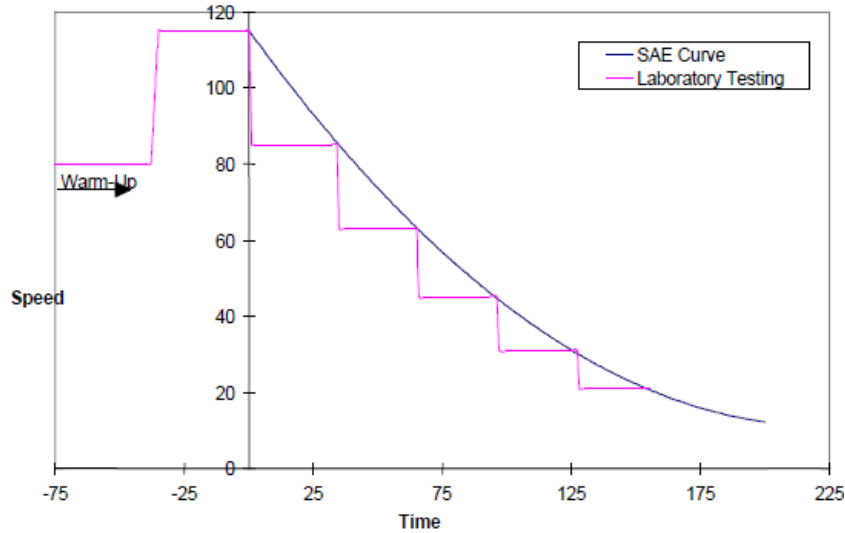


Figure 22: Theoretical and practical step-wise coast-down procedure [19].

The blue curve indicates the SAE coast-down curve. However, the test is conducted in step-wise manner in order to allow the system to stabilize before measurements are taken at the speeds of interest. The coast-down is performed in both the forward and reverse directions and the results are averaged. The results of the coast-down are then fitted to Model 3, given by the equation (5).

$$F_{RR} = P^{\alpha} * F_Z^{\beta} * (a + b * v + c * v^2) \quad (5)$$

where, v is the coast-down velocity and α, β, a, b and c are constants that are dependent on the pressure, P and load, F_Z of the tyres. The values of these constants are obtained by performing regression analysis on the RR data obtained from the coast-down procedure. This model has been validated for several tyres of different sizes, across different manufacturers [18].

In the SAE J2452 coast-down methodology, the RR is measured on a test drum (see Figure 23) which imposes a curvature to the tyre at its contact patch, resulting in higher deformation than observed on a flat surface. This higher deformation results in higher measured values of RR due to hysteretic losses. Clark S. K. and Dodge R.N [5] suggested a correction factor to the RR data obtained from drum measurements i.e.;

$$F_{RR(drum)} = F_{RR} * \sqrt{1 + \frac{R_{tyre}}{R_{drum}}} \quad (6)$$

The validity of equation (6) has been demonstrated for a number of passenger car and truck tyres. However, this correction factor must be applied with caution as it only weakly based of fundamental mechanics [19]. According to Barrant J. and Boker J.

[20], the surface of test drum used for measurement has either smooth steel or 80-grit 3 Mite coated paper which does not match the macro roughness of roads and thus tend to underestimate the actual RR force exerted on the tyres. Thus, the effect of the drum curvature and drum surface texture cancel out each other to closely relate the measured RR data to that observed on a real roads [20].

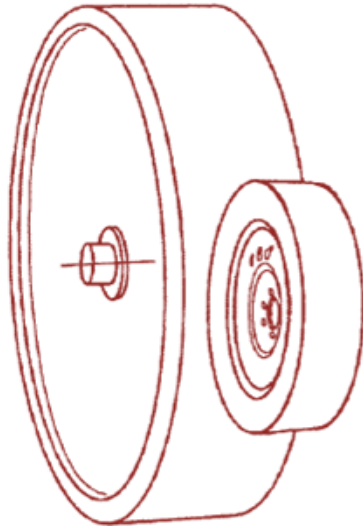


Figure 23: Schematic of a wheel on a test drum to measure its rolling resistance [19].

The three RR models presented in this section capture the influence of inflation pressure on RR force satisfactorily. However, Model 3 accounts for the change in RR with vehicle speed, which not only provides better accuracy in predicting the RR force but also improves the accuracy of fuel estimation, especially for a driving cycle with a velocity profile. Thus, Model 3 was adopted for developing the complete vehicle QSS model in this report.

Since Model 3 has been validated extensively, it is insufficient to simply rank tyres based on the traditional approach of comparing their C_{RR} , which is measured using the older SAE J1269 methodology [19]. Thus, a parameter called Mean Equivalent Rolling Resistance (MERF) will be used to compare the RR of tyres for a particular tyre and driving cycle combination [3, 18, 19]. Rather than directly using the RR versus speed and pressure curves for comparison of the tyres, MERF will provide a convenient means for easy comparison of RR values for a given driving cycle. MERF is defined as the average of RR values of all the individual speeds-time point in a driving cycle. Mathematically, it is defined by equation (7).

$$MERF_{cycle} = \frac{\int_{t_0}^{t_f} F_{RR} * dt}{\int_{t_0}^{t_f} dt} \quad (7)$$

where, $MERF_{cycle}$ is the Mean Equivalent Rolling Force for a driving cycle, F_{RR} is rolling resistance force given by Model 3 and t_0 , t_f are cycle start time and end time, respectively.

For a fixed load and tyre pressure, equation (7) can be simplified using standard numerical integration method to equation (8).

$$MERF_{cycle} = \frac{P^\alpha * Z^\beta * (a * t_f + b * \sum_{i=1}^f V + c * \sum_{i=1}^f V^2)}{t_f} \quad (8)$$

It should be remembered that equation (8) is dependent on the driving cycle used. That is, the MERF value for NEDC city driving cycle will be different from the value obtained for EPA city driving cycle (a standard cycle used in the North American market). Also, the comparison between tyres should be done under the same test reference conditions of load and pressure. The adoption of Model 3 to describe RR will benefit vehicle manufacturers in developing accurate vehicle models to meet the increasingly stringent EU pollution norms in a reliable manner.

3.1.3 QSS vehicle model

Using the QSS TBTM library, a simple model of a medium sized passenger car, Saab 9-3, was built in the Simulink® interface. The data for this vehicle was obtained from the division of Vehicle Dynamics at the department of Applied Mechanics at Chalmers University of Technology. The complete list of the vehicle parameters are shown in Table 10 in Appendix I. Due to lack of detailed engine data (engine load map), a simple engine model was used when building the QSS vehicle model.

In this simple engine model only its internal thermodynamic efficiency could be changed. Thus, the engine model had to be calibrated to closely represent the fuel efficiency of the real vehicle. The following methodology was used. First, the tyre pressure was adjusted to the manufacturer recommended pressure of 2.2 bars. Then the model was simulated over a NEDC city driving cycle to obtain its fuel consumption in litres/100 km. This value was then compared against the average mileage reported by owners of the same vehicle. The internal thermal efficiency of the engine was then changed within acceptable limits to match the fuel consumption of a real vehicle. Some of the key parameters are shown below in Table 1. Figure 24, shows a snapshot of the model created in Simulink® using QSS TB™.

Table 1: Main vehicle parameters; Saab 9-3 (2003).

<i>Engine specifications</i>	4-cylinder, 2-Litre Turbo.
<i>Maximum torque [Nm]</i>	265 @ 2500-4000 RPM
<i>Maximum power [hp]</i>	175 @ 5500 RPM
<i>Curb weight [Kg]</i>	1675
<i>Wheelbase [m]</i>	2.675
<i>COG to front axle [m]</i>	1.150
<i>COG to rear axle [m]</i>	1.525
<i>Aerodynamic drag coefficient [-]</i>	0.29
<i>Rolling resistance coefficient [-]</i>	0.0089
<i>Gear ratios [1st-5th, Differential]</i>	[3.385,176,1.179,0.894,0.66,4.05]

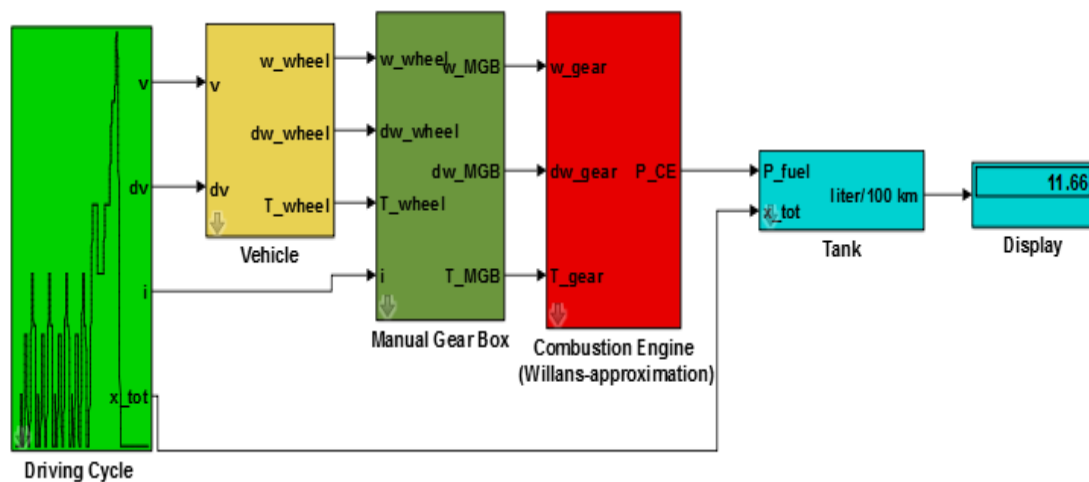


Figure 24: QSS vehicle model showing a fuel consumption in L/100 km at nominal tyre pressure of 2.2 bar.

In Figure 24, the NEDC 'Driving Cycle' block (green) passes the velocity v and acceleration dv data to the 'Vehicle' block (yellow). In the 'Vehicle' block the overall resistance forces (shown in Figure 1 in Section 2.1) acting on the vehicle is calculated and converted to required torque at the wheel centre. This block then passes the angular velocity ω , angular acceleration, $d\omega$ and torque at the wheels T_wheel to the 'Manual Gear Box' block (dark green). The 'Manual Gear Box' block in turn calculates the angular velocity ω_MGB , angular acceleration $d\omega_MGB$ and torque, T_MGB at

the crank shaft of the engine based on the gear selection data provided by the driving cycle block, at different speeds. These values are then passed on the 'Combustion Engine' block (red), which is an engine model that uses Willians approximation to provide realistic simplifications to engine torque and efficiency characteristics [21].

The friction losses in this engine block are modelled using ETH Zürich's own semi-empirical friction model that accounts for a losses in the bearings due to addition of supercharger or turbochargers and also losses due to coolant and oil pumps [21]. The 'Combustion Engine' block then calculates the mechanical power required from the torque and speed at the crank shaft and in turn calculates the total power obtained from combustion of gasoline by dividing the engine power by the engine internal thermodynamic efficiency coefficient. This value is then passed on to the 'Tank' block (cyan) where the fuel consumption is calculated from the total distance travelled, x_{tot} and displayed in litre/100km.

In the original 'Vehicle' block in the QSS library, the RR force is calculated using the simple linear relationship between RR and load, involving the coefficient of RR, C_{RR} . However, for the model used in this report, the MERF values described in Section 3.1.2 have been used. RR data has been borrowed from the results presented in reference [3]. Figure 25 shows data of a radial tyre P195/70R14 90S, used for this modelling.

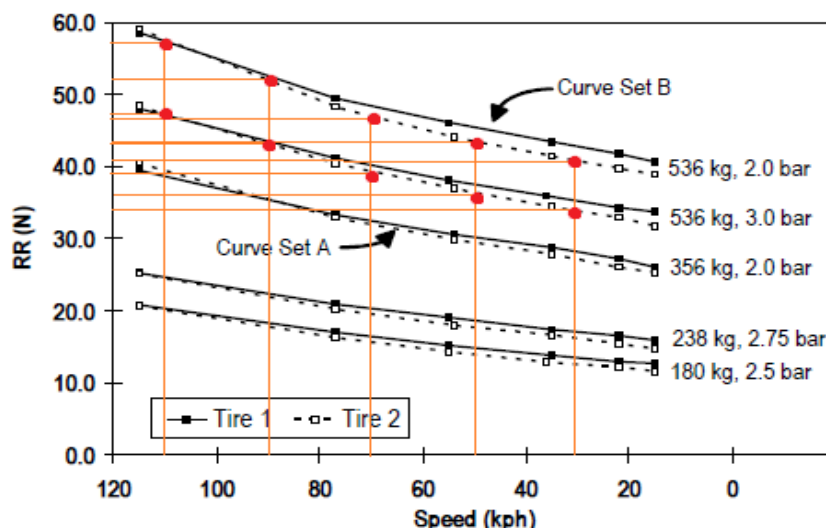


Figure 25: Rolling resistance force as a function of velocity, load and pressure,; P195/70R14 90S tyre [3].

From Figure 25, a number of data points were selected for the top two curves of Tyre 2, which were tested for the same load but at pressures of 2 bar and 3 bar. With this limited data, a linear interpolation was done between the 2 bar and 3 bar curves for a number of pressures to estimate the values of RR as shown in Figure 26.

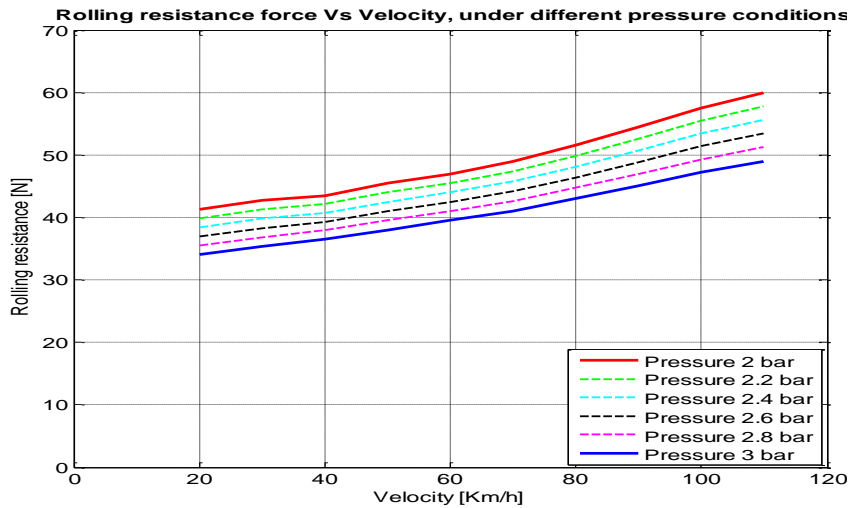


Figure 26: Rolling resistance as a function of velocity and pressure at 536 kg load.

Using the values from Figure 26, a non-linear regression was carried out to fit the data to equation (5) (Model 3) to determine the constants of regression, α , β , a , b and c . Figure 27 below shows the results of curve fit to the experimental data.

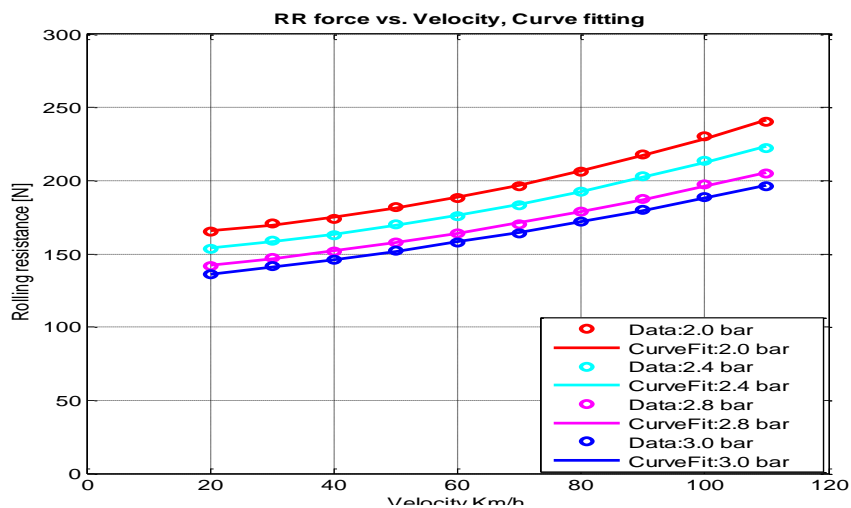


Figure 27: Results of curve-fit to the experimental data.

Once the constants of regression were determined, the MERF values were calculated at each pressure-load combination for the NEDC city driving cycle. These values are then used in the 'Vehicle' block of the QSS model to define the RR force. Also, as mentioned earlier, the RR data was borrowed from reference [3], where the size of the tyre is slightly smaller in dimension compared to the standard tyre recommended for our medium sized passenger vehicle. However, a justified compensation factor was applied to the MERF value to compensate for the size difference, based on the finding from literature review, particularly from [5, 3, 18, 19].

3.2 Vehicle lateral handling characteristics

Vehicle handling, in general, refers to the driver's perception of a vehicle's response to inputs such as steering, acceleration or braking. This term is objective in nature and can vary from one driver to another, making it difficult to quantify. In this thesis work the physical response of the vehicle to lateral forces will be referred to as vehicle handling. No scientific approach is presented to study the vehicle's behaviour from the driver's perspective. However, few inferences and suggestions are made in the Results and Discussion section (Section 4.2) to help visualize the results to some degree.

This section presents the development of a two-track vehicle model to study the influence of tyre pressure on the handling characteristics of the vehicle. The reliability of results obtained from a vehicle model is only as reliable as the tyre model used in it to define the tyre forces and moments. In this respect, the tyre is one of the most important components in a vehicle, which through its interaction with the road generates forces and moments required to manoeuvre a vehicle. Hence, two tyre models which incorporate the influence of inflation pressure in it are also discussed in this section.

3.2.1 Modelling approach

The analysis of vehicle cornering behaviour can be broadly classified into three approaches; low speed cornering, steady-state cornering and transient cornering. In low speed cornering approach, the inertial effects of the vehicle in motion is neglected as the vehicle speed is very low. The tyres do not develop a slip angle and are oriented perpendicular to the turn radius as shown by a simple bi-cycle model in Figure 28 a. Steady-state or quasi-steady state cornering refers to a turning situation where the vehicle is travelling at constant velocity or with low longitudinal accelerations (acceleration $< \pm 0.5 \text{ m/s}^2$). Due to the higher speeds, vehicle inertial effects must be included in the analysis of vehicle response to steering input. Figure 28 b shows a bi-cycle model of a vehicle in steady state turning manoeuvre.

Transient cornering approach is similar to steady-state cornering except now the longitudinal forces acting on the system are also included. The resultant acceleration acting on the vehicle is not in the radial direction and thus it needs to be treated with care when resolving the equations of motion. In order to effectively evaluate the influence of a dynamic TPRS on the lateral response performance of the vehicle, the transient cornering approach will be used. Figure 36 in Section 3.2.3 shows a two-track model of a vehicle in transient cornering.

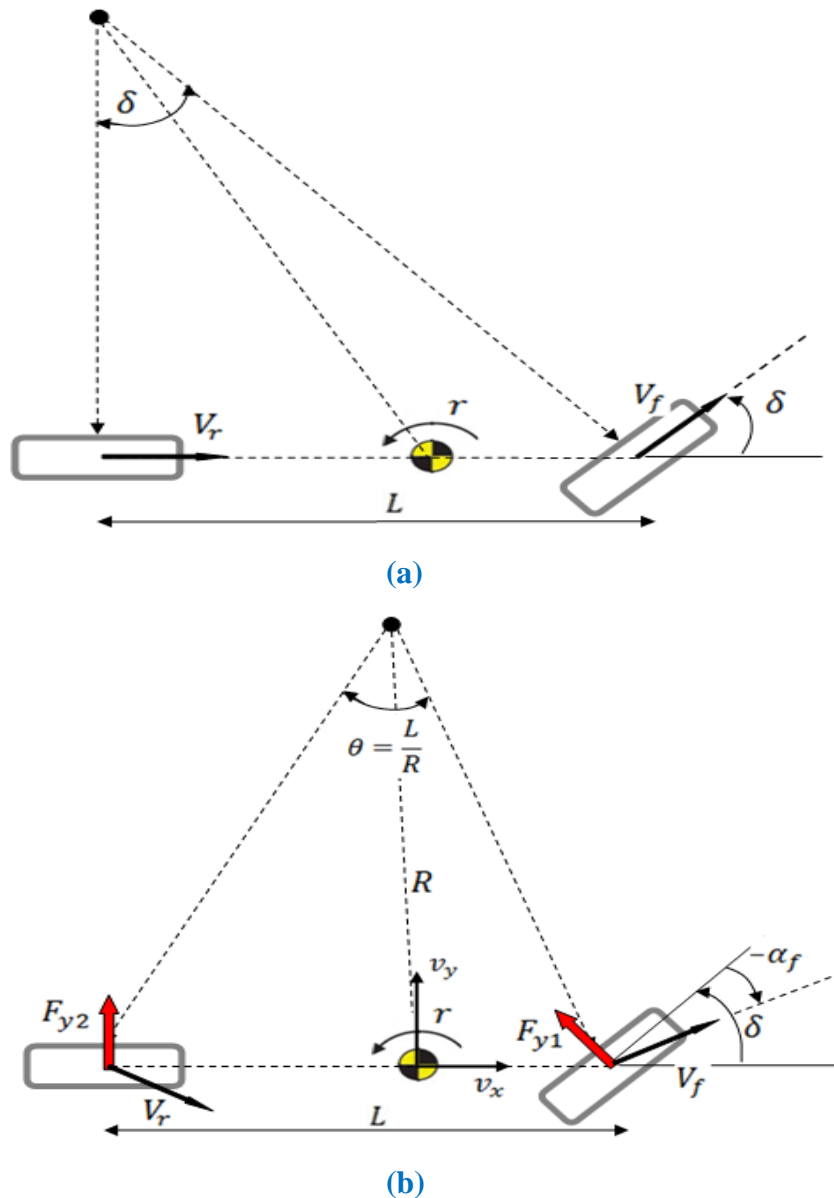


Figure 28: (a) Bi-cycle model in low-speed cornering (b) Bi-cycle model in steady-state cornering.

3.2.2 Tyre models

It is evident that the reliability of results obtained from simulation of vehicle models, are almost exclusively dependent on the accuracy and validity of the tyre model used to define the force and moment characteristics at the tyre-road interface. The tyre models used to study force and moment characteristics can be broadly classified into three groups; theoretical models, empirical models and finite element models. Theoretical models provide a mathematical expression for defining tyre force and moment characteristics and are essentially based on the physical behaviour of tyre structure. They have good predictive power and rely on very little experimental data involving tyre deformations. However, these models can become complex when accurate results are required.

Empirical models on the other hand rely on experimental data and utilize regression techniques to fit the data to mathematical models. This model gives accurate results but lacks the ability to predict results when the operating conditions are changed. Then regression techniques need to be applied all over again to a new set of data, at the desired operating condition. A well known empirical formula is the 'Magic tyre formula' which has been validated extensively. In finite element tyre models, the physical structure of the tyre is modelled in detail, mainly for structural analysis and to evaluate complex tyre behaviour in the contact patch. These models can be very complex and requires large computational capability, making them unsuitable for fundamental vehicle dynamic analysis.

Since the primary objective is to evaluate the change in vehicle response at different tyre pressures, the focus will be on only those tyre models that have incorporated the influence of tyre pressure on its force and moment characteristics. Two models are discussed below; the Radt/Milliken non-dimensional tyre model [22] and TNO Delft-Tyre model [23].

3.2.2.1 Radt/Milliken non-dimensional tyre model

This is a semi-empirical tyre model that uses both known operating conditions and assumptions about physical behaviour of a tyre to predict the net tyre force and moment.

The traditional inputs to the tyre model are:

α_{slip} - Side-slip angle,
 γ - Camber angle,
 κ - Slip ratio,
 F_z - Normal load, and
 μ - Surface friction coefficient.

and the output forces and moments are:

F_x - Longitudinal force,
 F_y - Lateral force,
 M_z - Aligning torque and
 M_x - Overturning moment.

This tyre model takes a unique approach to modelling tyre data. It involves the transformation of tyre variables to non-dimensional variables. After this transformation when a non-dimensional output variable is plotted against another non-dimensional input variable, a load and friction independent curve is obtained. To illustrate this behaviour let us consider two variables, α and F_y , where $F_y = f(\alpha)$ and apply the transformation to it (see equations (9) and (10)).

$$\bar{\alpha} = \frac{C * \tan(\alpha)}{\mu * F_z} \quad (9)$$

$$\bar{F}_y = \frac{F_y}{\mu * F_z} \quad (10)$$

where, $\bar{\alpha}_{slip}$ and \bar{F}_y are non-dimensional slip angle and lateral force, respectively. C_α and μ are the cornering stiffness coefficient and friction coefficient, respectively. Figure 29 shows a typical lateral force versus slip angle curve before transformation and Figure 30 shows the typical load and friction independent curve after transformation.

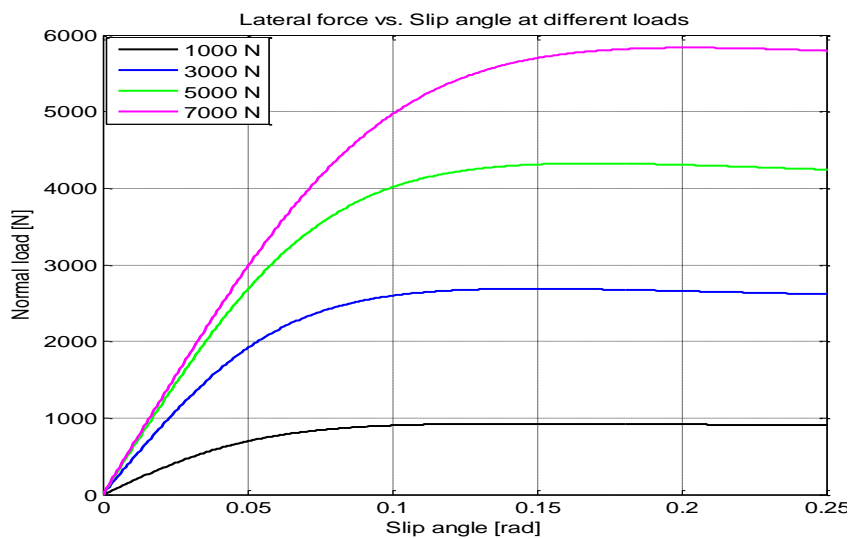


Figure 29: Lateral force variation with vertical load, at nominal tyre pressure.

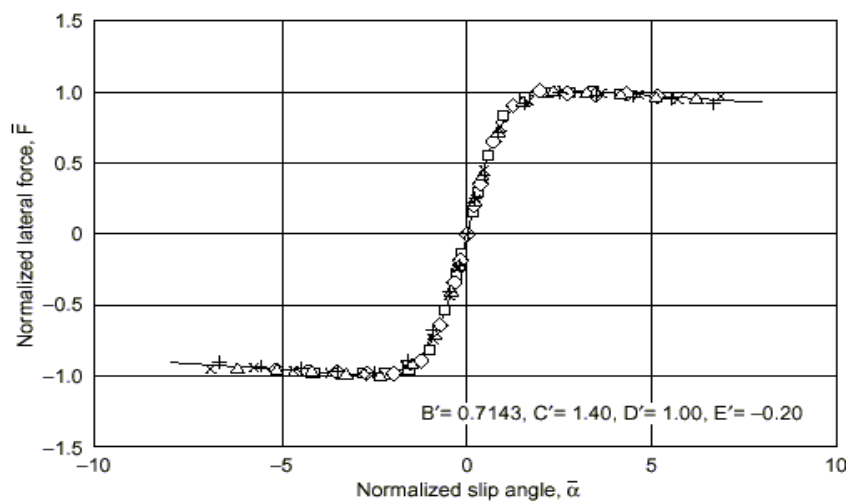


Figure 30: Non-dimensional lateral force versus slip angle curve [22].

However, Figure 30 describes the load-friction independent curve at only one fixed pressure. Edward M. Kasprzak and Kemper E. Lewis [22], suggested the inclusion of pressure in the definition of cornering stiffness, C_α and friction coefficient, μ used in the equations (9) and (10) such that $C_\alpha = f(F_z, p_i)$ and $\mu = f(F_z, p_i)$. Here, p_i is the inflation pressure. Prior to the inclusion of pressure, C_α and μ were modelled as a function of normal load F_z . Figure 31 shows the lateral force versus slip angle curves for a 13 inch Formula SAE racing tyre at different pressures represented by the different colours at two loads of $F_z=150$ lb (68 kg) and 350 lb (159 kg).

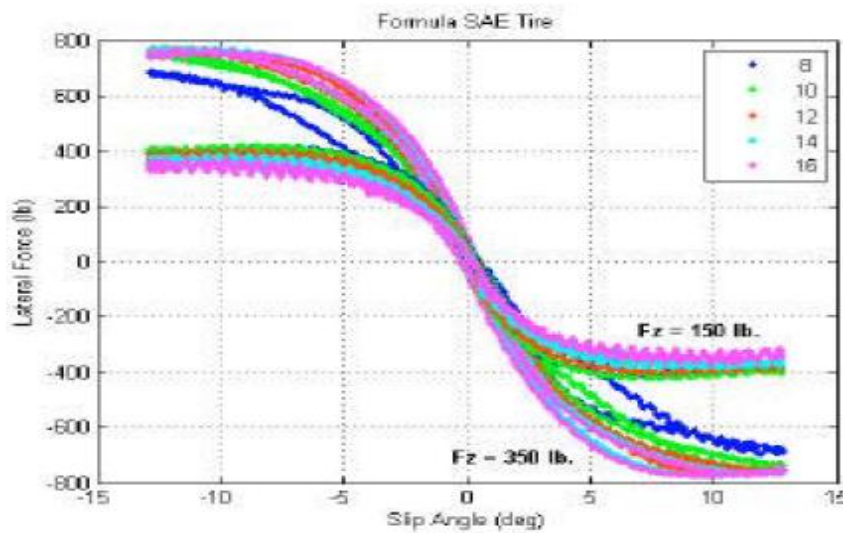


Figure 31: Lateral force versus side-slip for a 13'' Formula SAE racing tyre [22].

An interesting observation in Figure 31 is that the pressure trend is reverse at the two given loads! When the non-dimensional transformation is applied to this data, using the newly defined C_α and μ the curves can be successfully compressed to a load, friction and pressure independent curve as shown in Figure 32.

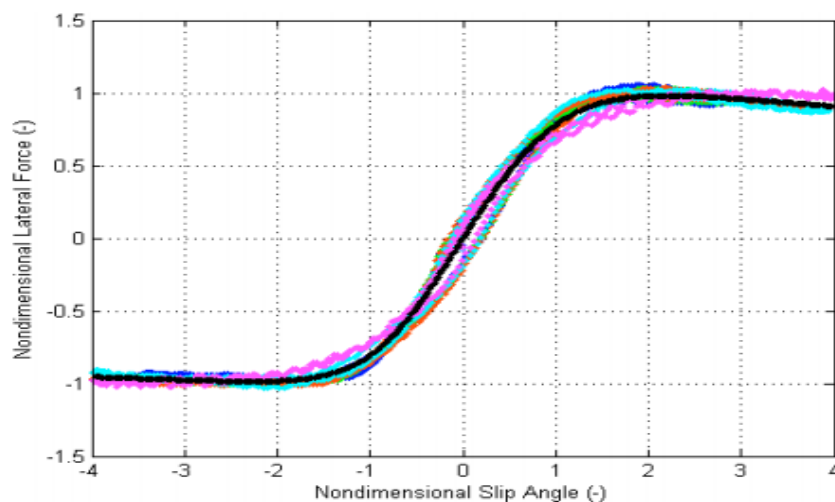


Figure 32: Load, friction and pressure independent non-dimensional curve [22].

In the above figure, the black line represents a single instance of Magic Formula fit to the non-dimensional curves. Although the Radt/Milliken tyre model is able of capture the influence of inflation pressure in the tyre's force and moment characteristics, for certain combinations of tyre load, pressure and other operating conditions, the transformation is unable to sufficiently capture the observed tyre behaviour. Figure 33 shows this deviant behaviour of the model near the peak values and beyond, for a radial racing tyre at different pressures and loads. It only shows a good fit in the tyre's linear operating range.

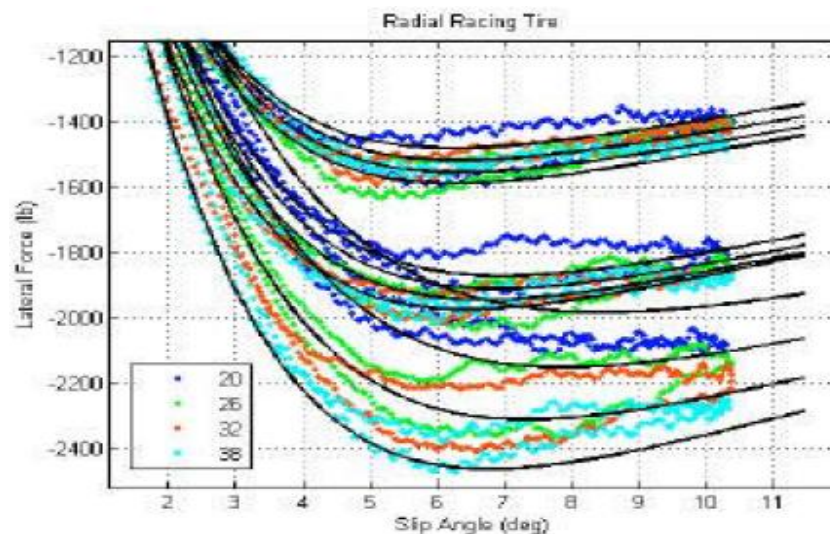


Figure 33: Lateral force versus slip angle for a radial racing tyre; deviation near the peak value [22].

The authors of [22] have suggested a post transformation modification technique to account for this deviant behaviour. However, this modification is not consistent with non-dimensional approach of modelling as the model's predictability of forces and moments, for different values of friction coefficient μ , is greatly reduced. Though this model shows potential, the lack of accuracy at higher slip angles has made it a liability to be used in our vehicle model.

3.2.2.2 TNO Delft-Tyre model

The TNO Delft-Tyre model is based on the renowned Pacjeka's 'Magic Formula' tyre model given by equation (11).

$$y = D * \sin [C * \arctan \{B * x - E * (B * x - \arctan (B * x))\}] \quad (11)$$

where y is the output variable, F_x , F_y or M_z and x is the input variable α_{slip} or κ . The Delft-Tyre model uses the ISO sign convention in defining forces and moments

(see Figure 34). For more information on the Magic Formula tyre model, the interested reader may be referred to [14].

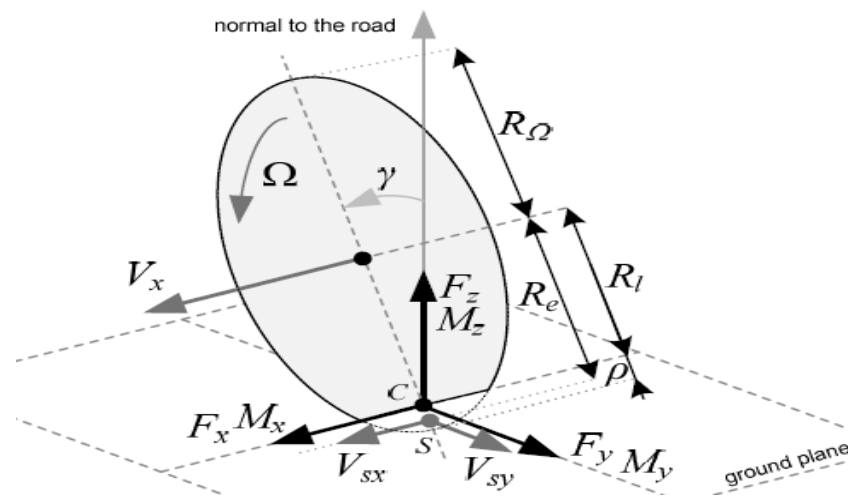


Figure 34: ISO sign convention for the wheel coordinate axis [30].

TNO Delft-Tyre is a semi-empirical tyre model that relies on both experimental data and physical attributes of the tyre to predict tyre force and moment characteristics. For a price, TNO Delft-Tyre provides a complete set of tools and services for detailed modelling of tyre-road interaction. Two tyre models are included in the package, namely, MF-Tyre and MF-Swift. With MF-Tyre it is possible to simulate steady-state and transient behaviour of the tyre making it ideal for vehicle handling simulations. MF-Swift is used for simulating dynamic tyre behaviour for inputs up to 100 Hz! This is ideally suitable for vehicle comfort analysis, vibration analysis and tyre durability tests.

However, in the package provided for this thesis work only MF-Tyre model was included. The tyre model has several modes of operation which gives the user the ability to conduct selective study of different tyre forces and moments based on the output of interest.

The slip forces may be calculated in any one of the five modes:

- I. Longitudinal forces/moments only (F_x, M_y)
- II. Lateral forces/moments only (F_y, M_x, M_z)
- III. Un-combined forces/moments (F_x, F_y, M_x, M_y, M_z)
- IV. Combined forces/moments (F_x, F_y, M_x, M_y, M_z)
- V. Combined forces/moments (F_x, F_y, M_x, M_y, M_z) + turnslip

The operation mode IV is used in the two-track model constructed for this thesis work. This option uses combined slip to calculate the tyre forces and moments. This tyre model also accounts for relaxation behaviour of the tyres, giving the user three choices:

- I. Steady-state
- II. Linear relaxation behaviour
- III. Non-linear relaxation behaviour

The steady-state evaluation does not account for any relaxation behaviour of the tyre. Linear relaxation behaviour mode is based on empirical relations that capture the linear transient effects of the relaxation behaviour. In non-linear relaxation behaviour, the tyre lag is calculated using a physical approach that takes the tyre carcass compliance into account. However, option II was chosen for the tyres used in the two-track vehicle model since it was expected that results using option III would be more tyre dependent.

The latest version of MF-Tyre/MF-Swift, version 6.1.2.1, incorporates the influence of tyre pressure on the tyre's force and moment characteristics. The pressure effects have been sufficiently validated for several tyres.

The inputs to the MF-Tyre model are:

- α_{slip} - Side-slip angle.
- γ - Camber angle.
- V_x - Longitudinal velocity at the wheel centre.
- V_{sy} - Lateral slip velocity, calculated at the slip point, S (see Figure 34).
- F_z - Normal load.
- $\dot{\psi}$ - Turn slip velocity.

Scaling - a set of scaling coefficients used to fine tune the fit of experimental data and

The output forces and moments are:

- F_x - Longitudinal force.
- F_y - Lateral force.
- M_z - Aligning torque.
- M_x - Overturning moment.
- M_y - Moment about y axis.
- M_{RR} - Rolling resistance moment.

The MF-Tyre model has been extensively validated for both steady state and transient tyre behaviours [23]. MF-Tyre model is capable of accurately calculating the output forces and moments for both pure and combined slip conditions based on the limited number of inputs described above. The model is valid for large side-slip angles (typically over 30 degrees), longitudinal slips ($\pm 100\%$), load variations and camber angles (including motorcycle camber angles). It can also predict linear and non-linear

tyre relaxation behaviour. Figure 35 shows how the combined slip is modelled in MF-Tyre for steady state conditions.

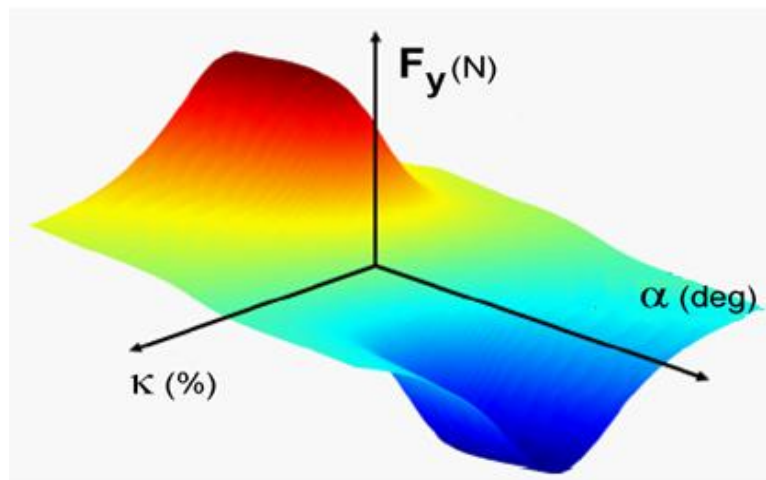


Figure 35: Lateral force as a function of side-slip angle, α and slip ratio, κ [23].

3.2.3 Two-track vehicle model

Due to the numerous advantages of the MF-Tyre model mentioned above, a two-track vehicle model was developed using this tyre model to study the influence of tyre pressure on vehicle handling. A two-track vehicle model was preferred over the Bi-Cycle model as it allows the tyre pressure to be independently changed in each of the four tyres, thereby bringing out the pros and cons of having an on-board dynamic TPRS. The MF-Tyre model was supplied on request by TNO, Netherlands, for use in this thesis work.

When evaluating the overall stability of a vehicle, the lateral forces generated from external disturbances such as wind, road gradient etc. must also be taken into consideration. However, these external factors are neglected in this two-track model for simplicity. The specification of a medium sized passenger car, same as the one used for the QSS model, was chosen for modelling the two-track vehicle model (see Table 10 in Appendix I). Figure 36 shows the free body diagram of the model.

In Figure 36, F_{yLi} , F_{yRi} are the lateral forces on the left and right wheels of the vehicle at the front ($i = 1$) and rear axles ($i = 2$), respectively and α_{Li} , α_{Ri} are the corresponding side-slip angles. Similarly, F_{xLi} and F_{xRi} represent the RR forces on the tyres. F_L and F_R are the traction forces. In this case the chosen vehicle is a front wheel drive. Track widths at the front and rear are given by s_1 and s_2 , respectively. The wheelbase is L and the centre of gravity is at a distance of a_1 and a_2 from the front and rear axle, respectively. The yaw rate about the Z axis at the centre of gravity is

given by r . In this model the steering wheel angle has been assumed to be the same on both the left and right front wheels, δ .

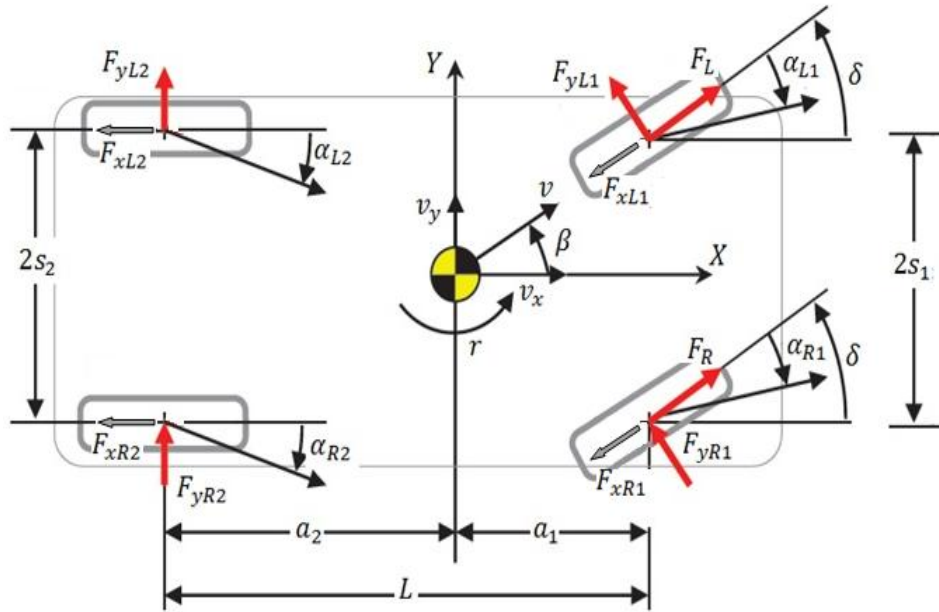


Figure 36: Free-body diagram of a two track vehicle model.

The equations of motion can be obtained from Figure 36. The forces and moments are resolved using the ISO standard coordinate system.

Sum of forces in lateral direction

$$M * (\dot{v}_y + v_x * r) = -F_{yL2} - F_{yR2} + (F_{yL1} + F_{yR1}) * \cos(\delta) \dots - (F_{xL1} + F_{xR1}) * \sin(\delta) \quad (12)$$

where, $\dot{v}_y + v_x * r$ represents the lateral acceleration, a_y .

Sum of forces in longitudinal direction

$$M * (\dot{v}_x - v_y * r) = -F_{xL2} - F_{xR2} - (F_{yL1} + F_{yR1}) * \sin(\delta) \dots - (F_{xL1} + F_{xR1}) * \cos(\delta) \quad (13)$$

where, $\dot{v}_x - v_y * r$ represents the longitudinal acceleration, a_x .

Moment about the z-axis passing through the COG

$$I_{ZZ} * \dot{r} = \left[\left\{ (F_{yL1} + F_{yR1}) \cos(\delta) - (F_{xL1} + F_{xR1}) \sin(\delta) \right\} * a_1 + (F_{yL2} + F_{yR2}) * a_2 - \left\{ F_{xR1} \cos(\delta) + F_{yR1} \sin(\delta) \right\} * s_1 \dots \right. \\ \left. + \left\{ F_{xL1} \cos(\delta) + F_{yL1} \sin(\delta) \right\} * s_1 + (F_{xL2} - F_{xR2}) * s_2 \right] \quad (14)$$

This two-track model also includes the effects of lateral and longitudinal load transfer. They are given by equations (15) and (16).

$$\Delta F_{zlong} = \frac{(M - M_{us}) * a_x * h}{L} \quad (15)$$

$$\Delta F_{zlat} = \frac{M_i * a_y * (h - h_i) - M_{\phi i}}{s_i} \quad (16)$$

where, $M_{\phi i}$ is the roll stiffness moment about the roll centre at the front ($i = 1$) or rear ($i = 2$) axles, calculated from the suspension stiffness and damping values. The influence of load transfer due to pitch of the vehicle body is neglected and only the effect of inertia is included. However, the lateral load transfer caused by the body roll has been taken into account.

In order to do a comparative study of the influence of changing tyre pressure on the four wheels independently, seven test Cases were developed. The description of these Cases are given below:

Normal Cases

Case I: Nominal pressure of 2.2 bar in all four tyres.

Case II: Low pressure of 1.8 bar in all four tyres.

Case III: High pressure of 2.8 bar in all four tyres.

Special Cases

Case IV: 2.8 bar pressure in outer tyres and 1.8 bar in inner tyres (while turning).

Case V: 2.8 bar pressure in inner tyres and 1.8 bar in outer tyres (while turning).

Case A: 1.8 bar on front tyres and 2.8 bar on rear tyres.

Case B: 2.8 bar on the front tyres and 1.8 bar on rear tyres.

The special Cases were developed to take advantage of having an on-board dynamic TPRS. Case IV in particular, was developed based on the tyre behaviour shown in Figure 15 in Section 2.4.1, where the cornering forces are higher at higher pressure and higher load. Since the two-track vehicle model accounts for body roll, it was only natural to develop the special Cases IV and V to study the influence of body roll on the cornering behaviour of the vehicle. Cases A and B were developed to see if there were any advantages to be gained in vehicle's cornering response and stability.

These seven test Cases will be subjected to the three inputs, a step input, ramp input and a Sine-With-Dwell (SWD) input. The vehicle model response will be evaluated on two surfaces; dry and wet. The step input will be used to investigate the change in yaw rate and trajectory of the vehicle at different tyre pressures, while the ramp input will be used to develop the handling diagram of the vehicle at different tyre pressures. A SWD input is also given to this model to illustrate the difference in the yaw response of the vehicle for the seven Cases mentioned earlier.

The dry and wet surface conditions are approximated by changing the value of peak longitudinal and lateral friction coefficient in the MF-Tyre model's tyre file. Due to the lack of sufficient tyre and test data, the influence of parameters such as tread depth and design, standing water height, road surface roughness etc. are not explicitly modelled to determine the tyre forces and moments, but approximated by simply changing the limiting friction value at the tyre-road interface.

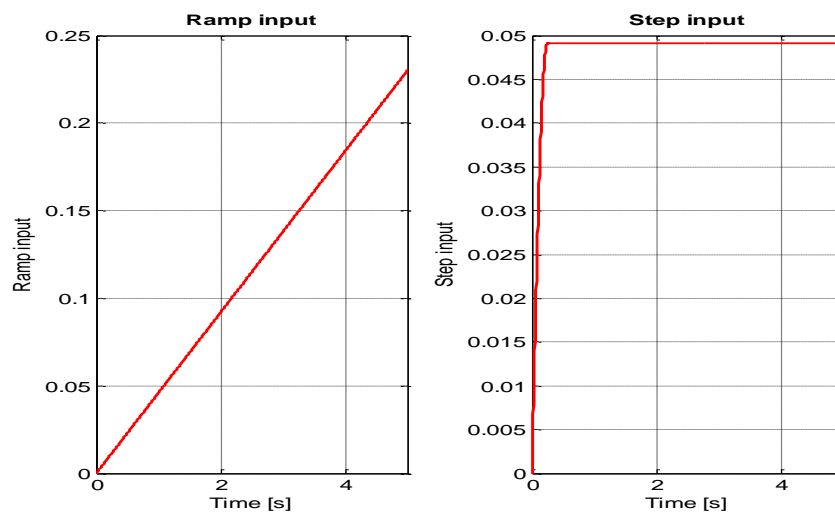


Figure 37: Ramp input and step input, respectively.

3.2.3.1 Ramp input

A ramp input is a signal that starts at a specified time and increases in value at a particular rate (see Figure 37). Using this input at the steering wheel the handling diagram for the seven Cases were evaluated, on both dry and wet surfaces.

3.2.3.2 Step input

The step input is shown in Figure 37. With this input the vehicle's yaw rate and global displacement (longitudinal versus lateral displacement) were evaluated for the seven tyre pressure Cases.

3.2.3.3 Sine-With-Dwell input

The SWD input is capable of inducing an over-steer in virtually any vehicle and is the basis for NHTSA FMVSS-126 (U.S.A) regulation, which is used to evaluate the over-steer intervention of different yaw-stabilizing systems in vehicles, such as ESC (Electronic Stability Control) and DSC (Dynamic Stability Control) systems. However, in this thesis work, only a part of the standard NHTSA's SWD test methodology will be used to illustrate the yaw response of the vehicle for the seven tyre pressure Cases.

In the SWD manoeuvre the vehicle is subjected to two tests where the manoeuvre is started by turning the steering wheel in the clockwise direction for the first test and in the anti-clockwise direction for the second test. The results are then averaged. The steering is given a sine-wave like input as shown in Figure 38.

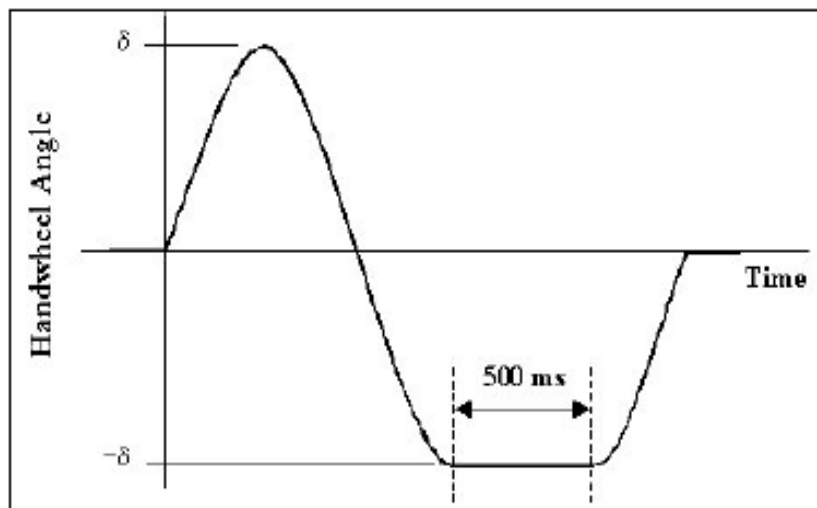


Figure 38: Sine With Dwell steering pattern [24].

The frequency of the sine wave is 0.7 Hz and at the second peak, the steering wheel is held at its maximum position for 500 millisecond before returning to the initial zero position. For a detailed description of standard operating procedure the reader is referred to [25]. For a vehicle to pass this regulation it must pass two stability criterions and one manoeuvrability criterion.

Stability Criterion I: The Yaw Rate Response (YRR), one second after completion of steer, must be less than 35 % of the peak yaw rate observed at the second peak (i.e. at the start of the 'dwell' region of the manoeuvre; see Figure 39).

The YRR is mathematically defined as:

$$Y_{RR} = \frac{r_t}{r_{peak}} * 100 \quad (17)$$

where Y_{RR} is the yaw rate response, r_t is the yaw rate at any time t and r_{peak} is the peak yaw rate measured at the second peak. Figure 39 shows a typical YRR of a vehicle for SWD manoeuvre with time T_0 indicating completion of steer. The red circle indicates the second peak. The YRR for Criterion I is measured at time $T_0 + 1$.

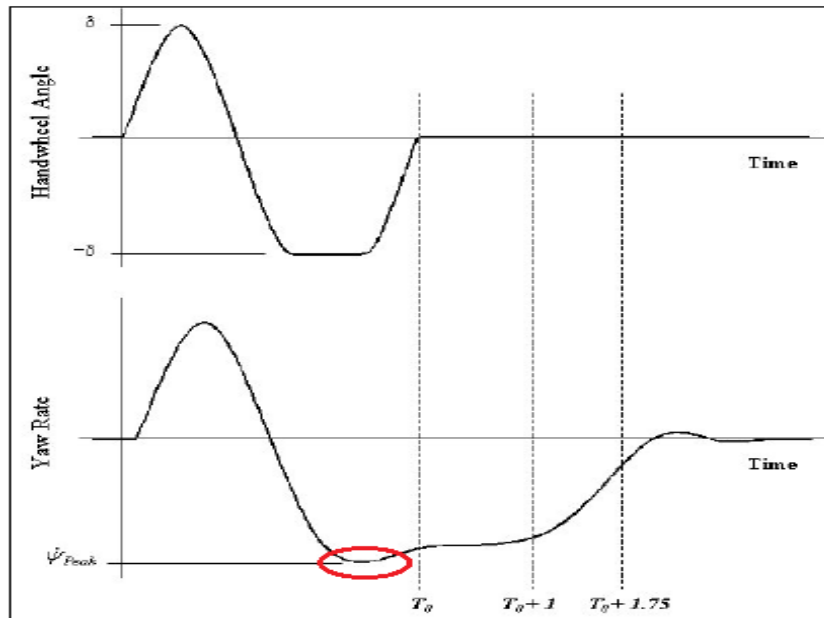


Figure 39: Typical yaw rate response of a vehicle to the SWD manoeuvre [24].

Stability Criterion II: The YRR, after 1.75 seconds after completion of steer, should be less than 20% of the peak yaw rate. From Figure 39, this value is measured at time, $T_0 + 1.75$.

Manoeuvrability Criteria I: The lateral displacement of the vehicle measured at 1.07 seconds after the beginning of steer must be 1.83 meters from the original path of the vehicle. This criterion ensures that the vehicle is not set up to be too under-steered and it is capable of avoiding an obstacle in time.

Using the stability and manoeuvrability criteria of the standard NHTSA's SWD test, a methodology is developed to evaluate the yaw response of the two-track vehicle model to the SWD input. First, the largest possible steering wheel amplitude, $\delta_{steering}$, which satisfies both the stability and manoeuvrability criteria is identified for Case I (nominal pressure in all four tyres). The yaw responses of the other test cases are determined using this $\delta_{steering}$ value and compared to Case I. This will help illustrate how a dynamic TPRS, can help a vehicle regain yaw stability by simply changing the inflation pressures in the four wheels.

In the SWD manoeuvre, the inner and outer sides of the vehicle (with respect to a turn) changes sides. Due to this fact and the lack of access to the source code of the MF-Tyre model, the true YRR of Cases IV and V could not be determined. Instead, the results of Cases IV and V presented in this report for the SWD input, show the vehicle's behaviour if the TPRS system were to fail after the initial steering input of the SWD manoeuvre.

3.3 Vehicle ride characteristics

An ideal suspension is one which is capable of isolating road irregularities while effectively transmitting the vehicle control forces of steering, braking and traction between vehicle and ground. For low frequency vibration analysis and ride simulations, the behaviour of pneumatic tyres and suspension components can be sufficiently captured by an equivalent mass-spring-damper system.

Several mathematical ride models have been developed over the years, a summary of which can be seen in [26] with a more complex seven Degree of Freedom (7-DOF) full-car model used in [27]. However, in this report, a four DOF half-car model is used for the ride quality analysis. Since the rear wheels naturally follow the same track as the front wheels, the front and rear tyres are excited by the same input, but out-of-phase. Thus the model's response will be more representative of the real vehicle.

3.3.1 Modelling approach

A four DOF half-car models was developed to study the influence of tyre pressure on ride characteristics of the vehicle. First, the equations of motion of the vehicle model is set up from the free body diagram of the vehicle model. It is then transformed to the equations in state-space form. The system thus obtained is a Linear Time Invariant (LTI) system which is then modelled in the Matlab /Simulink[®] interface. One model was created in the Simulink interface to evaluate the response of the vehicle to step input and sinusoidal input. Using the step input, the bounce displacement, bounce acceleration and pitch angle of the sprung mass are evaluated at different tyre inflation pressures. Using the sinusoidal input, the tyre-road contact characteristics are illustrated at different tyre pressures

The four DOF model is also re-created in the Matlab[®] interface to evaluate the influence of inflation pressure on the frequency responses of the vehicle's vertical acceleration and the tyre's road holding capability using Bode plots. Road holding or road grip may be defined as the ability of the vehicle and tyre to maintain continuous contact with the road at all frequencies of excitations. The frequency response of the vehicle's vertical acceleration is also evaluated for a random road surface profile input, which is defined according to ISO 8608 standards [15, 28, 29]. The frequency response thus obtained not only provides a better representation of a real vehicle's frequency response but also enables the direct calculation of RMS value of the accelerations at the frequencies of interest. The RMS values of the vehicle's sprung mass vertical acceleration are calculated for a range of frequencies and compared to the ISO 2631 standard [15, 16], which give detailed guidelines for evaluation of human exposure to whole body vibrations.

3.3.2 Four DOF half-car model

The four DOF half-car model is developed by approximating the vehicle, its suspension and tyres as a mass-spring-damper system. Several authors [13, 15, 26] have shown this to be a reasonable approximation of the vehicle when studying the vibrations in the low-to-mid frequency range. The vehicle body, indicated by mass M_B , is free to move vertically along the Z axis by an amount Z_B and rotate about Y axis by θ . The un-sprung masses at the front and rear, M_{uf} and M_{ur} , can move vertically along Z axis by Z_{uf} , Z_{ur} , respectively. K_f , K_r and B_f , B_r are the front and rear suspension stiffness and damping values, respectively. Similarly, K_{tf} , K_{tr} , B_{tf} and B_{tr} give the stiffness and damping values of the front and rear tyres. L is the wheel base and the COG is located at a distance of a_1 and a_2 from the front and rear axle respectively. U_1 and U_2 are the vertical inputs at the front and rear tyres, with U_2 being the same as U_1 but with a phase delay given by $\frac{L}{V_x}$. Figure 40 shows the four DOF model that was developed in this thesis work to analyse the influence of tyre pressure on vehicle ride characteristics.

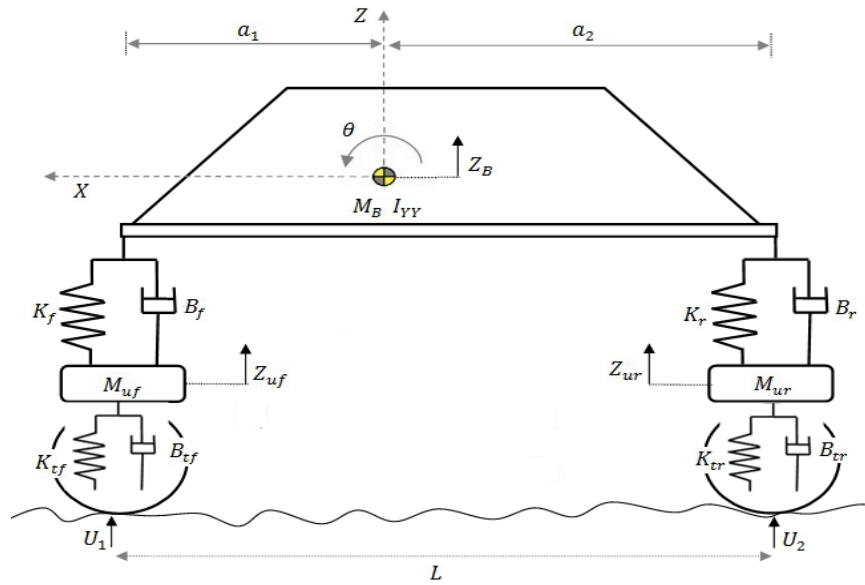


Figure 40: Four DOF half-car model.

Equations (18) to (21) give the equations of motion for the 4-DOF vehicle model developed using Lagrange's method, applied to lumped rigid bodies.

Equations of motion

$$\begin{aligned}
 M_{uf} \cdot \ddot{Z}_{uf} - K_f \cdot Z_B - K_f \cdot a_1 \cdot \theta + (K_f + K_{tf}) \cdot Z_{uf} - K_{tf} \cdot Z_f - B_f \cdot \dot{Z}_B \dots \\
 - B_f \cdot a_1 \cdot \dot{\theta} + (B_f + B_{tf}) \cdot \dot{Z}_{uf} - B_{tf} \cdot \dot{Z}_f = 0
 \end{aligned} \tag{18}$$

$$\begin{aligned}
M_{ur} \cdot \ddot{Z}_{ur} - K_r \cdot Z_B + K_r \cdot a_2 \cdot \theta + (K_r + K_{tr}) \cdot Z_{ur} - K_{tr} \cdot Z_r - B_r \cdot \dot{Z}_B \dots \\
+ B_r \cdot a_2 \cdot \dot{\theta} + (B_r + B_{tr}) \cdot \dot{Z}_{ur} - B_{tr} \cdot \dot{Z}_r = 0
\end{aligned} \tag{19}$$

$$\begin{aligned}
M_B \cdot \ddot{Z}_B + (K_f + K_r) \cdot Z_B + K_f \cdot a_1 \cdot \theta - K_r \cdot a_2 \cdot \theta_r - K_f \cdot Z_{uf} - K_r \cdot Z_{ur} \dots \\
+ (B_f + B_r) \cdot \dot{Z}_B + (B_f \cdot a_1 - B_r \cdot a_2) \cdot \dot{\theta} - B_f \cdot \dot{Z}_{uf} - B_r \cdot \dot{Z}_{ur} = 0
\end{aligned} \tag{20}$$

$$\begin{aligned}
I_{YY} \cdot \ddot{\theta} + (K_f \cdot a_1 - K_r \cdot a_2) \cdot Z_B + K_f \cdot a_1^2 \cdot \theta - K_f \cdot a_1 \cdot Z_{uf} \dots \\
+ K_r \cdot a_2^2 \theta + K_r \cdot a_2 \cdot Z_{ur} + (B_f \cdot a_1 - B_r \cdot a_2) \cdot \dot{Z}_B + B_f \cdot a_1^2 \cdot \dot{\theta} \dots \\
- B_f \cdot a_1 \cdot \dot{Z}_{uf} + B_r \cdot a_2^2 \cdot \dot{\theta} + B_r \cdot a_2 \cdot \dot{Z}_{ur} = 0
\end{aligned} \tag{21}$$

3.3.2.1 Step input

As mentioned earlier the vehicle model was subjected to a step input to evaluate the influence of tyre pressure on sprung mass bounce displacement, bounce acceleration and pitch displacement. A step size of 0.025 meters was chosen at a vehicle speed of 60 km/h.

The equations of motion developed earlier are transformed to the equations in state-space form, through suitable selection of state variables. Assume the following state variables:

$$\begin{aligned}
x_1 &= Z_{uf} & x_5 &= Z_B \\
x_2 &= \dot{Z}_{uf} - \frac{B_{tf} \cdot Z_f}{M_{uf}} & x_6 &= \dot{Z}_B \\
x_3 &= Z_{ur} & x_7 &= \theta \\
x_4 &= \dot{Z}_{ur} - \frac{B_{tr} \cdot Z_r}{M_{ur}} & x_8 &= \dot{\theta}
\end{aligned}$$

The state-space equations take the following form:

$$\begin{aligned}
\dot{X} &= AX + BU \\
Y &= CX + DU
\end{aligned}$$

where, the state vectors are:

$$\begin{aligned}
X &= [x_1 \ x_2 \ x_3 \ x_4 \ x_5 \ x_6 \ x_7 \ x_8]^T \\
\dot{X} &= [\dot{x}_1 \ \dot{x}_2 \ \dot{x}_3 \ \dot{x}_4 \ \dot{x}_5 \ \dot{x}_6 \ \dot{x}_7 \ \dot{x}_8]^T \\
U &= [Z_{uf} \ Z_{ur}]^T
\end{aligned}$$

$$A = \begin{bmatrix} 0 & 1 & 0 & 0 & 0 & 0 & 0 & 0 \\ \frac{-(K_f + K_{tf})}{M_{uf}} & \frac{-(B_f + B_{tf})}{M_{uf}} & 0 & 0 & \frac{K_f}{M_{uf}} & \frac{B_f}{M_{uf}} & \frac{K_f \cdot a_1}{M_{uf}} & \frac{B_f \cdot a_1}{M_{uf}} \\ 0 & 0 & 0 & 1 & 0 & 0 & 0 & 0 \\ 0 & 0 & \frac{-(K_r + K_{tr})}{M_{ur}} & \frac{-(B_r + B_{tr})}{M_{ur}} & \frac{K_r}{M_{ur}} & \frac{B_r}{M_{ur}} & \frac{-K_r \cdot a_2}{M_{ur}} & \frac{-B_r \cdot a_2}{M_{ur}} \\ 0 & 0 & 0 & 0 & 0 & 1 & 0 & 0 \\ \frac{K_f}{M_B} & \frac{B_f}{M_B} & \frac{K_r}{M_B} & \frac{B_r}{M_B} & \frac{-(K_f + K_r)}{M_B} & \frac{-(B_f + B_r)}{M_B} & \frac{-(K_f \cdot a_1 - K_r \cdot a_2)}{M_B} & \frac{-(B_f \cdot a_1 - B_r \cdot a_2)}{M_B} \\ 0 & 0 & 0 & 0 & 0 & 0 & 0 & 1 \\ \frac{K_f \cdot a_1}{I_{yy}} & \frac{B_f \cdot a_1}{I_{yy}} & \frac{-K_r \cdot a_2}{I_{yy}} & \frac{-B_r \cdot a_2}{I_{yy}} & \frac{-(K_f \cdot a_1 - K_r \cdot a_2)}{I_{yy}} & \frac{-(B_f \cdot a_1 - B_r \cdot a_2)}{I_{yy}} & \frac{-(K_f \cdot a_1^2 + K_r \cdot a_2^2)}{I_{yy}} & \frac{-(B_f \cdot a_1^2 + B_r \cdot a_2^2)}{I_{yy}} \end{bmatrix}$$

$$B = \begin{bmatrix} \frac{B_{tf}}{M_{uf}} & 0 \\ \frac{1}{M_{uf}} * \left(K_{tf} - \frac{(B_f \cdot B_{tf} + B_{tf}^2)}{M_{uf}} \right) & 0 \\ 0 & \frac{B_{tr}}{M_{ur}} \\ 0 & \frac{1}{M_{ur}} * \left(K_{tr} - \frac{(B_r \cdot B_{tr} + B_{tr}^2)}{M_{ur}} \right) \\ 0 & 0 \\ \frac{B_f \cdot B_{tf}}{M_B * M_{uf}} & \frac{B_r \cdot B_{tr}}{M_B * M_{ur}} \\ 0 & 0 \\ \frac{B_f \cdot B_{tf} \cdot a_1}{I_{yy} * M_{uf}} & \frac{-B_r \cdot B_{tr} \cdot a_2}{I_{yy} * M_{ur}} \end{bmatrix}$$

Vectors C and D are dependent on the output of interest as shown below.

The outputs of interest are:

- I. Bounce displacement of sprung mass.
- II. Bounce acceleration of sprung mass.
- III. Pitch displacement of sprung mass.

Bounce displacement, Z_B

From the state-space equations the output, $Y_1 = Z_B = x_5$. Thus, vectors C and D become:

$$C = \begin{bmatrix} 0 \\ 0 \\ 0 \\ 0 \\ 1 \\ 0 \\ 0 \\ 0 \end{bmatrix} \quad D = \begin{bmatrix} 0 & 0 \end{bmatrix}$$

Bounce acceleration, \ddot{Z}_B

From the state-space equations the output, $Y_2 = \ddot{Z}_B$, Thus the vectors C and D can be obtained from the Lagrange's equation (20):

$$C = \begin{bmatrix} \frac{K_f}{M_B} \\ \frac{B_f}{M_B} \\ \frac{K_r}{M_B} \\ \frac{B_r}{M_B} \\ \frac{-(K_f + K_r)}{M_B} \\ \frac{-(B_f + B_r)}{M_B} \\ \frac{-(K_f \cdot a_1 - K_r \cdot a_2)}{M_B} \\ \frac{-(B_f \cdot a_1 - B_r \cdot a_2)}{M_B} \end{bmatrix} \quad D = \begin{bmatrix} \frac{B_f \cdot B_{tf}}{M_B} & \frac{B_r \cdot B_{tr}}{M_B} \end{bmatrix}$$

Pitch angle displacement, θ

From the state-space equations the output, $Y_3 = \theta = x_7$. Thus, vectors C and D become:

$$C = \begin{bmatrix} 0 \\ 0 \\ 0 \\ 0 \\ 0 \\ 0 \\ 1 \\ 0 \end{bmatrix} \quad D = \begin{bmatrix} 0 & 0 \end{bmatrix}$$

3.3.2.2 Sinusoidal Input

The four DOF half-car model is subjected to a sinusoidal input at the front and rear tyres in order to illustrate the influence of tyre pressure on the vehicle's ability to maintain full and continuous contact with the road. The maximum excitation of any system is observed at its natural frequency, thus making the natural frequency of the un-sprung mass a suitable choice as input frequency. The amplitude of the input is chosen such that the tyres, at its nominal inflation pressure of 2.2 bar, barely maintain contact with the road. The amplitude chosen is also comparable to the amplitude observed at the corresponding frequency in Class G road (ISO road representation; see Table 2 in Section 3.3.2.3 below), which is an extremely poor quality road, rarely found within city limits.

3.3.2.3 Frequency response

In order to study the ride behaviour of the vehicle to inputs at different frequencies, the frequency response of the vehicle's vertical acceleration and road holding capability were evaluated using Bode plots. The Bode plots reveal the amplification or attenuation of the system's gain at different frequencies. The vehicle's vertical acceleration frequency response is also examined using a standard random road profile, which is widely used across the automotive industry to study ride quality and passenger comfort. The most common representation of road profile is in the form of vertical displacement Power Spectral Density (PSD), $S_{rd}(n)$. The International Standards Organization (ISO) has proposed a road roughness classification based on vertical displacement PSD [15, 30, 28, 29].

Table 2: Road roughness classification according to ISO 8608 [30].

Class number (cn)	Road Class	$Sd_{(n=1)}^A$ ($\times 10^{-6} \text{ m}^3$)	$S_{RMS(n=1)}^B$ ($\times 10^{-3} \text{ m}$)	$S_{RMS(n=1)}$ (mm)
1	A	0.16	0.4	0.4
2	B	0.64	0.8	0.8
3	C	2.56	1.6	1.6
4	D	10.24	3.2	3.2
5	E	40.96	6.4	6.4
6	F	163.84	12.8	12.8
7	G	655.36	25.6	25.6
8	H	2621.44	51.2	51.2

Ob.: ^A: Geometric Mean; ^B: rms value; $n = 1$ meter, from ISO 8608.

Table 2 shows how the roads are classified into the different classes (A through H), with the corresponding class numbers and roughness coefficient values. The road profile is represented by a relationship curve between PSD of vertical displacement, $S_{rd}(n)$ and spatial frequency, n . However, a discontinuity generally appears in this spectrum and the relationship curve may be approximated by two straight lines at this point, with different slopes on a log-log scale. The displacement PSD is then given by the following relations:

$$S_{rd}(n) = \begin{cases} R_{class} * \left(\frac{n}{n_0}\right)^{-p1} & ; \text{for } n \leq n_0 \\ R_{class} * \left(\frac{n}{n_0}\right)^{-p2} & ; \text{for } n \geq n_0 \end{cases} \quad (22)$$

where, R_{class} is the road roughness coefficient, n is the spatial frequency of interest, n_0 is the spatial frequency at the discontinuity (at $1/2\pi$ cycles/m) and $p1$ and $p2$ are the slopes of the log-log curve.

However, for general ride modelling purposes it is sufficient to assume a single line with slope of -2. Then the above equations take the following modified form [28, 30].

$$S_{rd}(n) = R_{class} * \left(\frac{n}{n_0}\right)^{-2} \quad (23)$$

where, $R_{class} = 4^{(class+1)}$.

Figure 41 below, shows the PSD of vertical displacement profile of the road as a function of wavelength, obtained from equation (23).

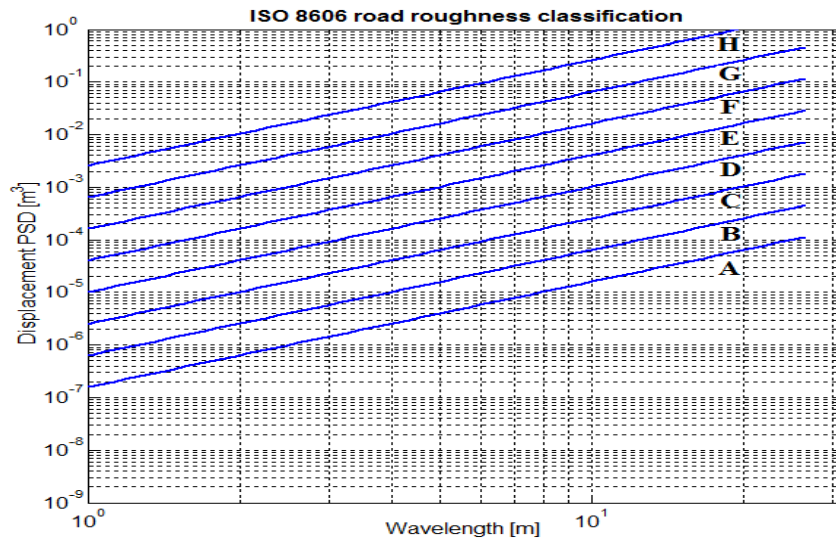


Figure 41: Power spectral density of vertical displacement of road surface profile.

Equation (23) can be rewritten in terms of angular frequency, ω using the relationship between time frequency, f and spatial frequency, n ; $f = n * V$ and $\omega = 2 * \pi * f$. Here, V is the velocity of the vehicle travelling over the given road profile. Now, equation (23) can be written in the form of equation (24).

$$S_{rd}(\omega) = (2 * \pi i)^2 * R_{class} * V * \left(\frac{1}{\omega}\right)^{-2} \quad (24)$$

For a linear time invariant system such as our four DOF model, if the input to the system is an ergodic, stationary, random process, then the output is also a stationary random process of similar characteristics. Hence, once we have determined the input to the system, the PSD of the output is obtained by multiplying the square of the magnitude of a frequency response function with the displacement PSD as shown in equation (25). Then, the PSD of vertical acceleration response of a vehicle can be calculated as follows:

$$S_{acc}(\omega) = |H(\omega)|^2 * S_{rd}(\omega) \quad (25)$$

The frequency response of the four DOF vehicle model is evaluated at a speed of 60 km/h and the PSD of vertical acceleration is determined using the ISO Class B (class number 2) random road profile. The frequency response is evaluated for three different tyre pressures Cases; Case I, Case II and Case III (see Section 3.2.3 for the Case descriptions). Other Cases have not been analysed since the model used is a half-

car model. Once the PSD plots are made the RMS value of vertical acceleration at any given frequency of interest, ω_j can be determined from the PSD of vertical acceleration using equation (26).

$$RMS_j(a_z) = \sqrt{S_{acc_j}(\omega) * \omega_j} \quad (26)$$

As mentioned in Section 2.5, humans are sensitive to vertical vibrations in a certain range of frequencies. The SAE and ISO have suggested that frequencies between 4 Hz and 8 Hz cause the most discomfort to humans [15, 16]. Figure 42 below gives the vertical acceleration ISO tolerance curves at different exposure times.

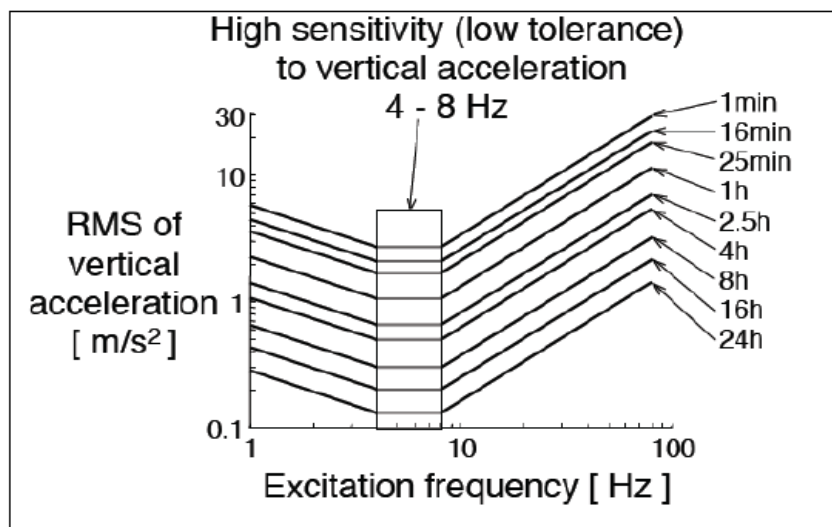


Figure 42: ISO 2631 tolerance curves [16].

It can be seen from the figure that the ability to withstand higher RMS value of accelerations increase, with the reduction in exposure time. In the Results and Discussion section below, the RMS values of acceleration for the frequencies between 4 Hz and 8 Hz will be presented at different tyre pressures.

4 Results and Discussion

This section presents all the results obtained from the simulation of the three vehicle models, namely the QSS model, the two-track model and the four DOF half-car model. Using these results, the influence of inflation pressure on the fuel consumption, vehicle ride and handling are discussed. Few personal inferences are also made to help correlate the results between the vehicle models and the real vehicle.

4.1 QSS vehicle model: Fuel estimation

In this section all the results from the simulation of the QSS full vehicle model is presented. First, fuel consumption estimations from the two RR models are compared to each other using the NEDC city driving cycle. This is done to illustrate the importance of including all the relevant tyre operating parameters, such as vehicle speed, load and tyre pressure, when estimating the fuel consumption. Second, the contribution of tyre RR to the overall fuel consumption of the vehicle is evaluated for the NEDC city driving cycle. Finally, the influence of tyre pressure on the rolling resistance is evaluated and discussed.

4.1.1 Contribution of rolling resistance to overall fuel consumption

Tyre manufacturers, even today, compare the RR of tyres using their coefficient of RR, C_{RR} values. However these C_{RR} values, as mentioned earlier in literature review, are determined from a RR model in which the RR force is defined as a linear function of load i.e., $F_{RR} = f(\text{load})$. This model, which will be referred to as RR-I in this section, does not account for the effects of other tyre operating parameters such as vehicle speed, inflation pressure etc, on the RR of tyres. Hence, this model will be compared against another model, RR-II, which accounts for the influence of vehicle speed, load and inflation pressure on RR of tyres. RR-II has already been defined earlier in Section 3.1.2 under the name of Model 3. Table 3 shows the fuel consumption estimates obtained for the two RR models from the QSS vehicle model.

Table 3: Comparison of fuel consumption for two RR models.

<i>RR Model No.</i>	<i>Fuel Consumption [L/100km]</i>
<i>RR-I</i>	11.77
<i>RR-II</i>	11.68

In the above Table 3, the tyre inflation pressure in both models are set to 2.2 bars and the vehicle's curb weight is assumed to be evenly distributed among the four tyres. It can be seen that the estimated fuel consumption is 1.1 % lower in model RR-II as compared to RR-I. Although the difference observed is small in this case, the fuel estimations can differ considerably depending on the choice of driving cycle and accuracy of tyre data provided. Figure 43 shows the difference between the two models, RR-I and RR-II. In this figure the load and tyre pressure is kept constant at 438 kg and 2.2 bar, respectively.

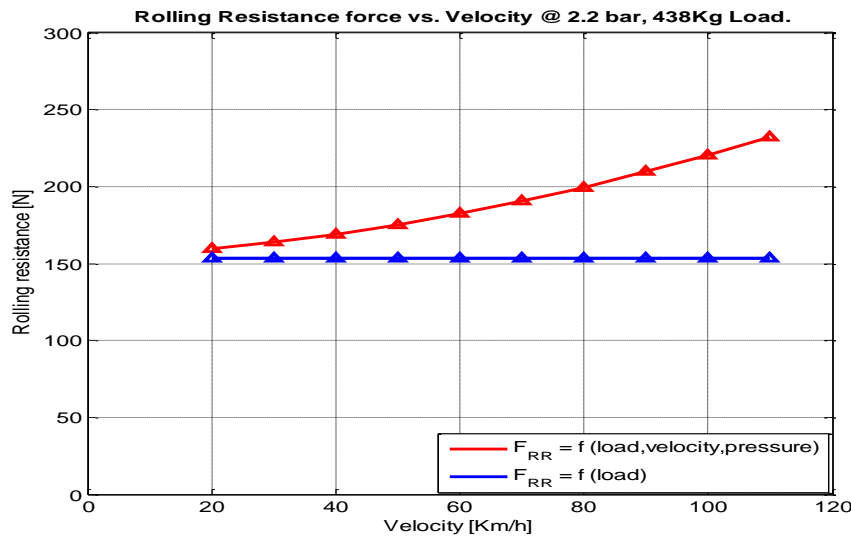


Figure 43: Difference between two rolling resistance models.

The red curve corresponds to model RR-II and the blue curve to RR-I. For a fixed load and inflation pressure, the RR force increases with velocity for RR-II while the RR force is unaffected by velocity for model RR-I. Table 4 below shows the effect of reducing rolling resistance by 10% on the corresponding change in fuel consumption estimation.

Table 4: Estimation of fuel consumption for two different RR models.

<i>RR Model No.</i>	<i>Fuel Consumption</i> [L/100km]	<i>Fuel Consumption- with 10% reduction in RR.</i> [L/100km]	<i>Percentage reduction</i> [%]
<i>RR-I</i>	11.80	11.64	1.355
<i>RR-II</i>	11.68	11.31	3.167

For the RR-I model, the fuel consumption had reduced by 1.36 %. However, for the non-linear model described by RR-II, a fuel consumption reduction of 3.17 % was observed for the same 10 % reduction in RR. According to sources [4, 19] and others, a 10 % reduction in RR can bring about 2 % reduction in the fuel consumption. Whether this 2 % estimation was made at fixed values of speed, vertical load and pressure is not clearly specified in the references, though it wouldn't be surprising if it were so. However, from the results in Table 4, it may be safely concluded that the usage RR-I model in a full vehicle model could lead to the overestimation of fuel savings obtained. Thus, it is imperative that tyre RR be accurately modelled for better estimation of fuel consumption.

Using the QSS model, the contribution of RR force to the total fuel consumption of a vehicle is determined for the NEDC city driving cycle. Figure 44 shows the percentage break-up of the fuel consumption due to each of the three resistive forces acting on the vehicle.

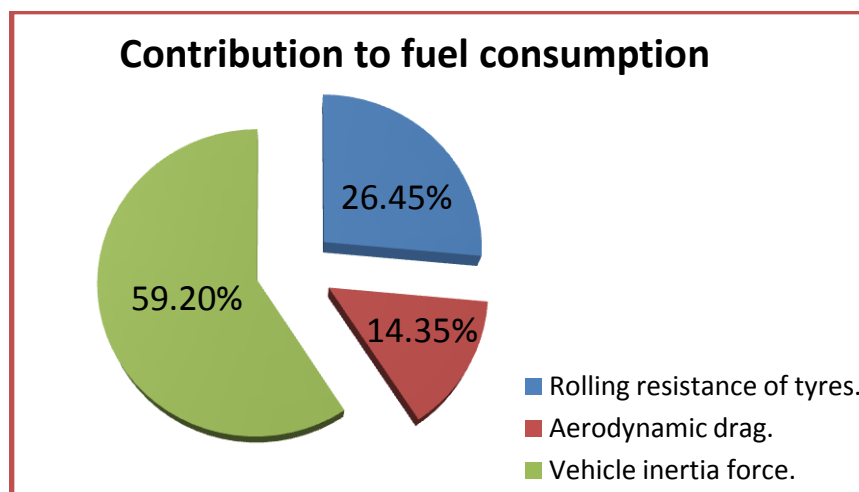


Figure 44: Factors contributing to fuel consumption for a NEDC city driving cycle.

It can be clearly seen that the RR of tyres contribute to nearly 27 % of the overall fuel consumption. Thus, any attempt at improving the fuel economy of a vehicle, without major vehicle redesign or resorting to exotic materials, should begin at the tyres. However, the entire 27 % may not be accessible for improving the vehicle's fuel efficiency with the current materials and technologies used in pneumatic tyres. Also, any changes made to the tyres to reduce its RR should not affect the tyre performance.

4.1.2 Influence of tyre pressure on rolling resistance

The QSS complete vehicle model used in this thesis work is capable of predicting fuel consumption of the vehicle between the inflation pressures of 2 and 3 bars. Among other standard inputs to the vehicle block (shown in Figure 24, Section 3.1.3), the block had been modified to accept tyre pressure and vertical load as inputs to the

vehicle model. Figure 45 shows the variation of rolling resistance of tyres with change in tyre inflation pressure.

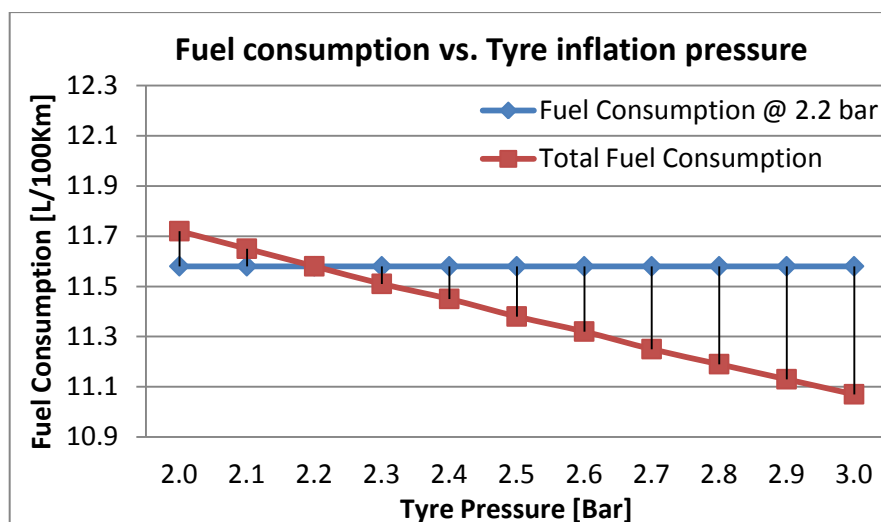


Figure 45: Influence of tyre pressure on fuel consumption.

The blue line (diamond markers) correspond to the fuel consumption at nominal pressure of 2.2 bar. The red curve (square markers) show the actual variation of fuel consumption with tyre inflation pressure. It can be seen that the fuel consumption reduces with increase in pressure. This is consistent with the findings in literature review. Between the pressure range of 2 bar and 3 bar fuel reduction of 5.2 % was observed. Here, it was assumed that the loaded tyre radius increases by 16 mm between pressure of 2 bar and 3 bar.

In reality, it may not possible to achieve such high value since the losses due to slippage has not been included. When the tyre losses were included in the simulation for the NEDC city cycle at an inflation pressure of 2.2 bar, the fuel consumption increased from 11.68 L/100km to 11.71 L/100km, indicating an increase of only 0.25%.

The reduction in fuel consumption with the increase in pressure can be observed even beyond 3 bars. However, this will be at the expense of reduced ride quality, poor traction and increased uneven tyre wear. Since the last three decades, tyre manufacturers have been constantly increasing the operating pressure of tyres to reduce the RR while simultaneously improving the tyre performance and ride comfort. In the next two sub-chapters the influence of tyre pressure on vehicle handling and ride quality will be evaluated.

4.2 Two track model

This section presents all the results obtained from the simulation of the MF-Tyre two-track vehicle model. The vehicle model is subjected to a step input, a ramp input and a SWD input for the seven tyre pressure Cases mentioned in Section 3.2.3. The vehicle's response to the step and ramp input are examined at three different velocities; 80 km/h, 60 km/h and 40 km/h on two surfaces; dry and wet. The results for the SWD manoeuvre test are also presented for the two surfaces but only at a test speed of 80 km/h.

4.2.1 Vehicle response to a step input

In this sub-section, the vehicle's yaw response and corresponding global displacement is presented for two surfaces, at two different velocities; 40 km/h and 80 km/h (results for 60 km/h are presented in Appendix I). Yaw rate may be defined as the rate of change of angular displacement of a vehicle about a vertical axis, perpendicular to the road and passing through the vehicle's COG. Yaw response on the other hand is the rate of change of yaw rate and it can be determined at any point on the yaw rate versus time plot, by the slope at that point.

Dry surface

Figure 46 to 51 give the vehicle's yaw response and the corresponding global displacements for the seven Cases on a dry surface at two velocities, 80 km/h and 40 km/h.

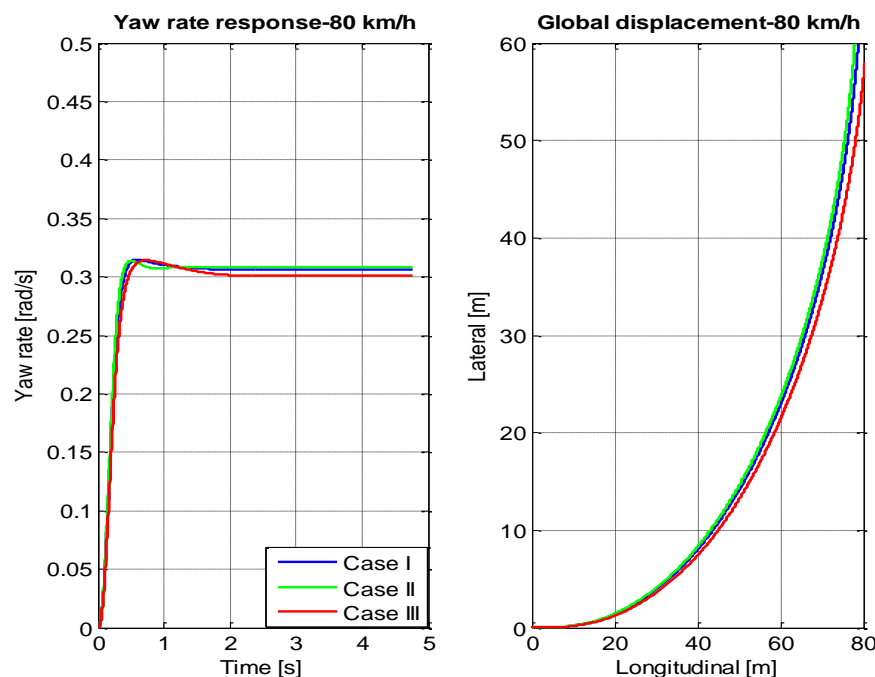


Figure 46: Yaw response to a step input at 80 km/h on dry surface and Cases I,II and III.

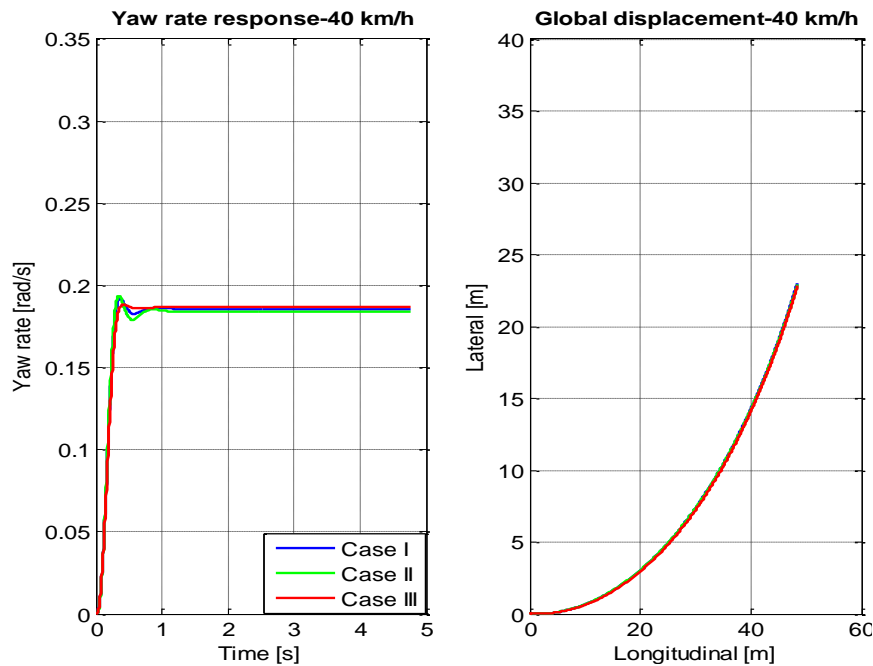


Figure 47: Yaw response to a step input at 80 km/h on dry surface on Cases I, II and III.

From Figures 46, 47 and 83 (in Appendix I), it can be concluded that the initial yaw response (rate of change of yaw rate) is better for Case II than Cases I and III. The impact this has on the turning capability can be seen from its global displacement plots, where the vehicle with lower tyre pressure is seen to turn marginally better, immediately after the application of the step input. This distinction is clearer at higher vehicle speeds.

Although the vehicle's initial yaw response is better with low pressure tyres, it takes longer to reach a steady state, especially at lower speeds of 40 km/h and 60 km/h (see Figures 47 and 83). The yaw rate reaches a peak and oscillates about a steady state value before reaching the steady state. However, at higher speed this trend is reversed, with Case III taking longer to reach steady state than Case II or Case I. This oscillation may be interpreted as a weaving motion, thereby affecting driver's confidence. Increasing the tyre pressure has a damping effect on these oscillations. For Cases I, II and III, the gain in lateral displacement versus longitudinal displacement is marginal, especially at lower speeds, making it inefficient to use a dynamic TPRS to change the vehicle trajectory.

Figure 48, 49 and 84 (in Appendix I) show the yaw response and the corresponding global displacements for Cases IV and V in comparison to Case I. Case IV shows better yaw response and a higher peak yaw rate than Case I and Case V at the three velocities. However at 80 km/h (see Figure 48), the yaw rate of Case IV vehicle does not reach steady state and continues to increase in magnitude even after the completion of the step input. The corresponding global displacement curve however, did not show any drastic change in turn radius. When Case IV was subjected to a ramp input, its yaw response showed a steady increase as expected (see Figure 86 in

Appendix I). Thus, the vehicle behaviour needs to be investigated further for Case IV at 80 km/h. However, at low to medium speeds, having high pressure on outer wheels and low pressure on inner wheels gave the vehicle noticeably improved turning capability.

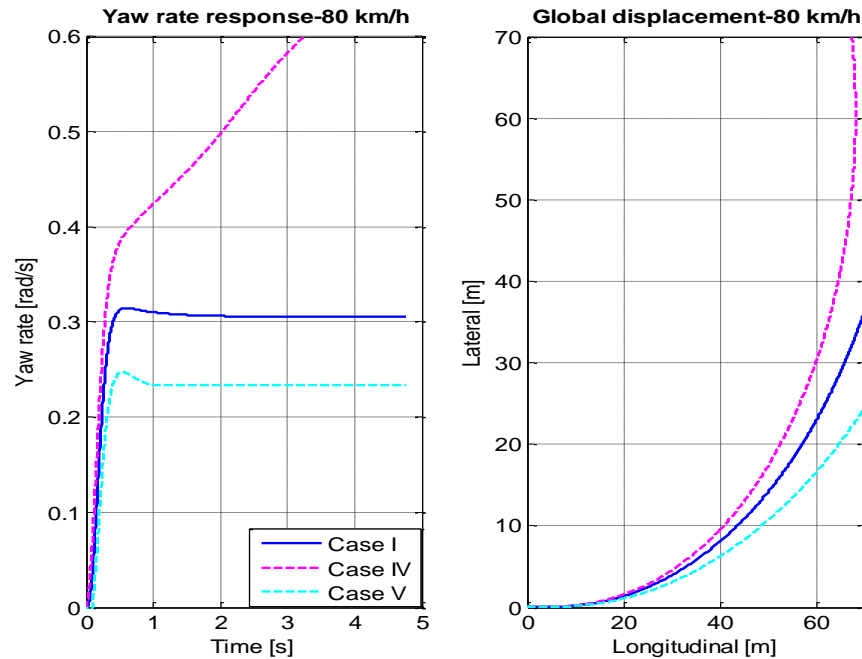


Figure 48: Yaw response to a step input at 80 km/h on dry surface on Cases I, IV and V.

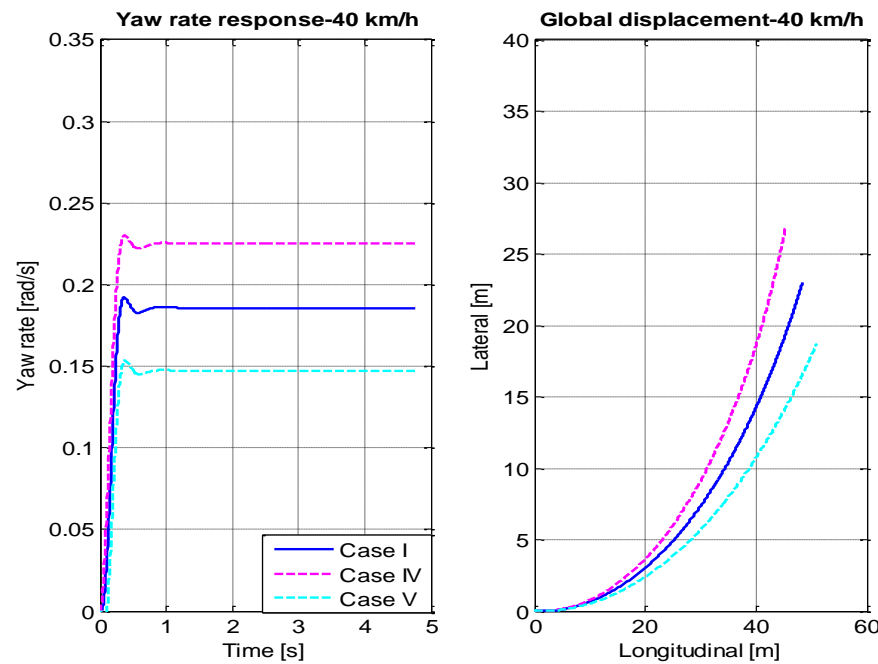


Figure 49: Yaw response to a step input at 40 km/h on dry surface on Cases I, IV and V.

Figure 50 and 51 show the yaw response and global displacement results of Cases A and B at 80 km/h and 40 km/h. The blue curve corresponds to Case I and is used for comparison.

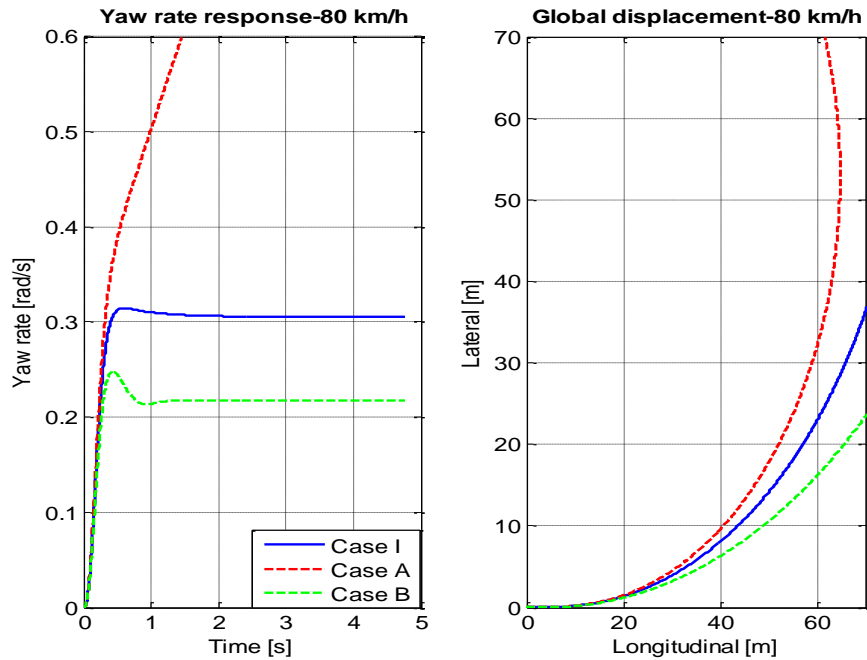


Figure 50: Yaw response to a step input at 80 km/h on dry surface for Cases I,A and B.

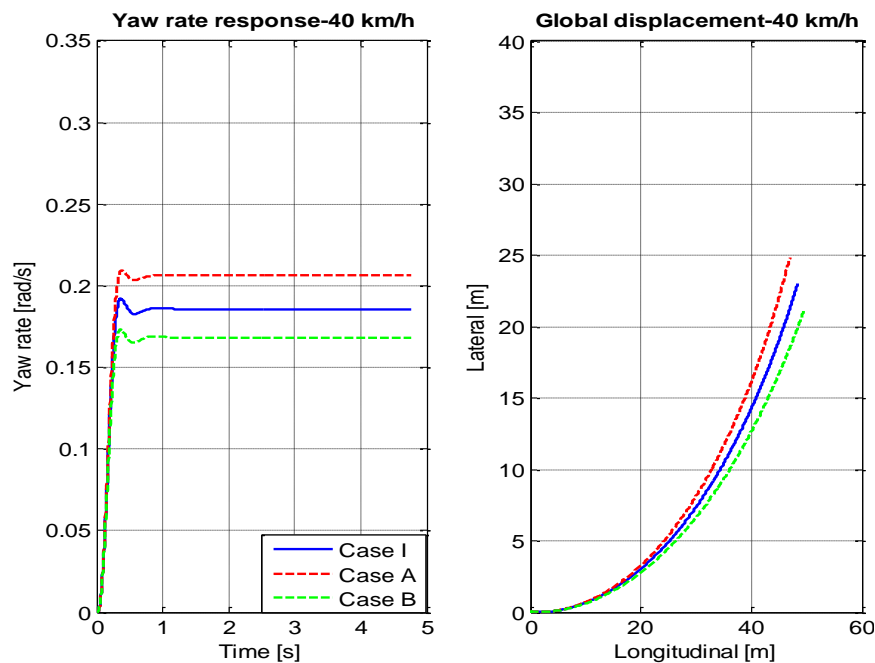


Figure 51: Yaw response to a step input at 40 km/h on dry surface for Cases I, A and B.

Unlike the earlier Cases, there are no clear trends visible for the yaw response of Cases A and B. A closer look at the figures, show that Case B has better yaw response

immediately after the application of step input. However, a quarter second later Case A shows better yaw response than Cases I and B. Case A also exhibits higher peak yaw rate at both velocities thus giving higher lateral displacement with the passage of time. At 80 km/h however, the yaw rate of Case A is similar to Case IV does not achieve a steady state and continues to increase steadily. However, the nature of this steady rising yaw rate needs to be examined further before concluding this Case as un-safe. Figure 86 in Appendix I shows the vehicle's yaw response to a ramp input, where the yaw rate increases steadily with the ramp input as expected.

From results shown in Figures 46 to 51 and Figures 83 to 86 in Appendix I, it may be concluded that by changing the tyre pressure between the front and rear wheels and/or inner or outer wheels, it is possible to change the handling characteristics of the vehicle in a turning manoeuvre. Thus, if a dynamic TPRS was to be used to improve the vehicle's cornering capability (assuming that the initial tyre pressure is higher than nominal, to take advantage of improved fuel economy), then Case IV or Case A tyre pressure setting could be used to take advantage of the improved turning i.e., either the inner wheel pressure could be reduced or the front wheel pressures could be reduced. If the dynamic TPRS could be designed to responds quick enough, it could be used in a safety critical situation to avoid an obstacle in the path of the vehicle.

Wet surface

Figure 52 to 57 show the yaw response and corresponding global displacements of a vehicle on wet surface at two velocities of 80 km/h and 40 km/h. As mentioned earlier, the wet surface is modelled by assuming reduced longitudinal and lateral peak friction coefficient and does not explicitly account for factors such as tyre tread design, tread depth, standing water height, tyre carcass compliance etc.

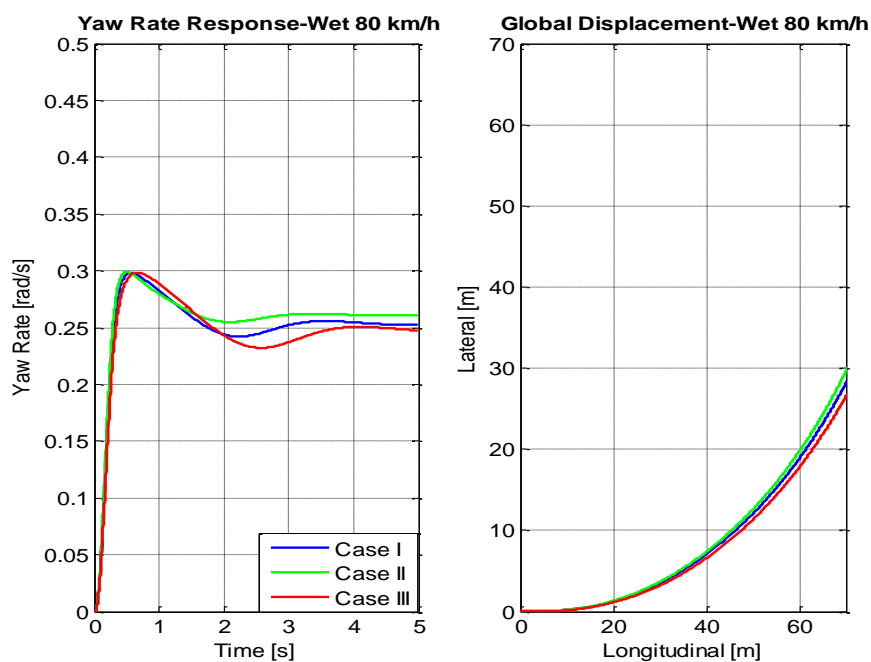


Figure 52: Yaw response to a step input at 80 km/h on wet surface for Cases I, II and III.

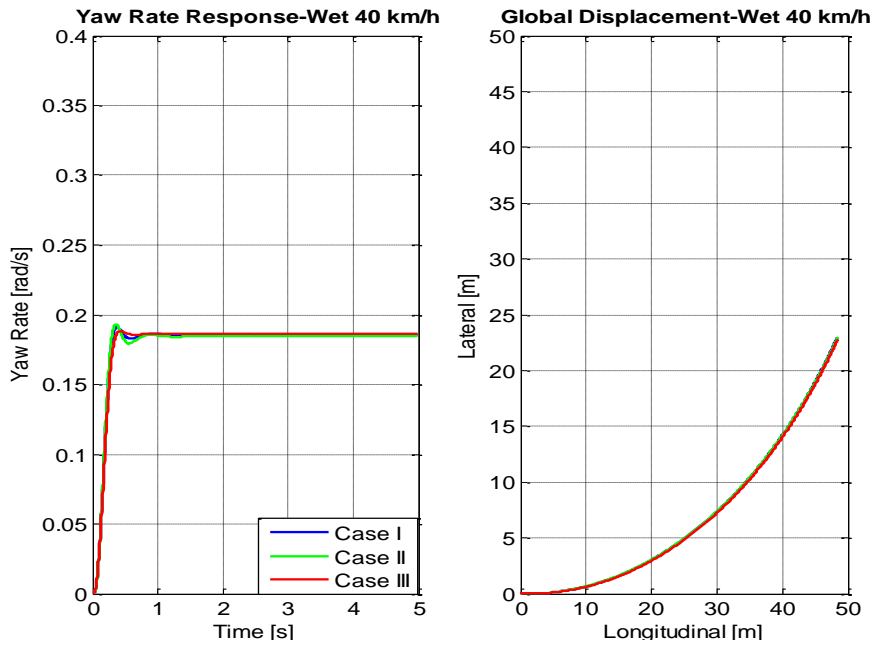


Figure 53: Yaw response to a step input at 40 km/h on wet surface for Cases I, II and III.

Figure 52, 53 and 87 (in Appendix I) show the yaw response and global displacement results for Case I, II and III on wet surface at three velocities. The trend is similar to that observed on dry surface at the corresponding speeds. However, the difference in the yaw response and global displacement is only marginal for the three Cases. As the vehicle speed increases, the difference between the three Cases become more clear. This may also be attributed to the higher steady state yaw rate for Case II at 80 km/h.

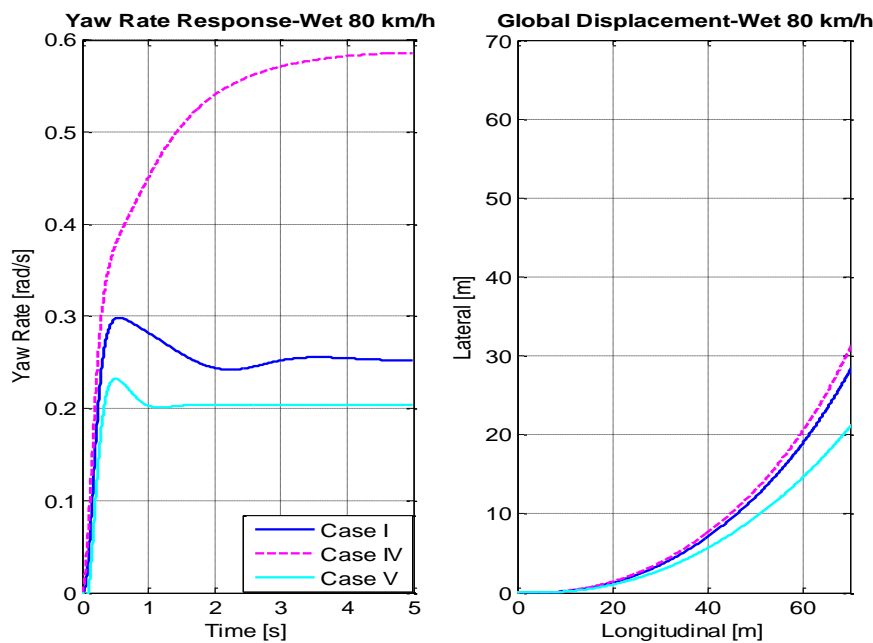


Figure 54: Yaw response to a step input at 80 km/h at wet surface for Cases I, VI and V.

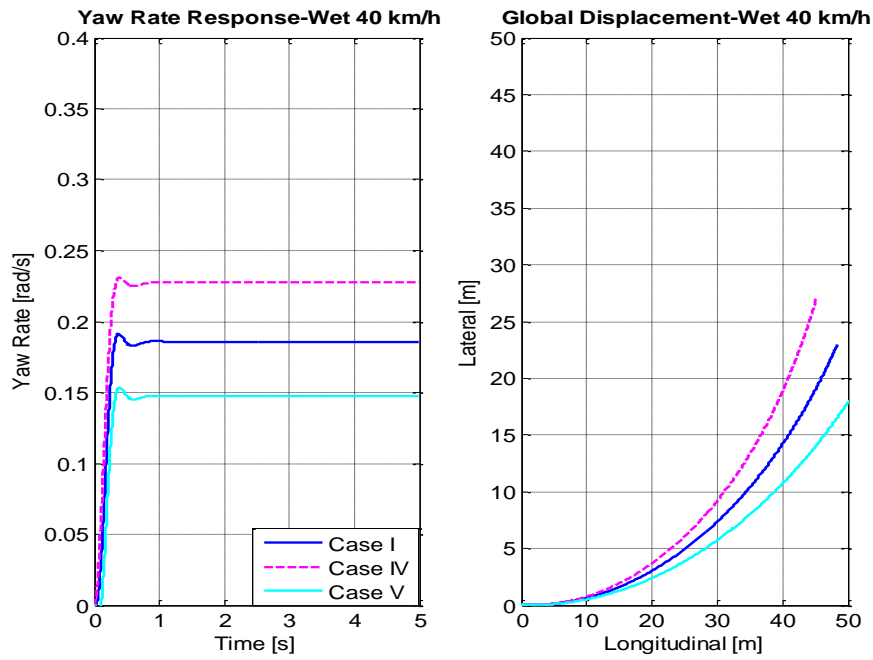


Figure 55: Yaw response to a step input at 40 km/h on wet surface for Cases I, IV and V.

Cases IV and V in Figure 54 and 55 show a trend similar to that seen on dry surface with Case IV showing better yaw response and a higher peak yaw rate than the other Cases. However, at 60 km/h (see Figure 88) and 80 km/h, the yaw rates continue to increase in magnitude even after the completion of the step input manoeuvre. However, their corresponding global displacements do not show a drastic change in the vehicle's trajectory. When Case IV was subjected to a ramp input at these two velocities, it showed a reasonably steady increase in yaw rate as expected (see Figures 90 and 91).

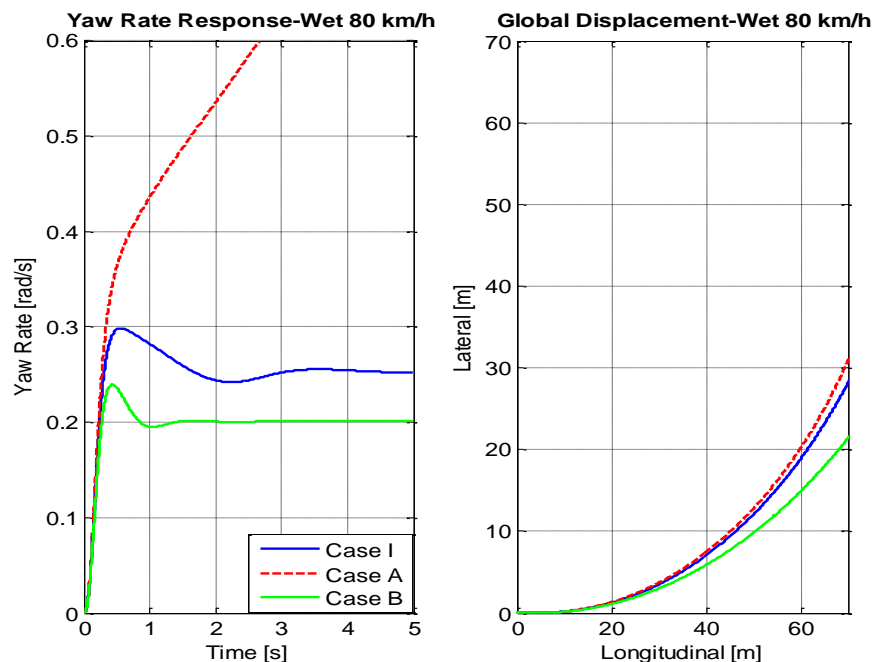


Figure 56: Yaw response to a step input at 80 km/h; Wet surface; Cases I, A and B.

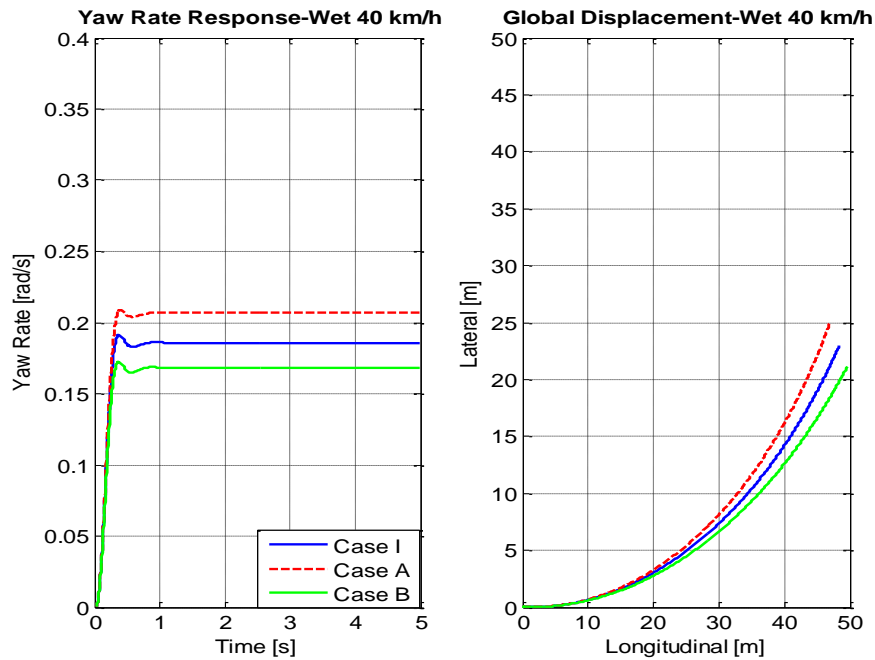


Figure 57: Yaw response to a step input at 40 km/h on wet surface for Cases I,A and B.

Figures 56, 57 and 89 show the yaw responses and corresponding global displacements observed for Cases A and B in comparison to Case I. The results for 40 km/h and 80 km/h are similar to that seen for dry surface. However at 60 km/h, the yaw rate of the Case A vehicle is not stable though no drastic change in trajectory is observed from its global displacement plot. When Case A was subjected to a ramp input at 60 km/h and 80 km/h, it showed a reasonably steady increase in yaw rate (see Figures 90 and 91). From the same figures, also notice that Case I vehicle shows instability, with its yaw rate oscillating instead of reaching a steady state.

So far, it has been shown that having higher pressure on the outer tyres and lower pressure on inner tyres or lower pressure on front wheels and higher on the rear wheels, can help improve the vehicle turning response considerably on both dry and wet surface at higher speeds, where an average car is most likely to under-steer. However, at these speeds, the stability of the yaw rate is a matter of further investigation. The results from step input show that the initial yaw response and turn-in is marginally better for a vehicle with low pressure tyres. In the next sub-section the handling diagrams for the seven Cases is presented. Similar conclusions can be drawn about the vehicle behaviour from these diagrams as well.

4.2.2 Vehicle response to ramp input

The two-track vehicle model is subjected to a ramp input in order to develop the Handling diagram of the vehicle for the seven tyre pressure Cases. In this section the results are presented for two velocities, 40 km/h and 80 km/h on two surfaces; dry and wet. The handling diagram gives the most basic information about the lateral behaviour of a vehicle in a cornering manoeuvre i.e., whether it over-steers or under-

steers. It is obtained by plotting the parameter $(\frac{L}{R} - \delta)$ against the normalised lateral acceleration, $\frac{a_y}{g}$. The slope of the handling curve with respect to the y-axis ($\frac{a_y}{g}$) gives the under-steer coefficient, κ_{us} of the vehicle. For more information on the construction of handling diagrams and its usage, the reader may be referred to [13, 14, 15].

Handling diagrams for dry surface

Figure 58 to 61 shows the handling diagrams for all the seven Cases at two velocities, 80 km/h and 40 km/h on dry surface.

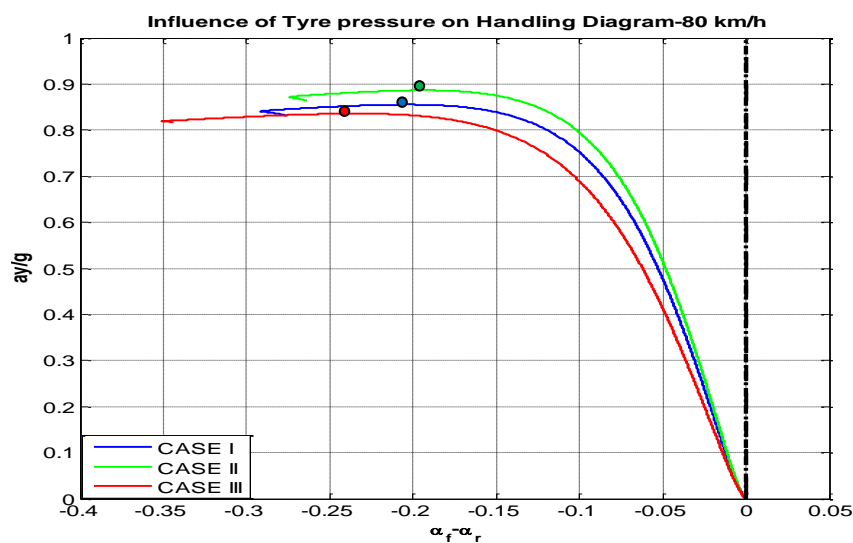


Figure 58: Handling Diagram for 80 km/h of dry surface for Cases I, II and III

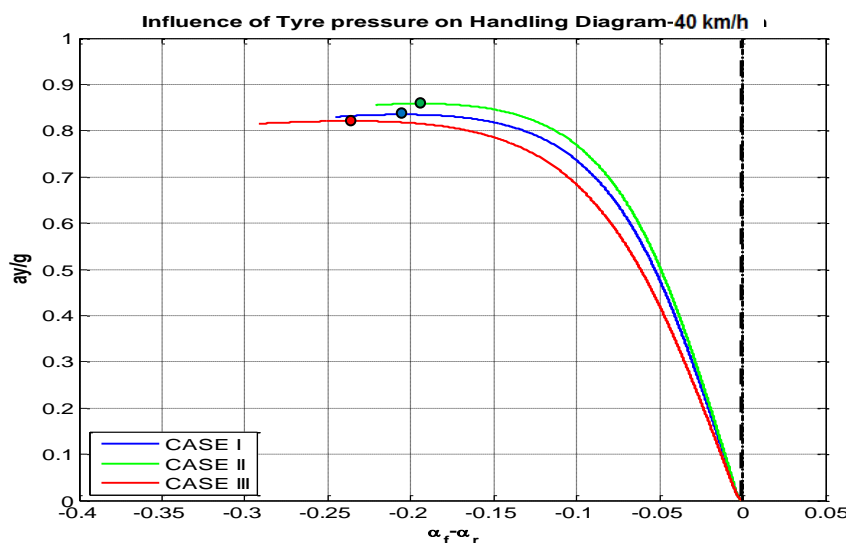


Figure 59: Handling Diagram for 40 km/h on dry surface for Cases I, II and III.

The results for 60 km/h are shown in Appendix I by Figures 92 and 93. The points shown in the handling diagrams, where the slope to the curve is infinity with respect to $\frac{a_y}{g}$ axis, indicate the loss of grip on the front axle. From Figures 58 and 59, three clear trends are visible at the two velocities. Firstly, Case II exhibits a lower under-steer coefficient κ_{us} compared to Cases I and III. Secondly, the peak lateral acceleration attained is higher for the vehicle with lower pressure tyres. Thirdly, the instability points (indicated by the points in the figures) occurs at a lower delta slip value at lower tyre pressure. These findings are consistent with the results obtained for the corresponding yaw responses and global displacements for a step input.

Figures 60 and 61 below, shows the handling diagram for the special Cases in comparison with the nominal Case I. Case V appears to show lower κ_{us} than Cases I and IV. However, a closer look at Case V curve near the origin reveals an anomaly in the expected handling diagram behaviour. The curve first crosses over to the right of the neutral steer axis and then changes direction to follow the same shape as other curves. This behaviour may be due to the fact that an initial yaw rate was observed for the vehicle, even before the ramp input was applied. This initial yaw rate may be attributed to the difference in forces generated due the difference in tyre pressures on the inner and outer wheels (refer Section 4.3.2). Leaving aside this anomaly, Cases IV and A exhibit lower κ_{us} than the nominal Case I at both velocities facilitating a better turn. These observations are consistent with the results obtained from the step input.

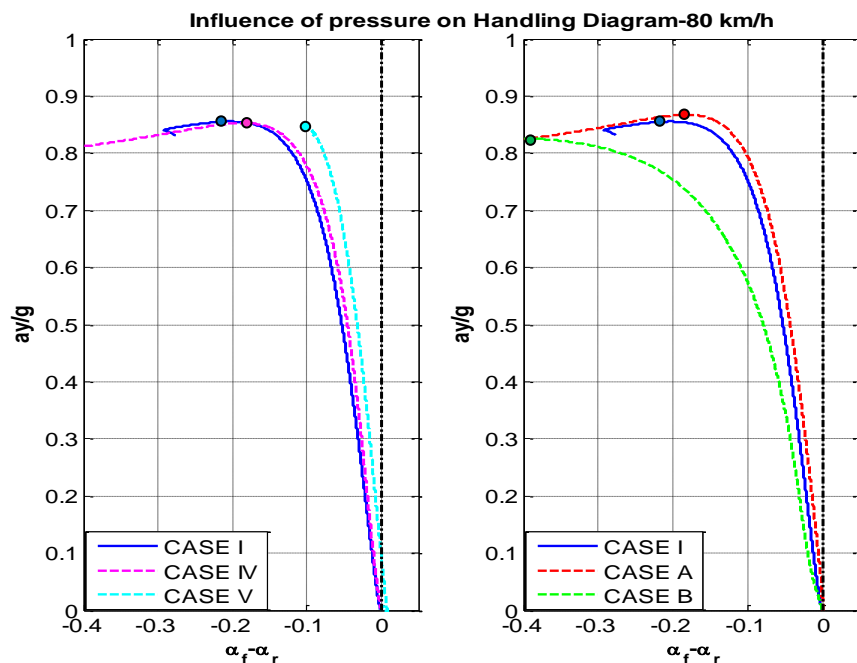


Figure 60: Handling Diagram for 80 km/h on dry surface on Cases I, IV, V, A and B.

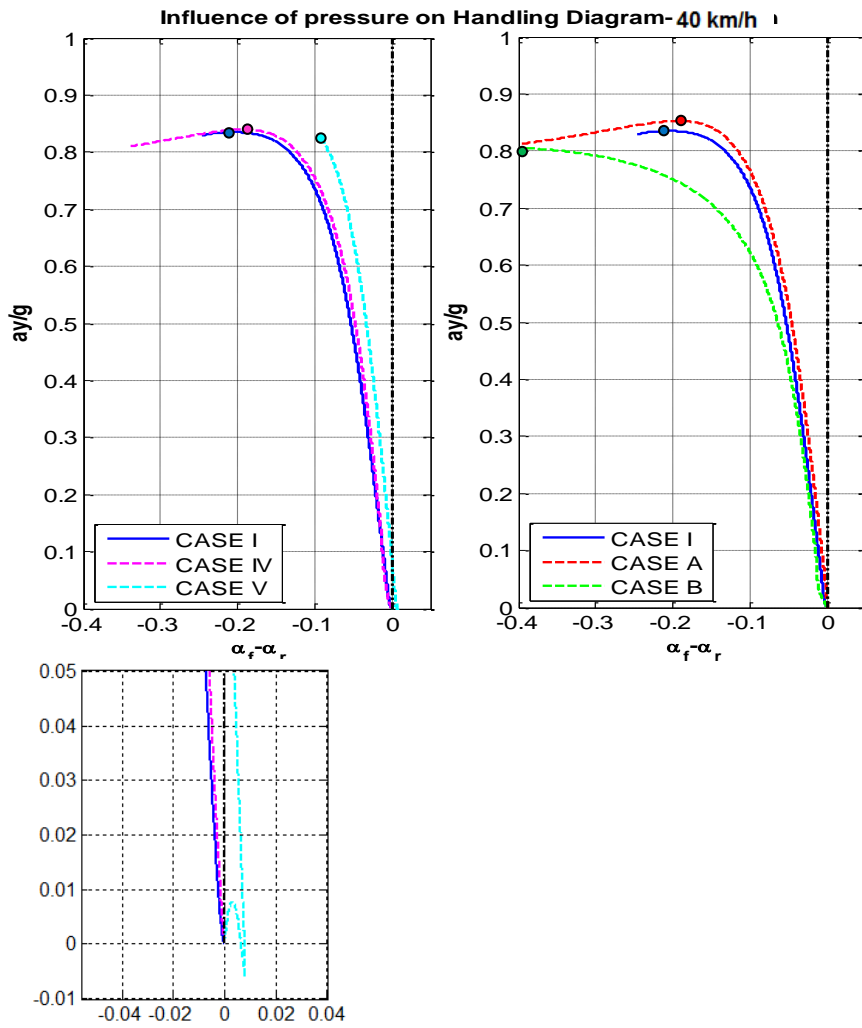


Figure 61: Handling Diagram for 40 km/h on dry surface for Cases I, IV, V, A and B.

Handling diagrams for wet surface

Figures 62 to 65 show the handling diagrams for the seven Cases on wet surface at velocities of 40 km/h and 80 km/h. The handling diagram for 60 km/h is given in Appendix I. Cases I, II and III in Figures 61 and 62 exhibit a trend similar to that observed on dry surface, with Case II vehicle exhibiting lower κ_{US} , higher lateral acceleration and instability at lower slip value.

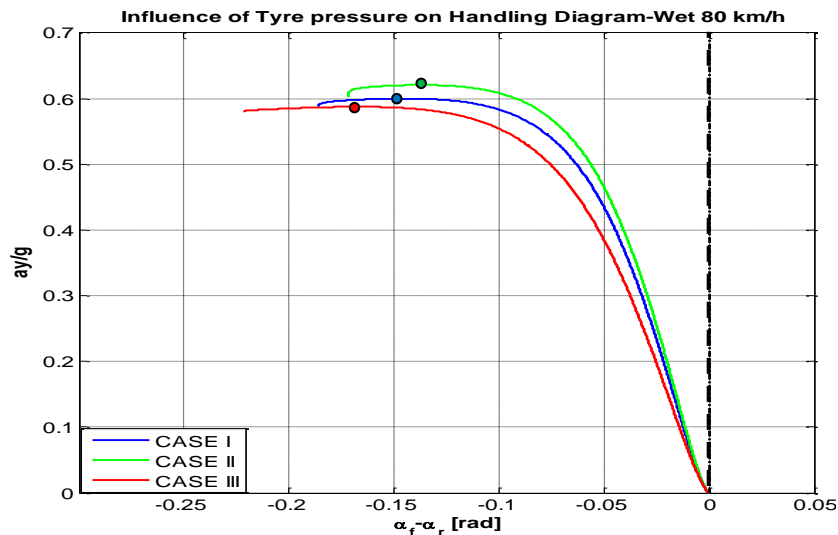


Figure 62: Handling diagram for 80 km/h on wet surface for Cases I, II and III.

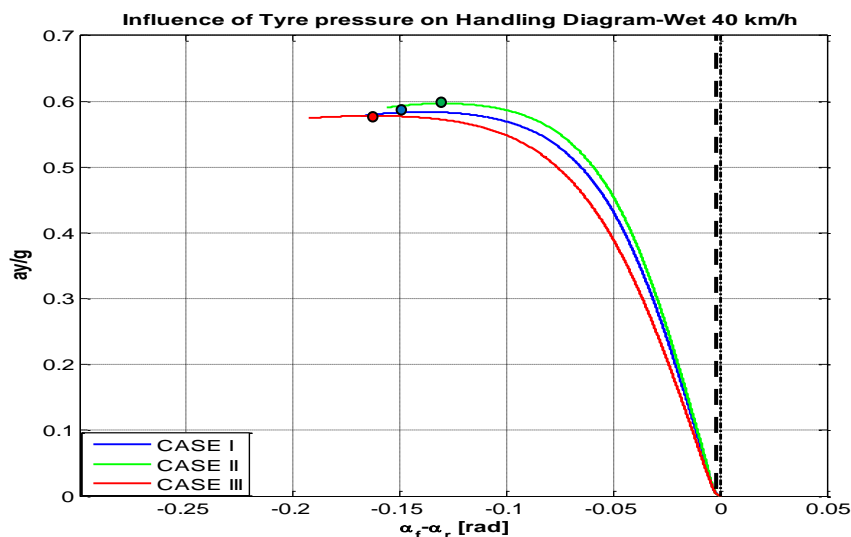


Figure 63: Handling diagram for 40 km/h on wet surface for Cases I, II and III.

Figures 64 and 65 show the handling diagrams for the special Cases in comparison to the nominal Case I. Cases IV and V shows trends similar to that seen on dry surface at the three velocities. However, Case B exhibits lower κ_{US} compared to Case A,

which should translate to the vehicle having a better turning capability. But from the yaw response and global displacement results for Case B, it can be seen that this is not true (see Figures 56 and 57). The instability point occurs at very low value delta slip for Case B and hence it may be concluded that the vehicle is highly unstable in cornering.

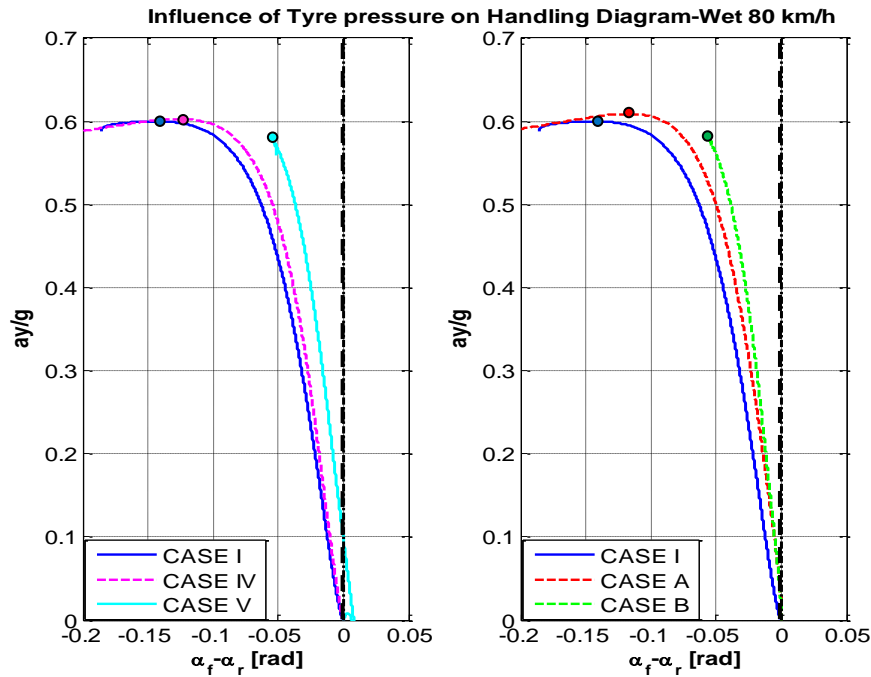


Figure 64: Handling Diagram for 80 km/h on wet surface for Cases I, IV, V, A and B.

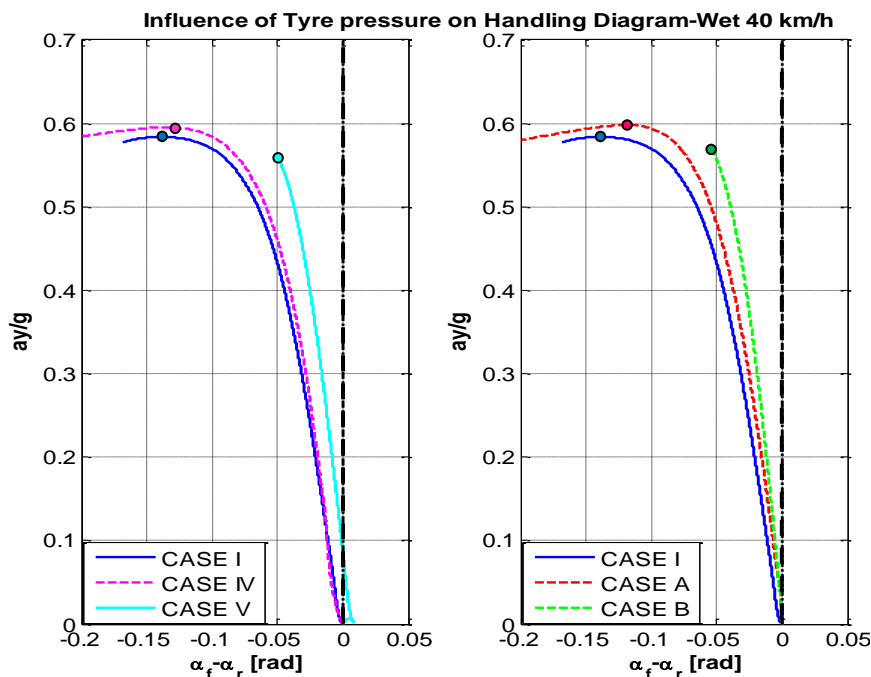


Figure 65: Handling Diagram for 40 km/h on wet surface for Cases I, IV, V, A and B.

4.2.3 Sine-With-Dwell input

This section presents the yaw response of the two-track vehicle model to the SWD input. As mentioned earlier, only some parts of the official NHTSA SWD test specifications were borrowed to illustrate the nature of vehicle's response for the different tyre pressures Cases. For Cases I, II, III, A and B, performing this test will illustrate the yaw stability of the vehicle in comparison to the nominal case, Case I. However, for Cases IV and V, this test only shows the nature of yaw stability of the vehicle if the TPRS system were to fail immediately after the first turn of the steering, at the beginning of the SWD manoeuvre.

Dry Surface

First, the vehicle with tyres at nominal pressure Case I, is subjected to the SWD input. Then using the stability and manoeuvrability criteria of the SWD test, the maximum steering wheel angle for which the vehicle is stable is determined. Using this methodology, the maximum steering stable wheel angle was found to be 72 degrees on the dry surface. Figures 66 to 68 show the yaw response to the SWD input at all the seven Cases. The blue curve in each figure represents the nominal tyre pressure case, Case I, and the vertical lines (black double-dash) indicate the time where the two stability criteria are measured.

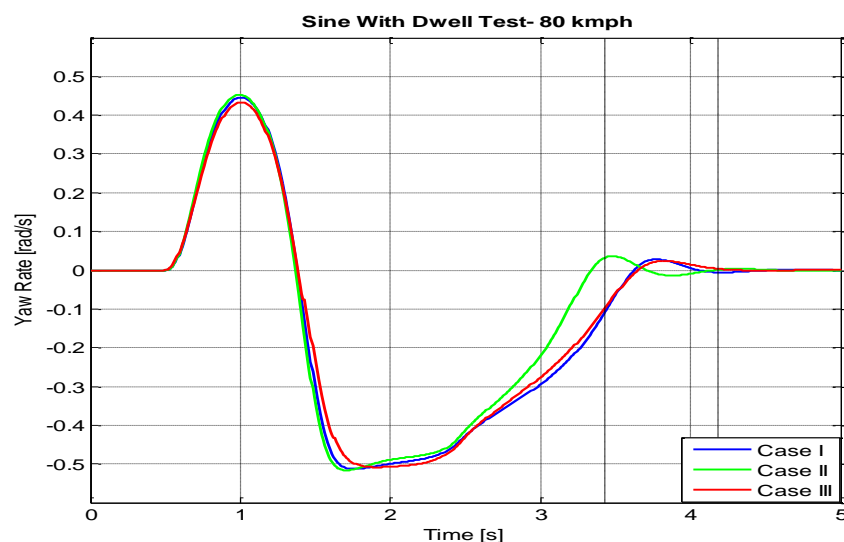


Figure 66: Yaw rate versus time for the SWD manoeuvre on dry surface for Cases I, II and III.

For Cases I, II and III, it can be seen that the yaw stability is better for the vehicle with lower pressure tyres (Case II) as the yaw rate approaches zero quicker than Cases I and III. It can also be seen that Case II has marginally better yaw response and higher peak yaw rate at the first peak, which is consistent with the findings for the yaw response to a step input. However, Case II shows a slight oscillating trend before reaching a steady-state. This may be interpreted as vehicle weaving from the driver's

perspective and could affect the driver's confidence in the vehicle's stability even though it gives a better response than the vehicle with nominal tyre pressure.

As the tyre pressure is increased it can be seen to have a damping like effect on the yaw response as it reaches the steady state value. Thus, such a weave may be corrected with a dynamic TPRS (this is only a hypothesis and hence needs to be validated through testing). It should be mentioned here that the tyre carcass compliance was not modelled into the vehicle model and hence it is possible to have result different to what is shown in Figure 66, especially for the low pressure results since tyre carcass compliance increases with decrease in tyre pressure. Table 5, gives the stability and manoeuvrability values for all the Cases. It can be seen that Cases I, II and III pass all the stability and manoeuvrability criterion.

Table 5: SWD stability and manoeuvrability criterions on dry surface.

Tyre Pressure	Peak yaw rate [rad]	Criterion I < 35%		Criterion I < 20%		Manoeuvrability Criterion $I < 1.83$ [meters]
		Yaw rate [rad]	%	Yaw rate [rad]	%	
<i>Case I</i>	- 0.513	- 0.11	21.4	- 0.005	0.01	2.312
<i>Case II</i>	- 0.516	0.032	6.20	0	0	2.424
<i>Case III</i>	-0.508	-0.089	17.5	0.003	0.06	2.10
<i>Case IV</i>	-0.477	0.057	11.9	0.060	12.5	3.293
<i>Case V</i>	No peak	-	+100	-	+100	1.172
<i>Case A</i>	No peak	-	+100	-	+100	2.643
<i>Case B</i>	-0.398	0.002	0.005	0	0	1.908

In Figure 67, it can be seen that Case IV gives significantly better yaw response than the nominal case, Case I. Case V shows both poor response and an unstable yaw response that diverges away from stability. However, for Cases IV and V, there are shifts in the initial yaw rate even before the start of the SWD manoeuvre. This shift may be attributed to a combination of two factors. Firstly, the tyre forces are a function of inflation pressure, with higher lateral force and RR force observed at lower pressures. Secondly, the MF-Tyre model used in this vehicle model uses combined slip to calculate the forces and moments at the tyres. It is believed that the limitation of available friction at the tyre-road interface gives rise to this shift.

As mentioned earlier, MF tyre model provides the option to calculate the tyre forces as a function of pure lateral slip, pure longitudinal slip or combined slip. When the SWD test was re-run with the tyre model calculating forces and moments based on lateral slip alone, the yaw rate shift had disappeared and the entire yaw response had changed for the exact same test conditions (this is shown in Figure 80 in the Appendix I). Thus, in Case IV, the vehicle has a positive yaw rate (in the direction of the turn) even before the start of the manoeuvre and for Case V, there is an initial negative yaw rate (opposite to the direction of turn). From Table 5, it can be seen that Case IV meets both stability and manoeuvrability criteria, whereas Case V does not meet either criteria.

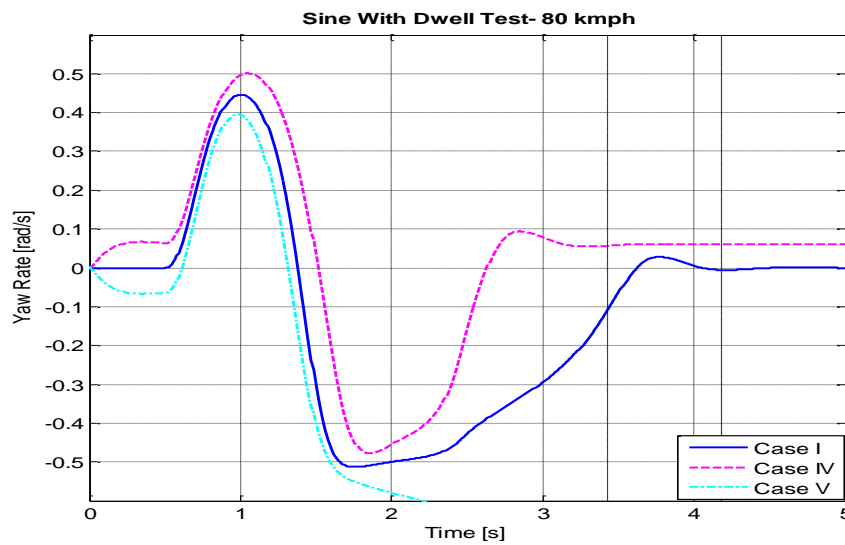


Figure 67: Yaw rate versus time for the SWD manoeuvre on dry surface for Cases I, IV and V.

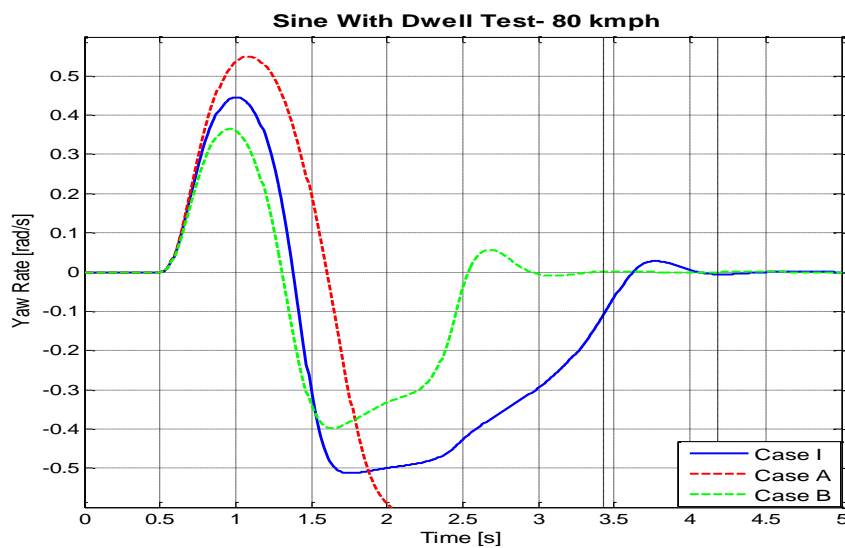


Figure 68: Yaw rate versus time for SWD manoeuvre on dry surface for Cases I, A and B.

From Figure 68, it can be seen that Case A gives an unstable yaw response to the SWD input. However, from the yaw response results obtained from the step input it was concluded that Case A provided better turning capability. Thus, it may be inferred that better turning capability is not always a better choice from the vehicle stability point of view. The SWD response for Case B in Figure 68 shows that vehicle is more stable in cornering when the rear wheels have better grip. However, Case B shows lower peak yaw rate at the first peak compared to Case I. The lateral displacement, needed to satisfy the manoeuvrability criterion of the SWD test, is dependent on the magnitude of yaw rate at the first peak. However, from Table 5 it can be seen that Case B passes the manoeuvrability criterion with a lateral displacement is 1.908 meters, when the minimum requirement is 1.83 meters. Case A on the other hand, shows an unstable yaw response and fails the two stability criterion although it passes the manoeuvrability criterion.

Wet surface

There is no standard test procedure for the SWD manoeuvre on wet surface, especially when the wet surface is only defined by its coefficient of friction values at the tyre-road interface, as mentioned in Section 3.2.3. However, it would be useful to see the change in yaw rate behaviour of the vehicle on wet surface and compare it to the results obtained for dry surface. The test methodology used to develop the yaw responses on wet surface is the same as that used for the dry surface. The stability criterions of dry surface will be borrowed to determine the maximum, stable steering wheel angle on the wet surface. The maximum steering wheel angle was found to be 55 degrees at vehicle speed and inflation pressure of 80 km/h and 2.2 bar, respectively. However, as predicted the dry surface's manoeuvrability criterion could be met with such a small steering wheel angle. Due to these limitations only the nature of yaw rate stability is discussed in this sub section, but not their absolute values.

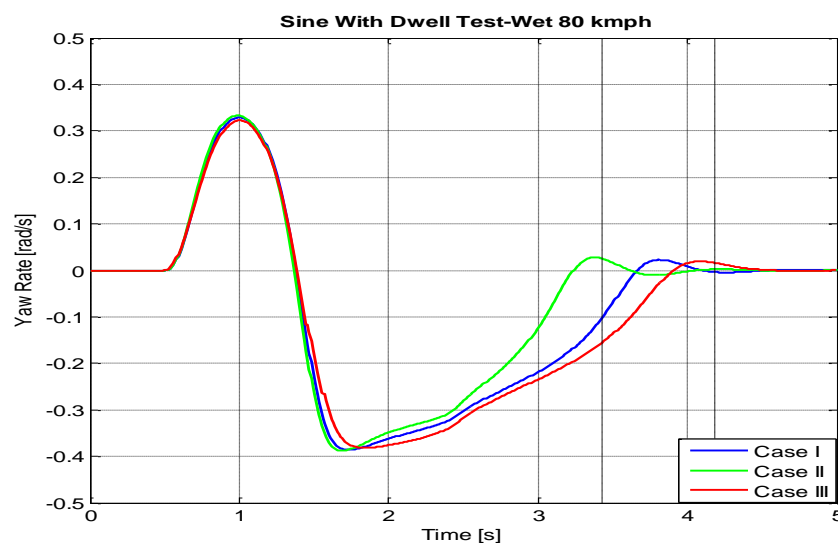


Figure 69: Yaw rate versus time for the SWD manoeuvre on wet surface for Cases I, II and III.

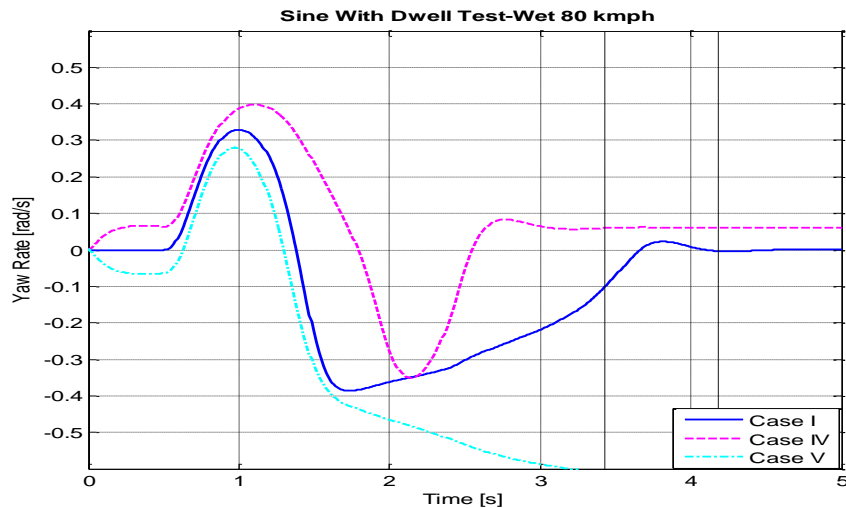


Figure 70: Yaw rate versus time for the SWD manoeuvre on wet surface for Cases I, IV and V.

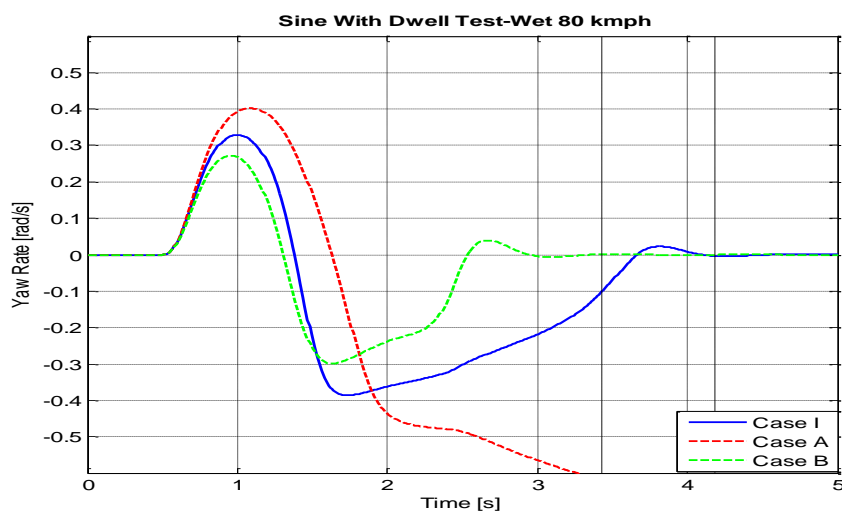


Figure 71: Yaw rate versus time for SWD manoeuvre on wet surface for Cases I, A and B.

Figure 69 to 71 show the yaw responses for the seven Cases on wet surface. The blue curve in the three figures represents the nominal case, Case I. The vertical black double-dash lines show the times where YRR are measured to determine the stability criterions. However, in these figures they have no significance but only serves as a reference.

In Figure 69, Cases I, II and III show the same trend as that observed for dry surface, with Case II showing marginally better yaw response at the first peak and reaching stability earlier than Cases I and III. Thus, from the yaw response results of Cases I, II and III on dry and wet surface, it may be concluded that the vehicle's over-steer stability may be improved by reducing the pressure in the four tyres. However, it must be noted that tyre carcass compliance has not been accounted for in the vehicle model.

From Figure 70 it can be seen that Cases IV and V have yaw responses similar to that seen on dry surface, including the initial shift in yaw rate. Cases A and B in Figure 71

also show trends similar to that seen on dry surface, with Case B exhibiting poor turning capability (lateral displacement versus longitudinal displacement) despite having a stable yaw response.

So far, from the simulation results obtained from the QSS complete vehicle model, it has been established that the rolling resistance of tyres and in turn the overall fuel consumption reduces with increase in tyre inflation pressures. From the step input given to the two-track model, it has been shown that the turning capability is not affected significantly when the tyre pressure is changed from its recommended pressure to high pressure, for low to medium speeds on dry surface. However, at higher speeds and wet surfaces there is noticeable difference in the turn radius. The handling diagram also confirms that the available friction at the tyre-road interface is reduced as the tyre pressure increases.

From the SWD test it was established that the yaw response did not change considerably for Cases II and III from Case I on dry surface. However, on wet surface, the vehicle stability was poorer for Case III compared to Case I. Thus maintaining higher pressure in all four wheels when cornering at higher speeds may not be a safe choice. However, the tyre's carcass compliance has not been considered in the simulation. This trend may even be reversed at some particular low value of tyre pressure, as compliance increases with reduction in pressure.

There are however alternative tyre pressure settings that are favourable to cornering i.e. Case IV and Case A. The results from step input indicate that the vehicle turns better for Cases IV and A. However Case A vehicle over-steered in the SWD test on both the dry and wet surfaces. This is further confirmed by the low under-steer coefficient and early instability point exhibited by Case A from the handling diagrams at 80 km/h, making it a poor choice at high speeds. At lower speeds, up to 60 km/h, Case A is also a safe option to turn better. The effectiveness of Case IV and Case A in providing better turning capability needs to be examined further through experimental data, since tyre carcass compliance had not been included in the simulations and only a linear tyre relaxation behaviour was modelled.

4.3 Four DOF half-car model

In this section the ride behaviour of the vehicle is analysed using the four DOF half-car model. As mentioned in Section 3.3, the model is subjected to a step input, a sinusoidal input and random road surface profile input at the front and rear axle to evaluate the response of the vehicle in both, the time domain and frequency domain. This section presents the results for three tyre pressure test Cases; Case I, Case II and Case III (Case descriptions are given in Section 3.2.3).

4.3.1 Response to step input

Bounce acceleration

Figure 72 shows the bounce acceleration response of the vehicle's sprung mass to a step input for Cases I, II and III. The step size chosen is 0.025 meters (approximation made from Janeway's criterion [15]) and the vehicle speed, 60 km/h.

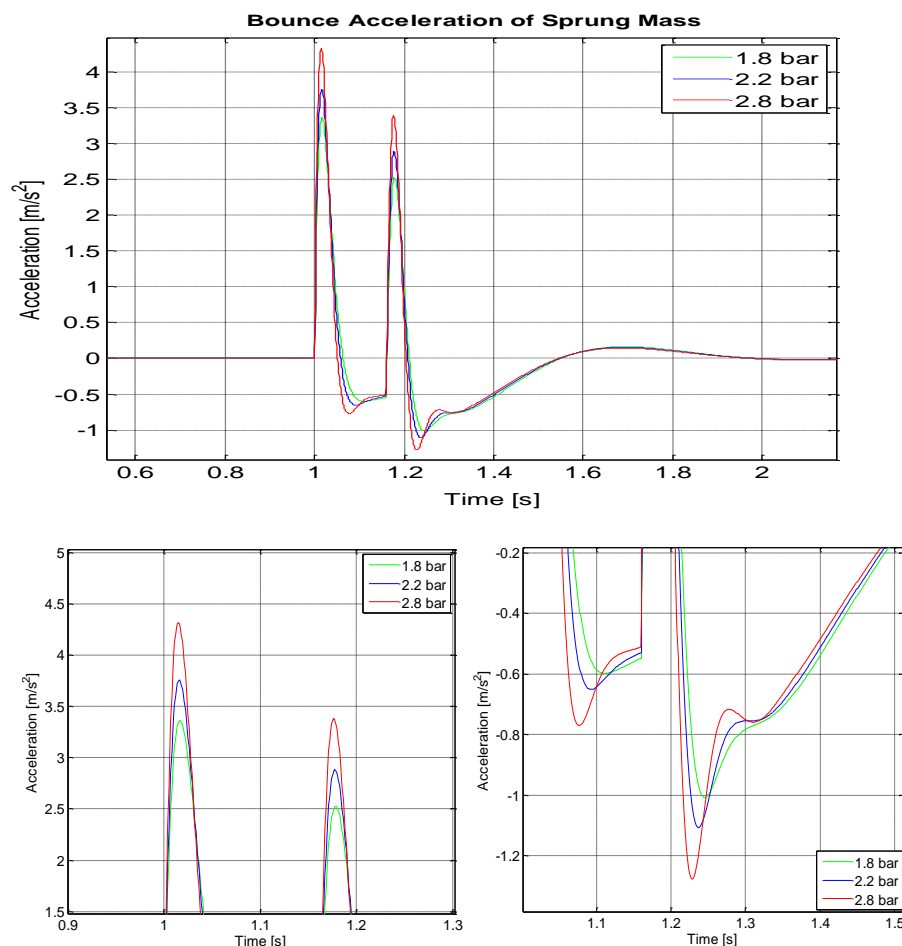


Figure 72: Bounce acceleration of the sprung mass at different pressures.

In Figure 72, the first peak corresponds to the response of front axle passing over the step and the second peak, to that of the rear axle. Closer look at the peaks reveal that the bounce acceleration experienced is higher at higher pressures. Though there is noticeable difference in peak acceleration in the three Cases, the rate of change of acceleration is also higher at high pressure i.e., the retention time of these forces will be lower and will thus be interpreted as a jerk. How this affects the comfort of passengers of different ages and sex is a matter of further investigation. With a proper design of passenger seat, these jerks may be attenuated to a considerable degree.

Bounce displacement

Figure 73, shows the bounce displacement of the sprung mass to a step input at different inflation pressures. A closer look at the peaks reveal that the vertical displacement reduces with increase in tyre pressures. However, the corresponding difference in peak displacement experienced in the three Cases is less than 1 millimetre. It may also be noted that this trend is completely opposite to that observed for bounce acceleration. Table 6 shows the peak accelerations and corresponding peak displacements for the three Cases, for a step input of 0.025 meters at 60 km/h.

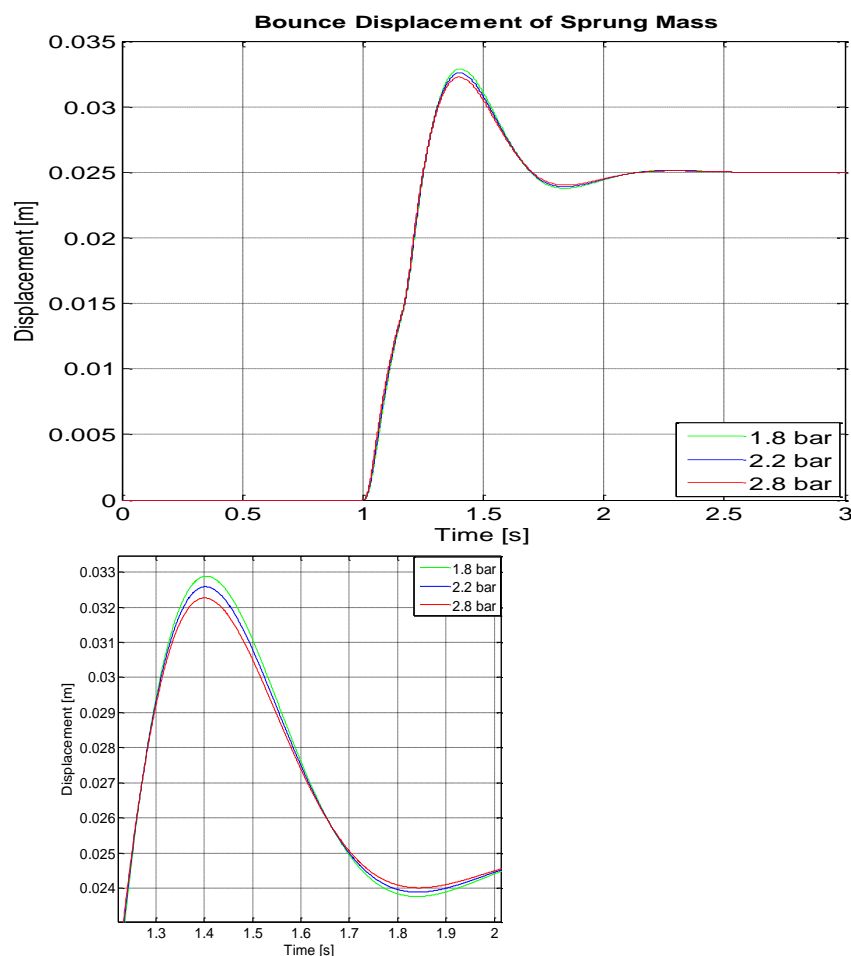


Figure 73: Bounce displacement of the sprung mass at different pressures.

Table 6: Results for peak bounce accelerations and displacements.

<i>Case No.</i>	<i>Peak Acceleration</i> [m/s ²]	<i>Peak displacement</i> [m]
<i>Case I (Nominal)</i>	3.75	0.0325
<i>Case II (Low)</i>	3.36	0.0328
<i>Case III (High)</i>	4.31	0.0322

Pitch angle

Figure 74, shows the pitch angle of the vehicle subjected to the same step input at the front and rear axle for Cases I, II and III. The trend is similar to that observed for bounce displacement i.e., the pitch angle is higher for lower pressures. The difference in the pitch angle magnitude is negligible for the three Cases.

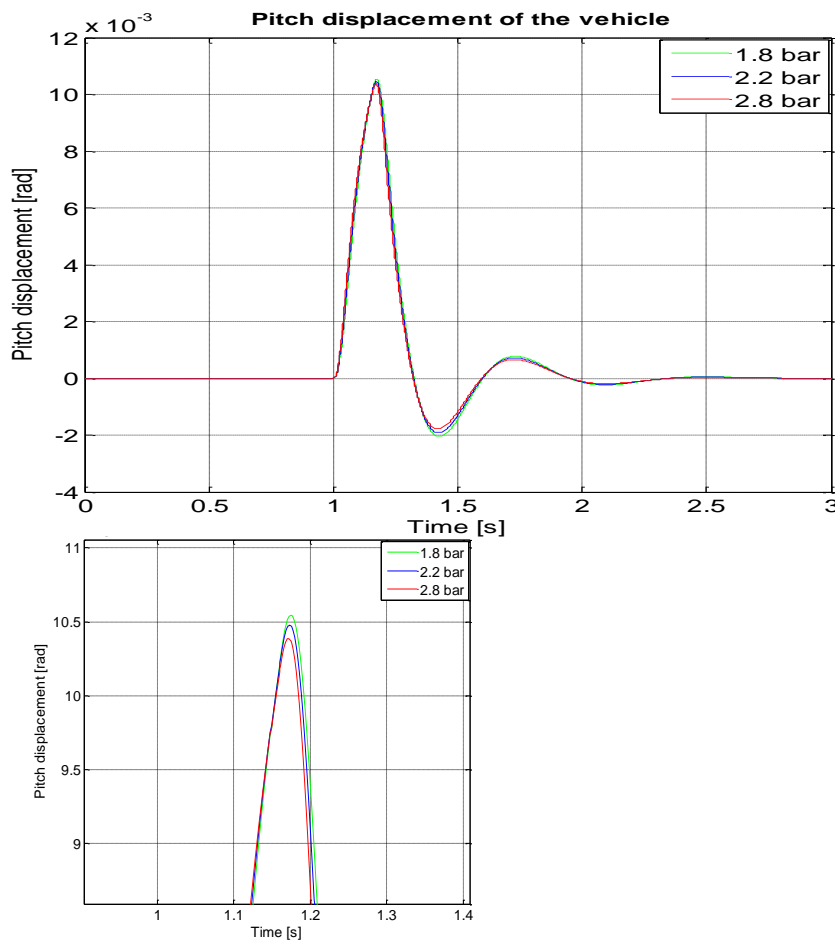


Figure 74: Pitch angle at different pressures.

4.3.2 Response to sinusoidal input

In this section, the vertical response of the vehicle model to sinusoidal inputs is examined to illustrate how the tyre-road contact changes with inflation pressure. The input amplitude chosen is 0.013 metres and the input frequency, 12.05 Hz (which is the natural frequency of the un-sprung mass obtained at the nominal tyre pressure of 2.2 bars). The reasons for choosing these values have been explained in Section 3.3.2.2. Figure 75 shows the displacement of the tyre (and un-sprung mass) at the front and rear axles for the three tyre pressure Cases; Case I, Case II and Case III. The three horizontal lines at the top of the figure indicate the static deflection of tyres for the three Cases. In order for the tyres to have continuous contact with the road the un-sprung displacement must not cross these lines.

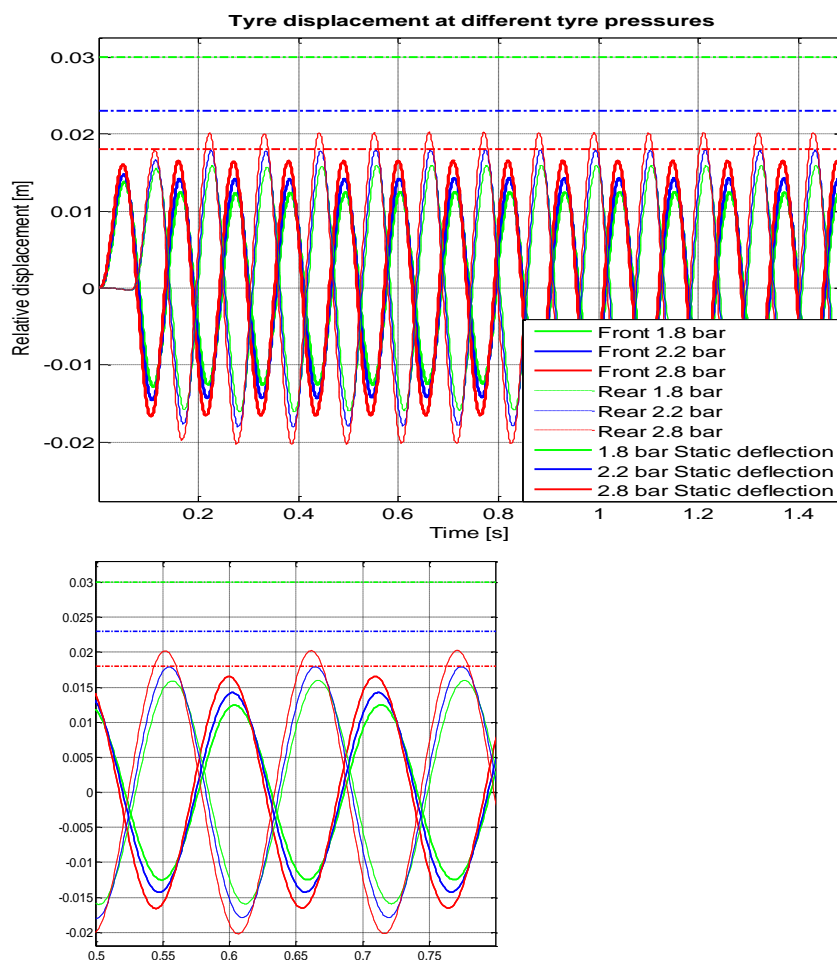


Figure 75: Relative displacement of tyre with respect to the sprung mass at the front axle.

One interesting observation from the figure is that the vertical displacement is higher at higher pressure, a trend which is completely opposite in nature to that observed for the sprung mass, in response to a step input (Section 4.3.1). This is because the input frequency chosen is the natural frequency of the un-sprung mass. Figure 75 shows that the rear axle will lose contact with the road when the pressure is changed from

Case I or II to Case III, as the red curve crosses above the red static tyre deflection line. It should be mentioned here that the weight on rear axle is lower than that on front axle (see Table 10 in Appendix I for vehicle specifications). The next subsection presents the frequency response of the vehicle, which shows the range of frequencies at which vehicle is likely to lose road contact/grip and experience maximum vertical bounce accelerations.

4.3.3 Frequency response

The Frequency Response Plot (FRP) is an instrument used to analyse the response of a system to periodic inputs of different frequencies. For a linear time invariant system, such as the four DOF half-car model used in this report, the FRP shows the system gain as a function of frequency. Figure 76, shows the bode plot for the vehicle's sprung mass vertical bounce acceleration.

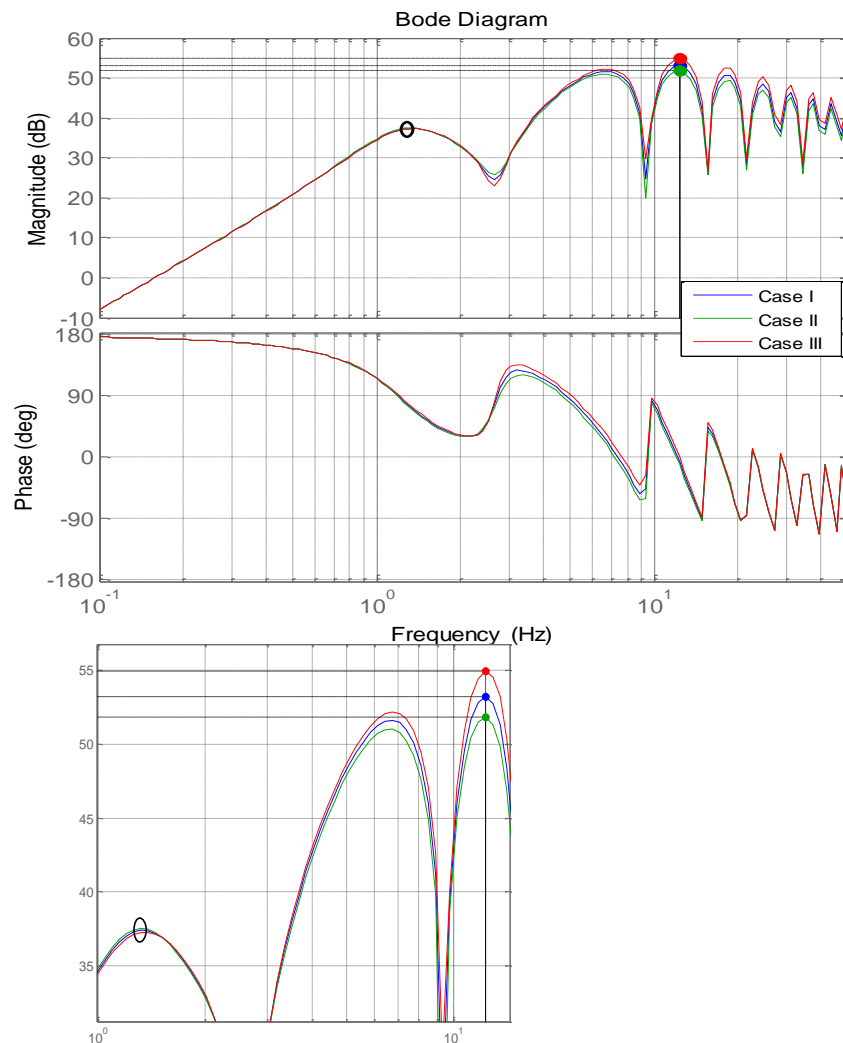


Figure 76: Bode plot for the vehicle's sprung mass bounce acceleration response.

The Bode plot is a type of FRF which shows the range of frequencies at which a dynamic system can experience amplification or attenuation of its output in response to a periodic input. This plot also gives information on the phase change between input and output. In Figure 76, the occurrence of several peaks in the curves may be attributed to the induced delay in the input, between the front and rear axles. The first peak corresponds to the natural frequency of the sprung mass, which is 1.32 Hz. Not much change in magnitude of acceleration was seen at this frequency, though the body experiences higher acceleration at lower pressures.

The natural frequency of the un-sprung mass, which is 12.05 Hz, has been indicated by the three dots corresponding to different tyre pressures. It can be seen that the accelerations are higher at higher pressures and also there is a noticeable difference in the magnitude. However, the difference between the three Cases is not too much to cause severe discomfort. Figure 76, shows the vehicle response to pure periodic inputs at the tyres, which is rarely seen in real life. A better representation of road profile is described in Section 3.3.2.3 from which one can obtain and examine the Power Spectral Density of acceleration response.

Figure 77, shows the PSD of vertical acceleration of the sprung mass at different frequencies for a class B road profile (refer Section 3.3.2.3) for Cases I, II and III.

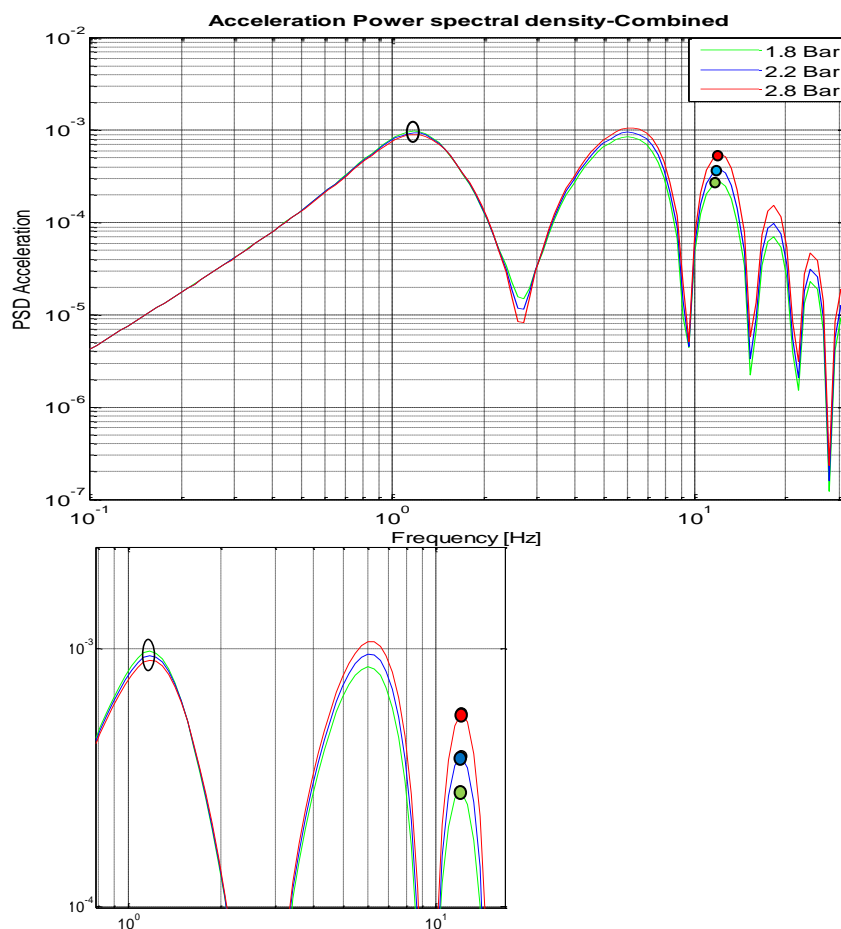


Figure 77: Power spectral density of vertical acceleration of sprung mass.

Again, the occurrence of multiple peaks may be attributed to the out-of phase inputs given at the front and rear axles [19]. The vehicle experiences amplified response in the frequency range close to the natural frequency of the sprung and un-sprung mass (indicated by the black circles in Figure 77). Close to the natural frequency of the sprung mass, higher acceleration is experienced at lower pressures whereas at the natural frequency of the un-sprung mass, higher pressure causes higher excitation (which can also be confirmed from Section 4.3.2). Table 7 below shows the RMS values of vertical acceleration of the sprung mass for frequencies between 4 Hz and 8 Hz for Cases I,II and III. The results are presented for two ISO 8606 Classification of roads; Class A and B.

Table 7: RMS values of vertical acceleration of the sprung mass between 4 Hz and 8 Hz at different tyre pressures.

<i>Tyre Pressure</i>	<i>CLASS A</i>			<i>CLASS B</i>		
	<i>4 Hz</i>	<i>6Hz</i>	<i>8 Hz</i>	<i>4Hz</i>	<i>6Hz</i>	<i>8Hz</i>
<i>Case II (1.8 bar)</i>	0.0462	0.0894	0.0473	0.0923	0.1789	0.0946
<i>Case I (2.2 bar)</i>	0.0483	0.0948	0.0531	0.0967	0.1896	0.1063
<i>Case III (2.8 bar)</i>	0.0503	0.1000	0.0596	0.1006	0.1999	0.1193

Two clear trend can be observed from Table 7. First, the RMS values are lower at lower inflation pressures at the three given frequencies. Second, the RMS values at 6 Hz for the three Cases are higher compared to the values at 4 Hz and 8 Hz for both classes of roads. The higher values at 6 Hz may be due to the interaction between the inputs at the front and rear wheels and this can be seen clearly from Figure 77, the second peak occurs around 6 Hz. When the RMS values from Table 7 are compared to the ISO 2631 tolerance curves (Figure 42), it can be seen that the RMS values for Class A road lie well below the 24 hours tolerance curve limit at the three frequencies. For Class B road, the RMS values at 4 Hz and 8 Hz are still below the 24 hours tolerance limit. However, at 6 Hz the values lie between the 24 hours and 16 hours tolerance curves limit, which is still within the acceptable range.

Road holding

Figure 78 and Figure 79 below show the frequencies for which there is good or poor tyre-road contact for three Cases at the front and rear axles. Since the system gain is reported in decibels (where, $db(x) = 20 * \log(x)$), zero db corresponds to a system gain of one. Thus, the system experiences amplification of the input for all values of gain (in dB) greater than zero, thereby increasing the risk of the tyres losing contact

with the road. The peak values and the corresponding frequencies have been tabulated in Table 8 and Table 9.

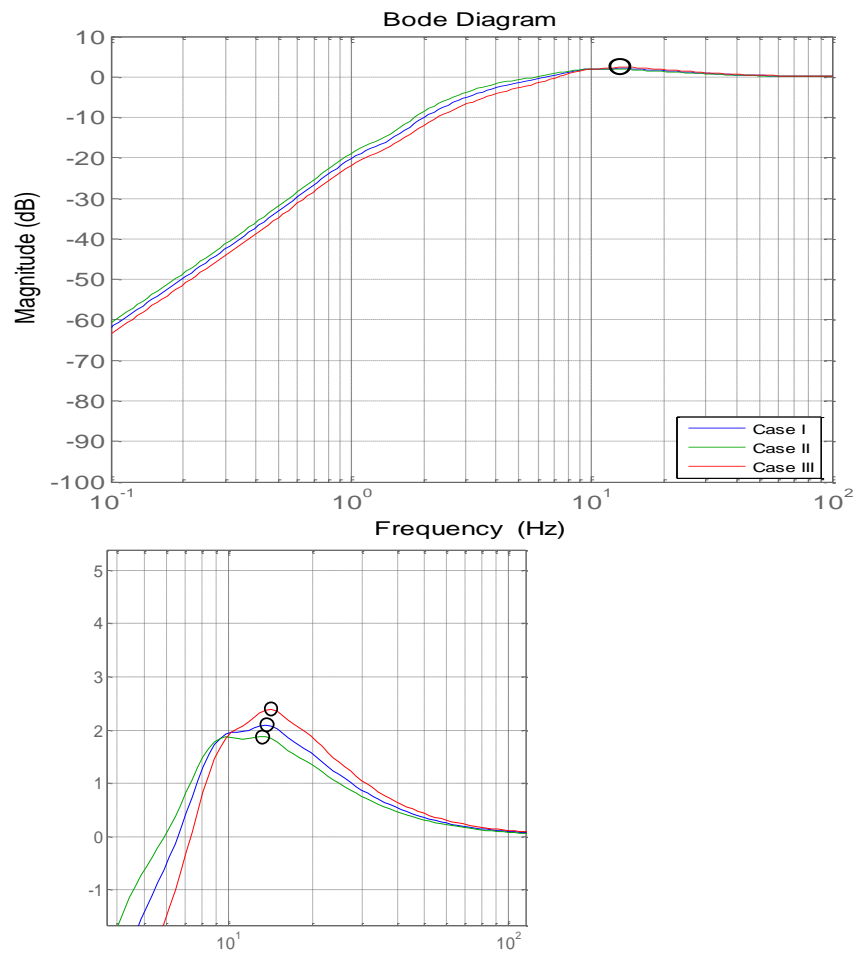


Figure 78: Bode plot for the dynamic tyre deflection at the front axle.

Table 8: Peak gain values for the dynamic tyre deflection for front axle.

<i>Tyre Pressure</i> <i>[bar]</i>	<i>Peak Gain</i> <i>[dB]</i>	<i>Peak Frequency</i> <i>[Hz]</i>
Case I (2.2 bar)	2.08	12.90
Case II (1.8 bar)	1.86	12.30
Case III (2.8 bar)	2.30	14.20

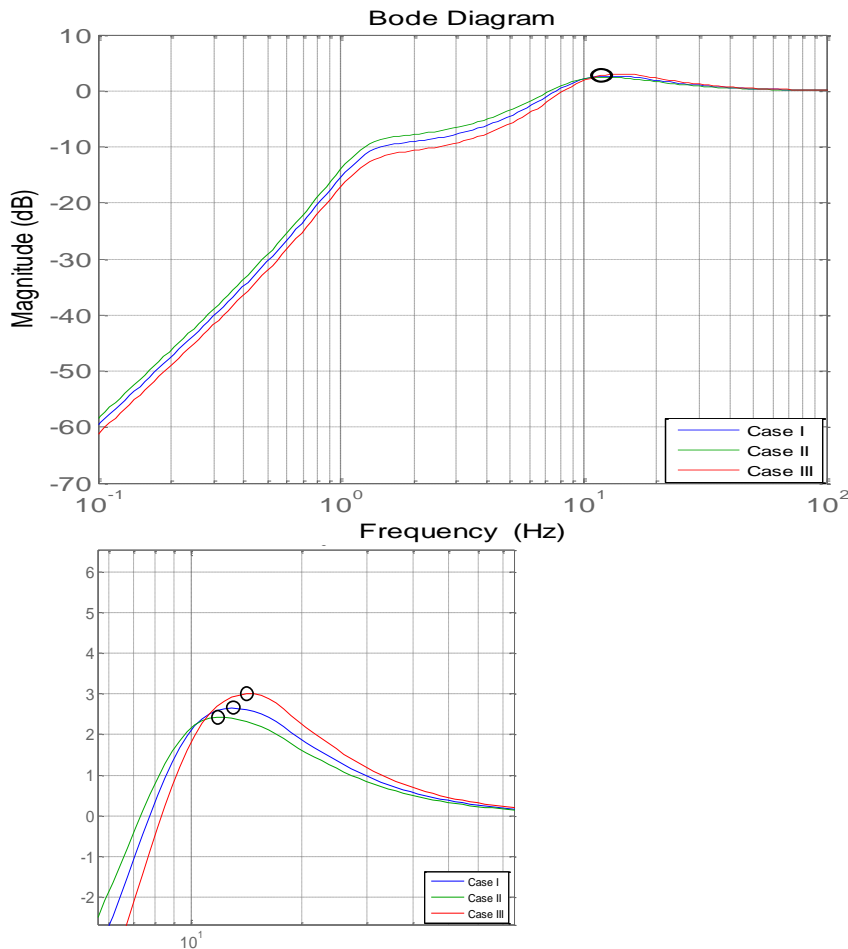


Figure 79: Bode plot for the dynamic tyre deflection for rear axle.

Table 9: Peak gain values for the dynamic tyre deflection for rear axle.

<i>Tyre Pressure</i> <i>[bar]</i>	<i>Peak Gain</i> <i>[dB]</i>	<i>Peak Frequency</i> <i>[Hz]</i>
<i>Case I (2.2 bar)</i>	2.65	12.9
<i>Case II (1.8 bar)</i>	2.42	12.3
<i>Case III (2.8 bar)</i>	3.0	14.2

Two observations can be made from Figures 78, 79 and Tables 8, 9. Firstly, near the natural frequency of the un-sprung mass, the system gain is higher at higher tyre pressures. Higher gain results in higher amplification of the input thereby increasing the risk of the tyres losing contact with the road (see also Figure 75). Secondly, the tyre at lower pressure (Case II) loses contact at a lower value of frequency compared to other Cases, for the same speed of travel of 60 km/h.

From Figures 78 and 79 it may be inferred that, when faced with a situation where the tyre loses contact with the road, the vehicle can either be slowed down or sped up to improve road holding, depending on which side of the peak response one finds oneself. Again, depending on the side of the response peak, the tyre pressure can either be increased or decreased to improve road contact. According to the vehicle's response the quickest way and safest way to improve road holding is to reduce the vehicle speed while simultaneously increasing the tyre pressure until uniform tyre-road contact is obtained. The combined front and rear axle road-holding response characteristics are shown in Figure 82 in Appendix I.

In this section, with the help of vehicle models, it was possible to successfully analyse the influence of tyre inflation pressure on fuel consumption, vehicle handling and ride quality. The next section gives a summary of all the major findings from these three vehicle models.

5 Conclusions and future work

In this section a brief summary of the main findings from this thesis work is presented. Some suggestions for future work are also given.

5.1 Conclusion

This work presents the influence of tyre inflation pressure and other parameters on RR of tyres and in-turn its influence on the overall fuel economy of the vehicle. The impact of tyre pressure on vehicle handling and ride characteristics have also been evaluated and discussed. Three vehicle models were developed in the Matlab/Simulink[®] interface, one each to simulate the effects of tyre pressure on fuel economy, vehicle handling and vehicle ride characteristics. The main findings from these models are discussed briefly in the sections below.

5.1.1 QSS vehicle model / Fuel consumption

A complete vehicle model of a medium sized passenger car was developed in Simulink, using the QSS TB toolbox designed by ETH Zürich. In this toolbox, the tyre RR force is mathematically modelled as a linear function of vertical tyre load. However, this RR model was substituted with another model which takes speed, load and tyre inflation pressure into account. The RR data of the tyre was obtained from [3], to which regression analysis was done to fit the data to a curve.

First, the contribution of tyres to the overall energy loss in a vehicle was estimated using the QSS vehicle model. The QSS vehicle model accepts tyre inflation pressure and load on the tyres as inputs, among other parameters, to generate the fuel consumption in litres/100 km as output. When the model was simulated over a NEDC city driving cycle, it was observed that tyres contributed to nearly 27 % of the net energy loss in a vehicle. However, it may not be possible to utilize the entire 27 % to improve the vehicle's fuel efficiency without affecting the tyre performance.

When the influence of tyre pressure on fuel consumption was analysed for the same NEDC city cycle, it was observed that the fuel consumption reduced by 4.4 % when the tyre pressure was increased from the nominal pressure of 2.2 bar to 3 bar, and a reduction of 5.2 % was observed between 2 bar and 3 bar. These results are consistent with the findings in literature review.

5.1.2 Two-track model / Handling

A two-track model of a medium sized passenger vehicle was modelled in Simulink using an advanced tyre model called the TNO Delft MF-Tyre[®]. This tyre model is based on the 'Magic Formula' tyre model and has been extensively validated for

effectively capturing the effects of inflation pressure on the tyre forces and moments. Using this two-track vehicle model, the transient response behaviour of the vehicle is analysed. In order to effectively analyse the lateral behaviour of the vehicle a number of test Cases were developed, based on the findings from literature survey regarding the role of inflation pressure on tyre force and moment characteristics. Refer Section 3.2.3 for the definition of these Cases. The vehicle's responses are evaluated for seven Cases, on two surfaces; dry and wet and three different velocities.

On both surfaces, it was observed that low pressure tyres gave better yaw response and higher lateral acceleration compared to the nominal Case I. The corresponding lateral displacement with respect to longitudinal displacement was also marginally higher, especially at higher vehicle speeds. Another interesting observation for the step input was that the Case IV vehicle (high pressure on outer wheels and low pressure on inner wheels) and Case A vehicle (high pressure at the front wheels and low pressure at the rear) showed better yaw response and cornering capability compared to Case I. However, at higher speeds, the yaw rates of Cases IV and A took longer time to stabilize to the steady state value. Thus, the nature of these yaw rates need to be analysed further through testing.

From the modified SWD test used in this thesis work, it was concluded that by reducing tyre pressure in all wheels, the vehicle was able to regain yaw stability when it was on the verge of over-steering, especially on wet surface. The yaw stability of Cases IV and V could not be simulated for the SWD test due to the lack of access to the source code of the MF-Tyre model. Thus the results of Cases IV and V presented in this report, only shows the vehicle behaviour if the TPRS system were to fail after the initial steering input in the SWD manoeuvre. Finally, it should be duly noted that the effectiveness of dynamic TPRS in a safety critical situation needs to be validated since, the tyre carcass compliances was not included in the tyre model.

5.1.3 Four DOF half-car model / Comfort

A four DOF half-car model was modelled in Simulink[®] and Matlab[®] to analyse the influence of tyre pressure on the vehicle's ride characteristics. The vehicle response was analysed for only the first three tyre pressure Cases; Case I, II and III. When the vehicle model was subjected to a step input of 0.025 meters at a speed of 60 km/h, it was observed that the peak bounce acceleration of the sprung mass was higher at higher tyre pressures. Between the nominal pressure of 2.2 bar and high pressure of 2.8 bar, the peak acceleration calculated at the COG increased in magnitude by nearly 0.5 m/s^2 . However, the vertical acceleration acts only for a very short time (see Figure 72). Thus, it is possible to attenuate these jerks (high frequency forces) to a considerable extent with a proper seat design.

As expected, the bounce displacement of the sprung mass showed higher peak value at lower tyre pressures. The peak displacement measured at the vehicle's COG reduced by only 0.005 meters when the tyre pressure was reduced from 2.2 bars to 1.8

bars. The influence of tyre pressure on the vehicle model's pitch angle was only marginal and for the pitch acceleration (see Figure 81 in Appendix I) the behaviour observed was similar to that seen for the Bounce acceleration.

A sinusoidal input was used to illustrate the influence of tyre inflation pressure on the tyre-road contact characteristics. It was observed that the tyre was most likely to lose contact with the road at higher inflation pressures (see Figure 75). This can be further confirmed from the road-holding frequency response Figures 78, 79 and from Tables 8 and 9 in Section 4.3.2. From these Bode plots it can be concluded that tyre pressure has a reasonably small impact on the road-holding capability of the vehicle, with higher pressure giving marginally higher gain near the natural frequency of the un-sprung mass. The vertical acceleration Bode plot showed that the vehicle with low pressure tyres exhibited marginally higher vertical accelerations at the COG compared to the vehicle with nominal pressure tyres, at the natural frequency of the sprung mass. However, at the natural frequency of the un-sprung mass, lower tyre pressures gave lower vertical acceleration gain.

The vehicle response to a random road surface profile defined by ISO 8608, was also examined with the help of a vertical acceleration PSD plot. From the PSD values, the RMS values of the vertical acceleration was calculated at three frequencies; 4 Hz, 6 Hz and 8 Hz. At 4 Hz and 6 Hz, the RMS values of vertical acceleration did not change more than 5 % when the pressure was changed from 2.2 bar to 2.8 bar or 1.8 bar. However, at 8 Hz there was 12 % change in RMS value at both low and high pressures, compared to nominal pressure. All the RMS values, except values at 6 Hz for Class B road were within the 24 hour tolerance limit (compare values in Table 7 to Figure 42). Whether this change of 5 % and 12 % at the corresponding frequencies is acceptable to the passenger, is a matter of further investigation.

Overall, fuel consumption could be reduced up to 4 % and noticeable improvement in handling was observed. However, ride comfort did not vary too much at different tyre pressures on smooth roads.

5.2 Future work

This thesis work is a pre-study to evaluate the pros and cons of a dynamic TPRS primarily from fuel consumption point of view. However, through this work, the different advantages of such a system from the vehicle handling and ride characteristics points of view have also been highlighted. A clear trend of the influence of tyre pressure on the different parameters such as rolling resistance, vehicle cornering forces and moments and vertical forces have been established. The models used in this work may be classified as having medium accuracy, in its ability to capture and represent the vehicle and tyre parameters. However, with access to

better vehicle and tyre data, more accurate vehicle models could be built to quantify and validate the gains in fuel efficiency, cornering and ride quality.

Due to the time limitation on this work, the effect of inflation pressure on the vehicle's longitudinal performance could not be evaluated through a vehicle model. Also, from literature review it was concluded that tyre pressure does not have much impact on the braking performance of a vehicle equipped with ABS. However, the traction performance could be studied in the future. From literature review it can be concluded that it would be advantageous to have slightly lower-than-nominal inflation pressure in the tyres while accelerating from standstill. The new vehicles with downsized engines entering the market have high torque available at lower engine speeds. With a dynamic TPRS, it could be possible to put this torque more efficiently on to the road simply by altering the tyre pressure.

As mentioned earlier, results obtained from vehicle model simulations are only as accurate as the results of a tyre model. Thus, if sufficient tyre data is available at different tyre pressures, then it is possible to make a reliable tyre model using Artificial Neural Network (ANN). ANN is a useful data modelling tool that is able to capture and represent complex relationships between inputs/outputs parameters. However, the neural network model needs to be trained initially with large amounts of tyre data at different tyre design and operating points, using a backward propagation algorithm. The model capable of processing multiple inputs in parallel depending on the training. It can reinforce some input variables while diminishing others, to generate reliable outputs for inputs that lie even outside the range of original training data. Thus, it could be a promising area of research for developing an intelligent tyre model.

6 References

- [1] International Energy Agency (2005): Technology and Policies to Improve Vehicle In-Use Fuel Economy, *Organisation for Economic Co-operation and Development (OECD), France*, ISBN 92-821-0343-9. pg 32,51,52.
- [2] Adams B. T., Reid J. F., Hummel J. W., Zhang Q, Hoeft R. G. (2004): Effects of central tire inflation systems on ride quality of agricultural vehicles. *Journal of Terramechanics*, No. 41, pp. 199-207.
- [3] Grover P. S., Bordelon S. H. (1999): New Parameters for comparing Tire Rolling Resistance. SAE International, Paper No. 1999-01-0787.
- [4] Tire Rack, Inc. (2003) : Air Pressure versus Wet Performance, Michelin North America, Website: <http://www.tirerack.com/tires/tiretech/techpage.jsp?techid=175> .
- [5] Clark S. K., Dodge R. N. (2003): A Handbook for the Rolling Resistance of Pneumatic Tires, U.S Department of transportation, Cambridge, Massachusetts, U.S.A. 3 pp.
- [6] Egger M. (2010): Rolling fiction of low resistance tires. SAE International, SAE Paper No. 20109110, pp. 2.
- [7] Rubber Engineering-Indian Rubber Institute-K. S. Loganathan-McGraw-Hill.
- [8] Andre M., Hammarstrom .U, Raynaud I. (1999): Driving Statistics for the Assessment of Pollution Emission from Road Transportation, INRETS-Laboratoire Transports et Environnement, France, Report no. 9906, pp 88.
- [9] De' Hooge J. (2005): Implementing inflation pressure and velocity effects into Magic Formula Tyre Model, TNO Automotive and Technische Universiteit Eindhoven, The Netherlands, Report no. DCT 2005.46.
- [10] PressureGuard™ (2013): Industry Standard on Tyre Pressure Effects, Fleet Air LLC, Cleveland, U.S.A.
Website: <http://www.fleet-air.com/wp content/uploads/Industry Info on Effects.pdf>
- [11] Website: Car Bibles.
http://www.carbibles.com/tyre_bible_pg3.html
- [12] Marshek K. M., Cuderman II J. F., Johnson M. J. (2002): Performance of Anti-Lock Braking System equipped passenger vehicles-Part III: Braking as a function of tire inflation pressure. SAE International, SAE Paper No. 2002-01-0306
- [13] Gillespie, T. D., (1992) Fundamentals of Vehicle Dynamics, Society of Automotive Engineers, Warrendale, PA, 1992, pp 57, 345.
- [14] Pacejka H. B. (2012): Tire and Vehicle Dynamics. Elsevier Ltd. , Oxford, UK.
- [15] Wong J. Y. (2001): Theory of Ground Vehicles. John Wiley & Sons, Inc., New York.

- [16] B. Jacobsson (2012): *Vehicle Dynamics Compendium*, Chalmers University of Technology, Göteborg, Sweden.
- [17] Zoz F. M., Grisso R. D., (2003): Traction and tractor performance. American Society of Agricultural Engineers, Publication No. 913C0403.
- [18] Grover P. S.(1998): Modelling of Rolling Resistance Test Data. SAE International, Paper No. 980251.
- [19] Hall D. E., Moreland J. C. (2001): Fundamentals of Rolling Resistance, Rubber Chemistry and Technology, Vol 74 No. , pp 529.
- [20] Barrand J., Boker J. (2008): Reducing Tire Rolling Resistance to save fuel and lower Emissions. SAE International, Paper No. 2008-01-0154, pp 10.
- [21] Guzzela L., Sciarretta A. (2007): *Vehicle Propulsion Systems: Introduction to modelling and optimization*. Springer, Berlin, Germany.
- [22] Kasprzak E. M., Lewis K. E., Milliken D. L. (2006): Inflation Pressure Effects in the Non-Dimensional Tyre Model. SAE International, Paper No. 2006-01-3607, pp all.
- [23] TNO Automotive (2012): MF-Tyre/MF-Swift 6.1.2.1 Help Manual. *TNO Automotive, The Netherlands*.
- [24] Forkenbrock G. J., Elsassar D., O' Harra B. (2005): NHTSA's Light Vehicle Handling and ESC Effectiveness Research Program, *Transportation Research Centre, Inc., USA*, Paper no. 05-0221.
- [25] Forkenbrock G. J., Elsasser D., O'Harra B. (2004): NHTSA's Light Vehicle Handling and ESC Effectiveness Research Program. NHTSA and Transportation Research Centre, Inc., U.S.A, Paper no.05-0221.
- [26] Talukdar S., Mazumdar A., Mullaseril M., Kalita K., Ujjwal A. (2012): Mathematical modeling in Vehicle Ride Dynamics. SAE International, Paper No.2012-01-0056, pp all.
- [27] Barak P., Panakanti N., Desai T. (2004): Effect of Chassis Design Factors (CDF) on Ride Quality using a 7 Degree of Freedom Vehicle Model. SAE International, Paper No. 2004-01-1555, pp all
- [28] Soliman A. M. A., Kaldas M. M. S., Abdalla S. A. (2013) Influence of Road Roughness on Ride and Rolling Resistance for Passenger Car. SAE International, Paper No. 2013-01-0993, pp all
- [29] Soliman A. M. A., Moustafa S. M., Shogae A. O. M. (2008): Parameters Affecting Vehicle Ride Comfort using Half Vehicle Model, SAE International, Paper No. 2008-01-1146, pp all
- [30] Barbosa R. S. (2011): Vehicle Dynamic Response due to Pavement Roughness. *Journal of Brazilian Society of Mechanical Sciences and Engineering*, Brazil. Volume 33, No.3.

[31] Besselink I.J.M., Schmeitz A.J.C, Pacejka H.B (2008): An Improved Magic Formula/Swift Tyre Model that can handle Inflation Pressure changes, *Eindhoven University of Technology, The Netherlands*.

[32] Website: Yokohama tyres.

http://global.yokohamatire.net/technology/tirecareandsafety/rolling_resistance.html

7 Appendix I

Table 10: *Vehicle specifications; Saab 9-3 2003 model*

Vehicle specifications	
Engine specifications	
Inline 4 cylinder,16 valves DOHC, Turbo	
<i>Displacement. [L]</i>	1.998
<i>Bore. [mm]</i>	86
<i>Stroke. [mm]</i>	86
<i>Maximum speed. [RPM]</i>	6500
<i>Idle speed. [RPM]</i>	900
<i>Engine power at idle. [kW]</i>	2.60
<i>Power required by Auxiliaries. [kW]</i>	0.3
<i>Engine Torque at fuel cut-off. [N/m]</i>	5.0
<i>Willian's Parameter 1: Engine internal thermodynamic efficiency. [-]</i>	0.29
<i>Willian's Parameter 2: Maximum boost ratio. [-]</i>	2
Measured Performance	
<i>Top speed [km/h]</i>	220
<i>Acceleration 0-100 km/h [s]</i>	8.5
<i>Acceleration 60-100 km/h [s]</i>	8.5
<i>Acceleration 80-120 km/h [s]</i>	12.5
Chassis	
<i>Air drag coefficient [-]</i>	0.30

<i>Auxiliary roll stiffness, front [N/rad]</i>	16.22
<i>Auxiliary roll stiffness, rear [N/rad]</i>	7.837
<i>Curb weight [kg]</i>	1675
<i>Distance from COG to front axle [m]</i>	1.524
<i>Distance from COG to rear axle [m]</i>	1.515
<i>Front roll centre height [m]</i>	0.045
<i>Frontal area [m²]</i>	2.17
<i>Height of COG from ground [m]</i>	0.543
<i>Max load carrying capacity [kg]</i>	450
<i>Rear roll centre height-front [m]</i>	0.101
<i>Suspension stiffness- front [N/m]</i>	30800
<i>Suspension stiffness- rear [N/m]</i>	29900
<i>Suspension damping-front [Ns/m]</i>	4500
<i>Suspension damping-rear [Ns/m]</i>	3500
<i>Total mass moment of inertia-x axis [kg-m²]</i>	540
<i>Total mass moment of inertia-y axis [kg-m²]</i>	2398
<i>Total mass moment of inertia-z axis [kg-m²]</i>	2617
<i>Track width- front [m]</i>	1.517
<i>Track width- rear [m]</i>	1.505
<i>Un-sprung mass [kg]</i>	180
<i>Wheelbase [m]</i>	2.675
<i>Tyre/Wheel 205/60 R15</i>	
<i>Unloaded radius [m]</i>	0.3135
<i>Nominal inflation pressure [pa]</i>	220000

<i>Nominal tyre vertical stiffness [N/m]</i>	209651.8
<i>Nominal tyre vertical damping [Ns/m]</i>	50
<i>Pressure effect on vertical stiffness [-]</i>	0.7098
<i>Nominal longitudinal stiffness [N/m]</i>	358066.3
<i>Nominal lateral stiffness [N/m]</i>	102673.5

Dry surface - SWD input

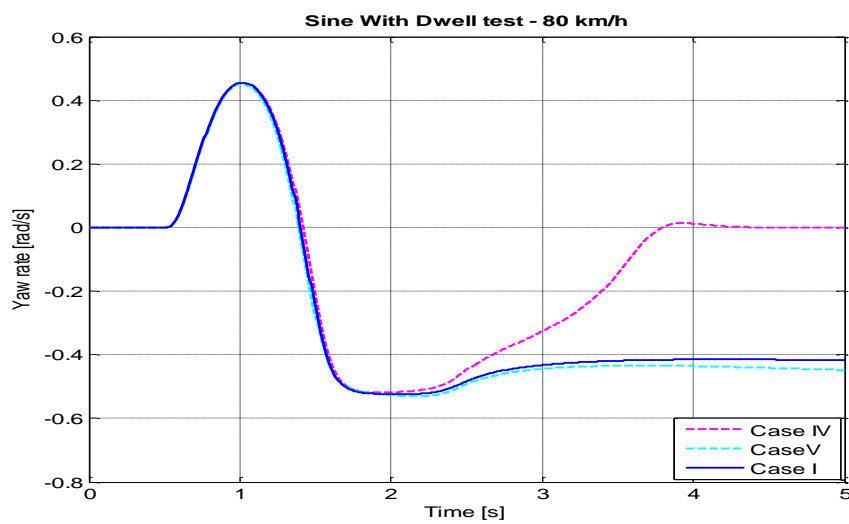


Figure 80: Yaw rate versus time for SWD manoeuvre where the lateral forces are computed by the MF-tyre model using only lateral slip; Dry surface; Cases I, IV and V.

Pitch acceleration

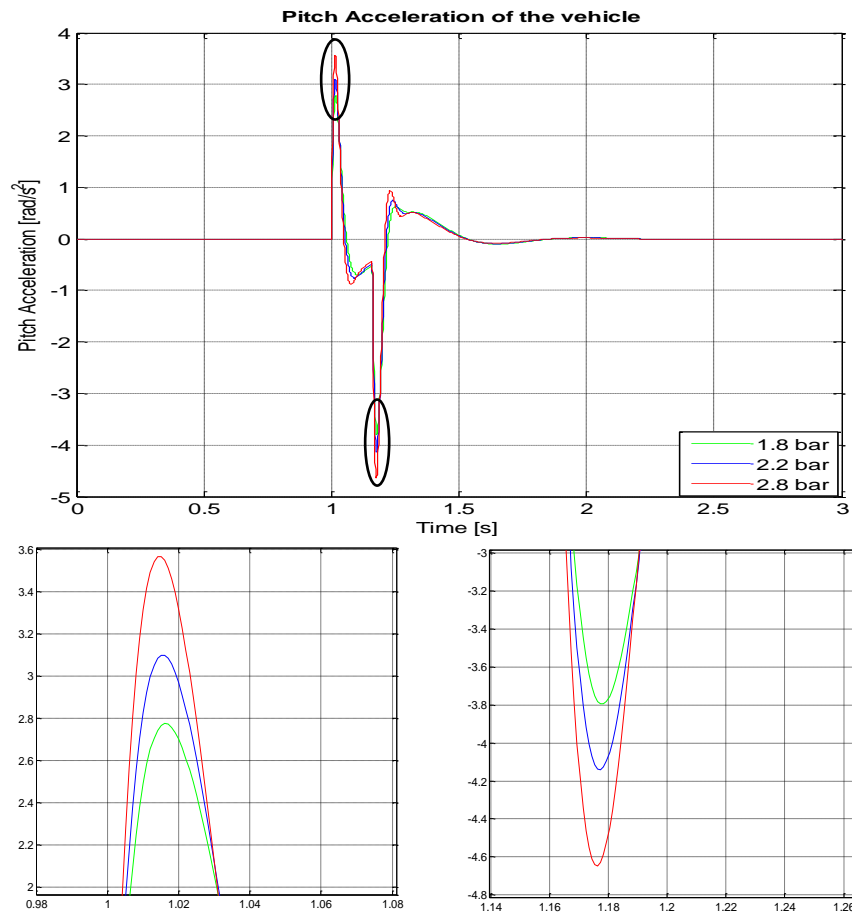


Figure 81: Pitch acceleration of the 4-DOF half-car model to a step input.

Bode plot - Road holding

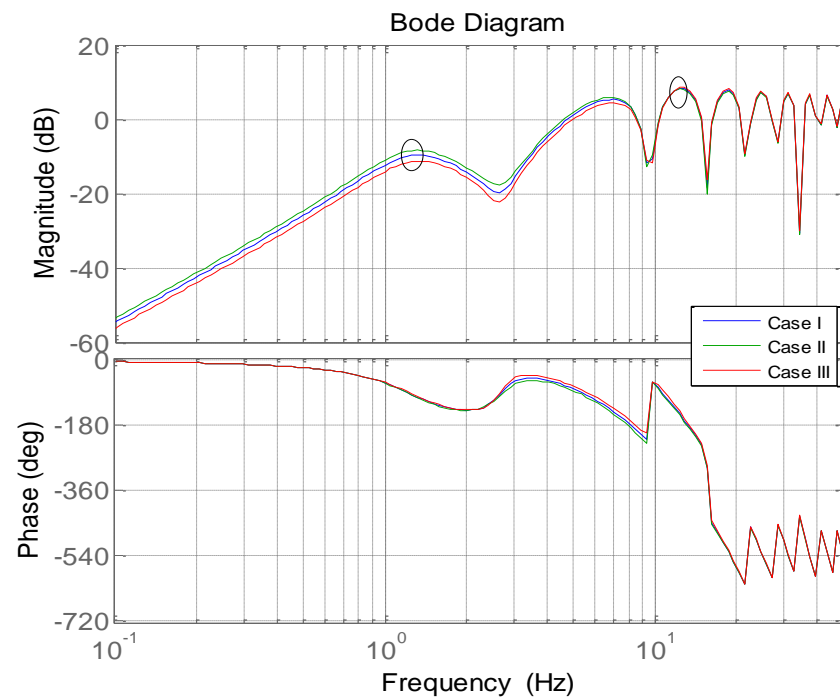


Figure 82: Combined front and rear axle Bode plot for road holding.

Dry surface - Step input

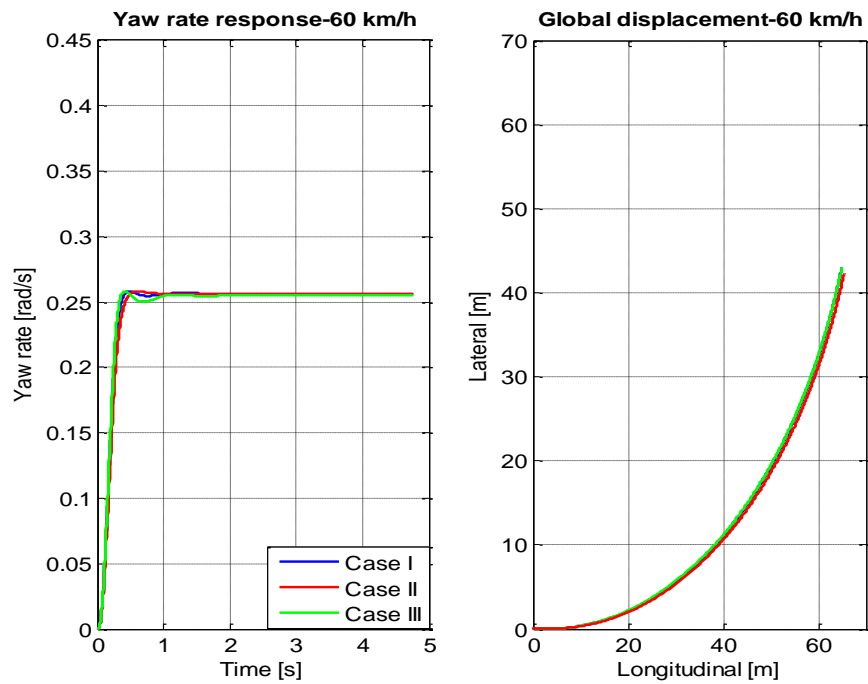


Figure 83: Yaw response to a step input at 60 km/h; Dry surface; Cases I, II and III.

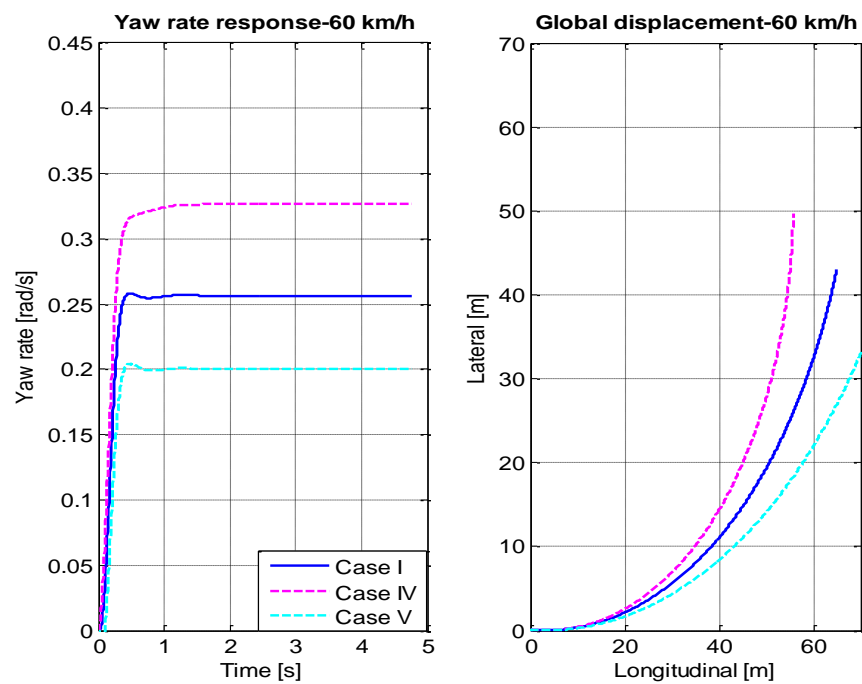


Figure 84: Yaw response to a step input at 60 km/h; Dry surface; Cases I, IV and V.

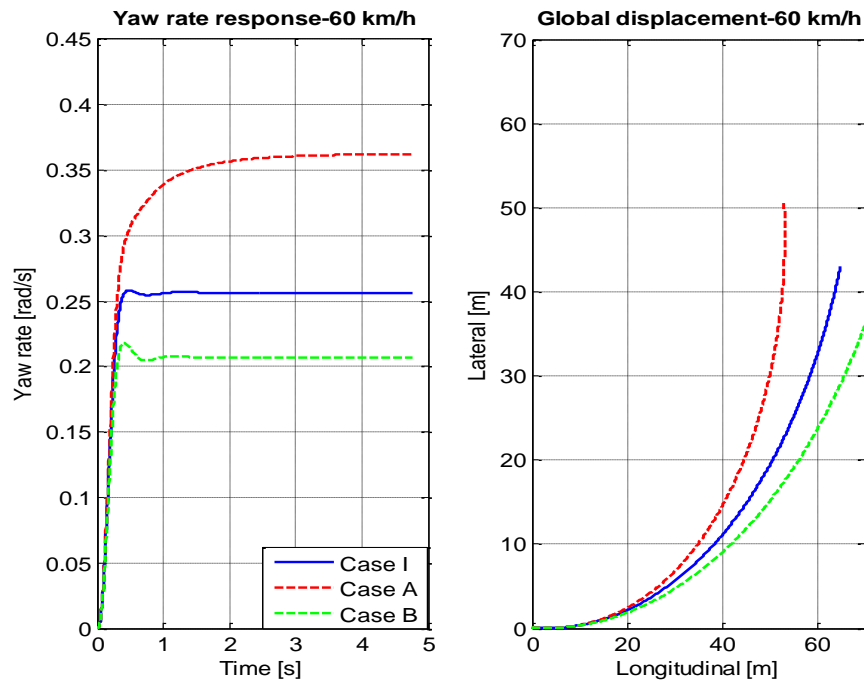


Figure 85: Yaw response to a step input at 60 km/h; Dry surface; Cases I, A and B.

Dry surface - Ramp input

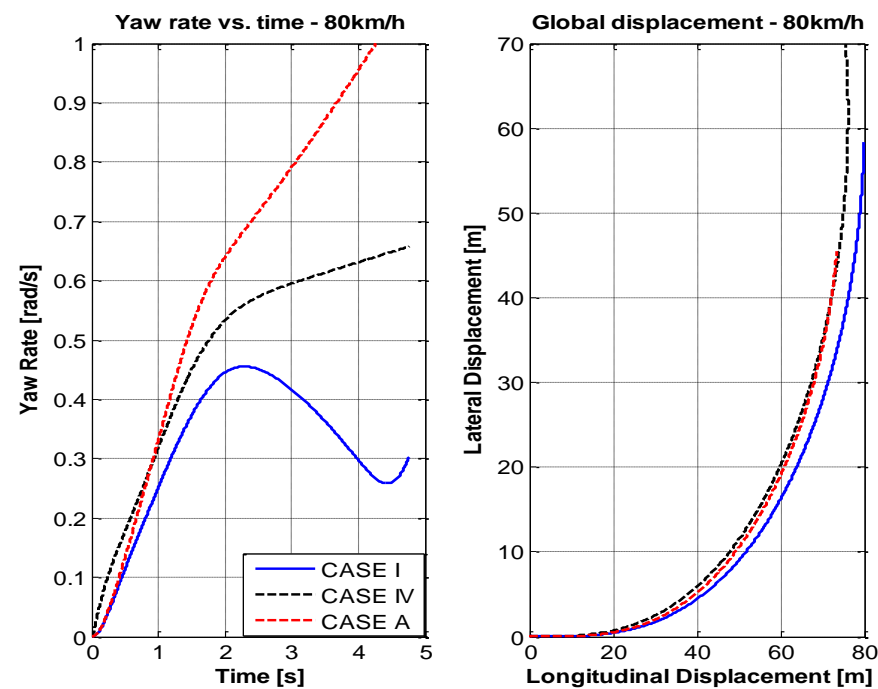


Figure 86: Yaw response to a ramp input at 80 km/h; Dry surface; Cases I, IV and A.

Wet surface - Step input

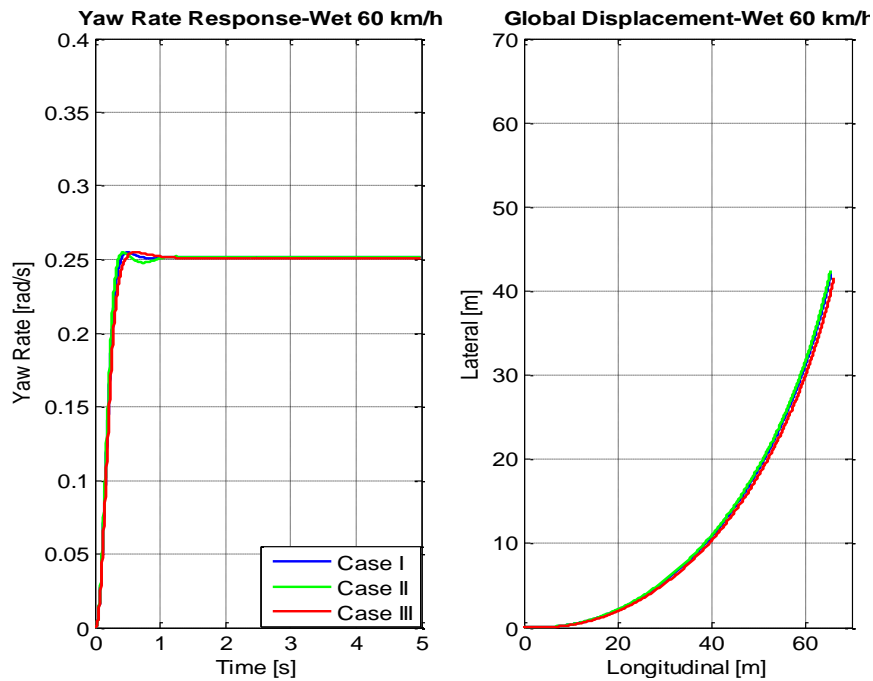


Figure 87: Yaw response to a step input at 60 km/h; Wet surface; Cases I, II and III.

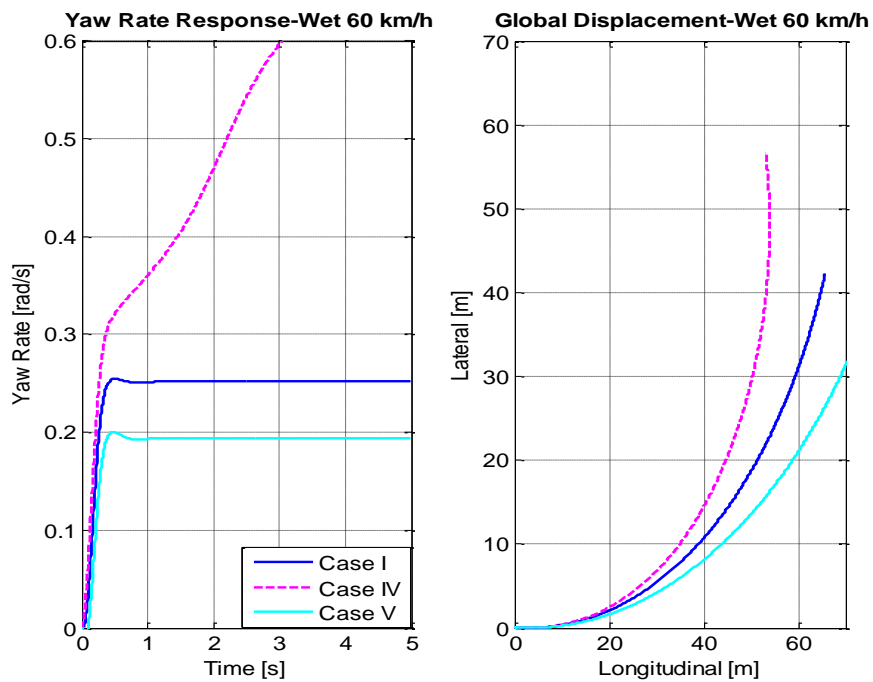


Figure 88: Yaw response to a step input at 60 km/h; Wet surface; Cases I, IV and V.

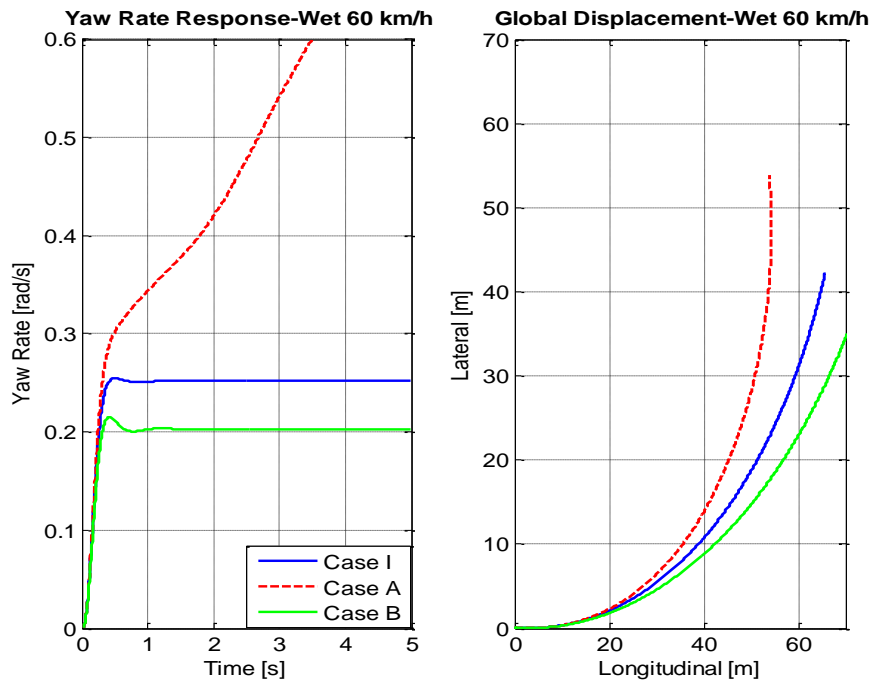


Figure 89: Yaw response to a step input at 60 km/h; Wet surface; Cases I, A and B.

Wet surface - Ramp input

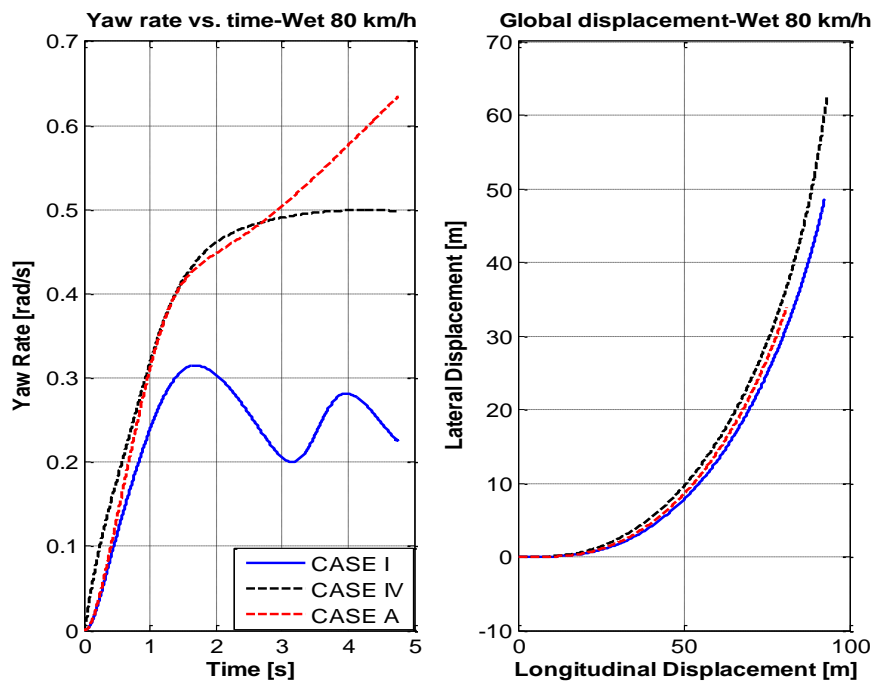


Figure 90: Yaw response to a ramp input at 80 km/h; Wet surface; Cases I, IV and A.

Dry surface - Handling diagram 60 km/h

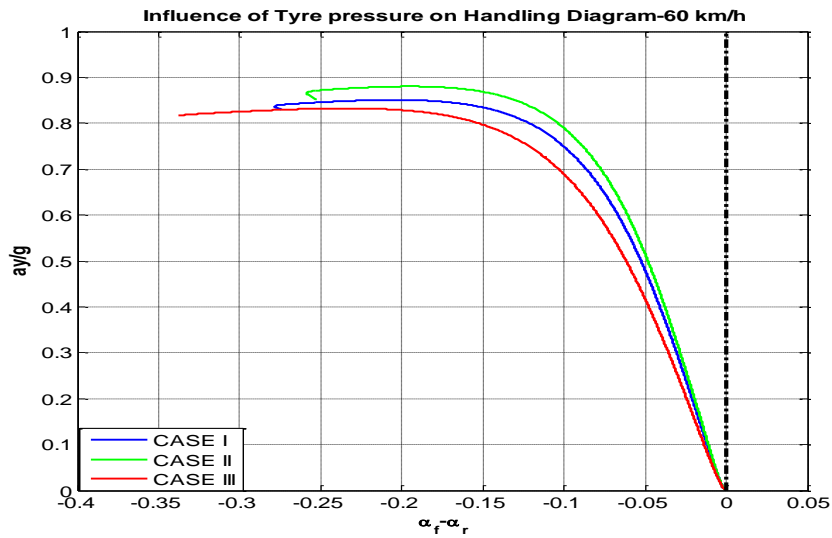


Figure 91: Handling Diagram for 60 km/h; Dry surface; Cases I, II and III

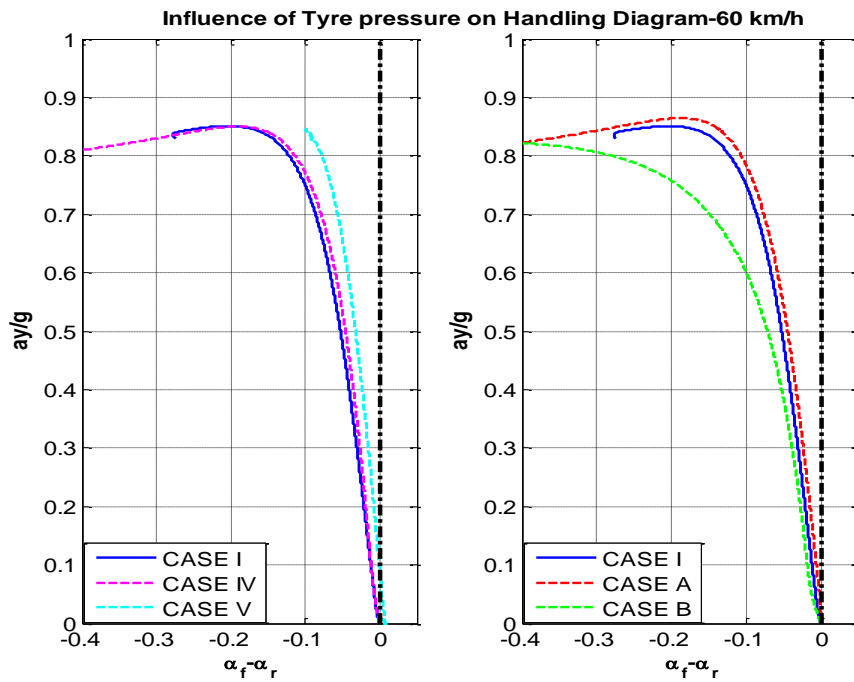


Figure 92: Yaw response to a step input at 60 km/h; Dry surface; Cases I, A and B.

Wet surface - Handling Diagram at 60 km/h.

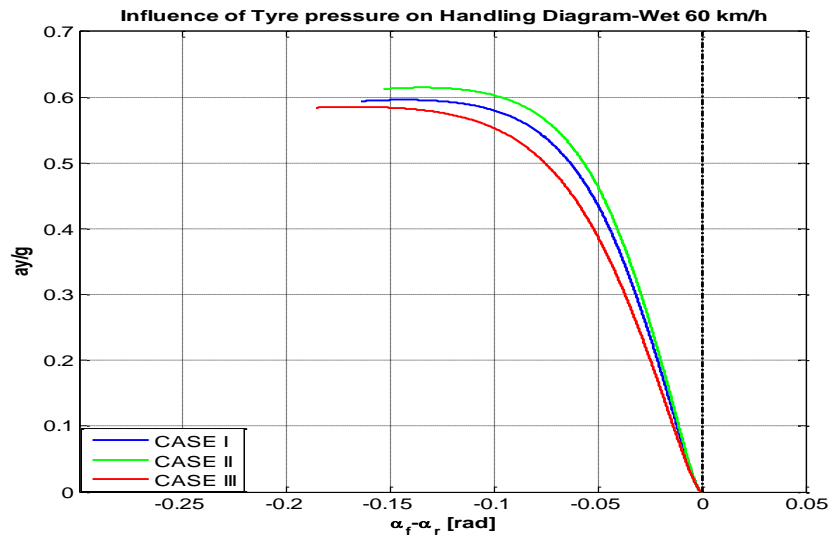


Figure 93: Handling Diagram for 60 km/h; Wet surface; Cases I, II and III

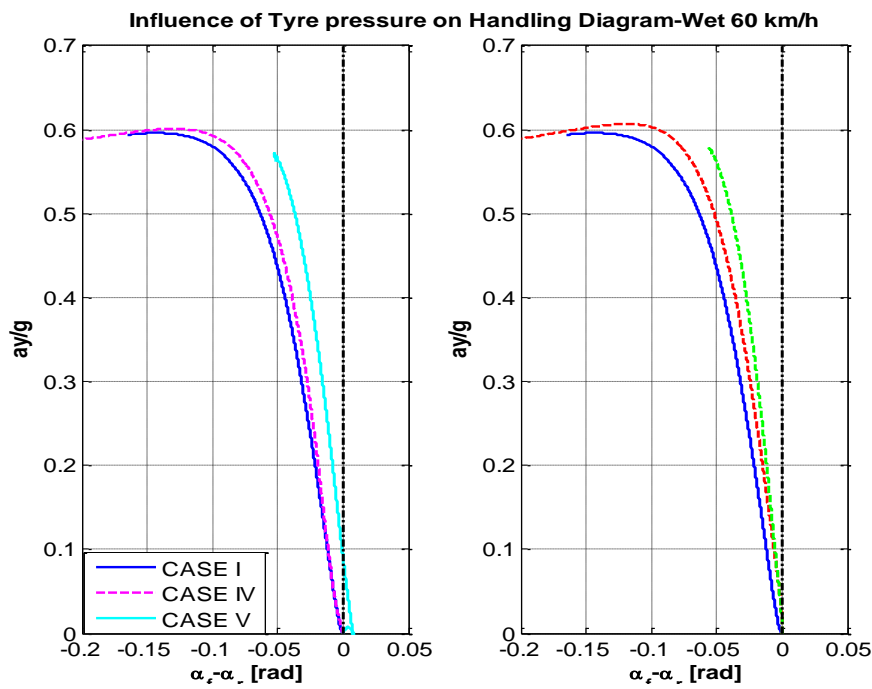


Figure 94: Handling Diagram for 60 km/h; Wet surface; Cases I, IV, V, A and B.